The Institute of Paper Science and Technology

Atlanta, Georgia

Doctor's Dissertation

A Computer Model of a Kraft Char Bed

Daniel W. Sumnicht

April, 1989

A COMPUTER MODEL OF A KRAFT CHAR BED

A thesis submitted by

Daniel W. Sumnicht

B. S. ChE., December 1983, University of Wisconsin, Madison

M. S., June 1986, The Institute of Paper Chemistry

in partial fulfillment of the requirements
of The Institute of Paper Chemistry
for the degree of Doctor of Philosophy
from Lawrence University
Appleton, Wisconsin

April, 1989

TABLE OF CONTENTS

LIST OF TABLES

LIST OF FIGURES

LIST OF FIGURES (Continued)

ABSTRACT

A computer model of a kraft char bed has been developed as part of a three-dimensional model of the recovery furnace. The char bed model calculates mass and energy exchange between the char bed surface and the gases in the furnace. The three-dimensional distribution of temperatures, gas velocities, and gas concentrations above the bed is used to calculate both local and global bed burning rates. The sulfate/sulfide cycle theory of char burning is used as a basis for calculating reduction efficiency.

The results of model calculations suggest that the bed influences gas flow patterns in the lower furnace and plays an important role in overall char combustion. Most of the char combustion can occur on the bed surface, and the C/CO_2 and C/H_2O reactions make a significant contribution to bed burning. The reduction efficiency is not threatened by a large oxygen supply as long as surface temperatures are high enough and there is sufficient char carbon present. Three bed shapes -- a high bed, a crater-shaped bed, and a low bed -- resulted in different flow patterns in the lower furnace for each case. The high bed forced the secondary jets upward while the crater bed and low bed resulted in the development of gas recirculation patterns above the bed.

INTRODUCTION

The recovery boiler has long been recognized as a production bottleneck at many kraft pulp mills. Other processes are optimized and equipment is upgraded until the most expensive unit -- the recovery boiler -- is the remaining obstacle to increased production. An extensive research effort is therefore warranted to obtain a fundamental understanding of recovery boiler processes with the goal of increasing boiler throughput within environmental and operational constraints. Experimental work has increased the understanding of the fundamental processes that determine the internal state of the recovery boiler. Knowledge of such conditions provides a basis for improving the operation of recovery boilers. The benefits of improved performance include enhanced burning rates, more efficient recovery of sodium sulfide, optimum vaporization of inorganic salts (fuming), height control of the char bed, and blackout prevention. This thesis is one of three theses at The Institute of Paper Chemistry devoted to modeling the recovery boiler using the best fundamental process knowledge available.

The operation of a recovery boiler depends on the combustion behavior of the fuel used. Spent pulping chemicals and dissolved wood components from the pulping process are concentrated into a combustible fuel known as black liquor. Black liquor is sprayed into the furnace through nozzles in a way that produces a distribution of drop sizes. Kraft black liquor drops proceed through several stages as they interact with the gases and boundaries of the furnace: drying, pyrolysis, char combustion, and smelt oxidation[1]. Drying removes the water and pyrolysis produces volatile organic compounds, leaving fixed carbon, a small amount of fixed hydrogen, and inorganic alkali salts. This residual mixture is referred to as char, and the organic carbon in the char is referred to as char carbon. Char combustion is the slowest stage of black liquor

combustion and may not be completed during the flight of the particle in the recovery furnace. In such a case, the particle is either carried out of the furnace or it eventually falls on the hearth where combustion of char carbon is completed and residual sodium sulfate (Na_2SO_4) is reduced to the active pulping chemical sodium sulfide (Na_2S). As char carbon becomes depleted, the inorganic salts form molten smelt which is drained from the furnace through spouts.

The location where char combustion occurs depends on the flight history of the individual particles. Char combustion may occur during flight, on the walls of the furnace, or on the pile of residual black liquor solids on the hearth of the furnace referred to as the char bed (or smelt bed). Small particles may complete combustion during flight and land on the furnace hearth as molten inorganic salts (smelt), or be carried out of the furnace by the upward flowing gases. Large particles may hit and stick to the furnace walls or land directly on the char bed in a wet or partially pyrolyzed state. The wet particles that stick to the wall may dry there, and the weight of the accumulating material eventually becomes great enough to cause chunks of solids to break off and fall to the char bed. Thus, char combustion can occur during flight, on the walls, or on the char bed on the hearth of the furnace.

In this thesis, "char combustion" will refer to the final stage of black liquor combustion, while "bed burning" will refer to the combustion processes that occur on the char bed. This thesis is concerned with bed burning which primarily involves char combustion but may also include drying and pyrolysis.

The behavior and structure of the char bed are determined by the material landing on it and interaction between the bed and combustion gases. The bed tends to grow, shrink, or maintain a quasi-stable height depending on the spray behavior and other furnace variables. In order to gain a better

appreciation for the form char beds may take, some experimental work on char beds will now be discussed.

LITERATURE REVIEW

CHAR BED CHARACTERISTICS

Smelt-water explosions can occur in recovery boilers if liquid water contacts molten smelt in the char bed. If it is suspected that water has entered the combustion chamber, an emergency shutdown procedure (ESP) is required. Smelt should be completely solidified before water washing begins, so beds which take a long time to cool increase the duration of the shutdown. Richardson and Merriam[2] studied the cooling rates of char beds in order to:

1) determine the mechanisms controlling cooling of the char bed;

2) determine the range of cooling and solidification rates in typical configurations;

3) assess methods for accelerating the cooldown in existing recovery boilers.

The study included measurements of bed temperature profiles, thermal properties, and composition. These measurements give some insight into the range of char bed characteristics that occur during normal operation.

Richardson and Merriam observed some differences between beds in Babcock and Wilcox (B&W) boilers and those in Combustion Engineering (CE) boilers. The designations "B&W bed" and "CE bed" will be used in the following discussion although B&W and CE beds may have features in common. The char bed measurements were performed on operating recovery boilers, so there was some difficulty in getting good measurements since access to the furnace was limited. The discussion of Richardson and Merriam's work is therefore a portrayal of their conclusions which are subject to the limitations of

the techniques used to gather the data.

B&W Char Beds

The char bed of a typical B&W boiler is depicted in Fig. 1. Most of the B&W beds observed had about the same geometry and all appeared to have an inactive core based on temperature measurement. The bed was observed to have a relatively flat top, level with the secondary air ports; the flow of secondary air was normally sufficient to limit the bed height at that level. This observation may only apply to the periphery of the bed since visibility through the primary ports would be limited by fuming and combustion processes.

The internal structure of the bed can be roughly divided into an active region and an inactive region. The distinction between an active zone and an inactive zone was based on temperature measurement. A zone was considered active if it was hot enough to carry out reaction in molten smelt (> 1400°F). The active region is a 6 - 8 inch layer of material in various states which depend on the local operating conditions of the furnace. Drying, pyrolysis, reduction, smelting, and fuming can all occur in the active zone, and the temperature varies accordingly between 1400 °F and 2200 °F. As the carbon is depleted, smelt forms, flows through the porous char, and collects in troughs around the perimeter of the bed. The smelt then flows down the sloping hearth to the smelt spouts.

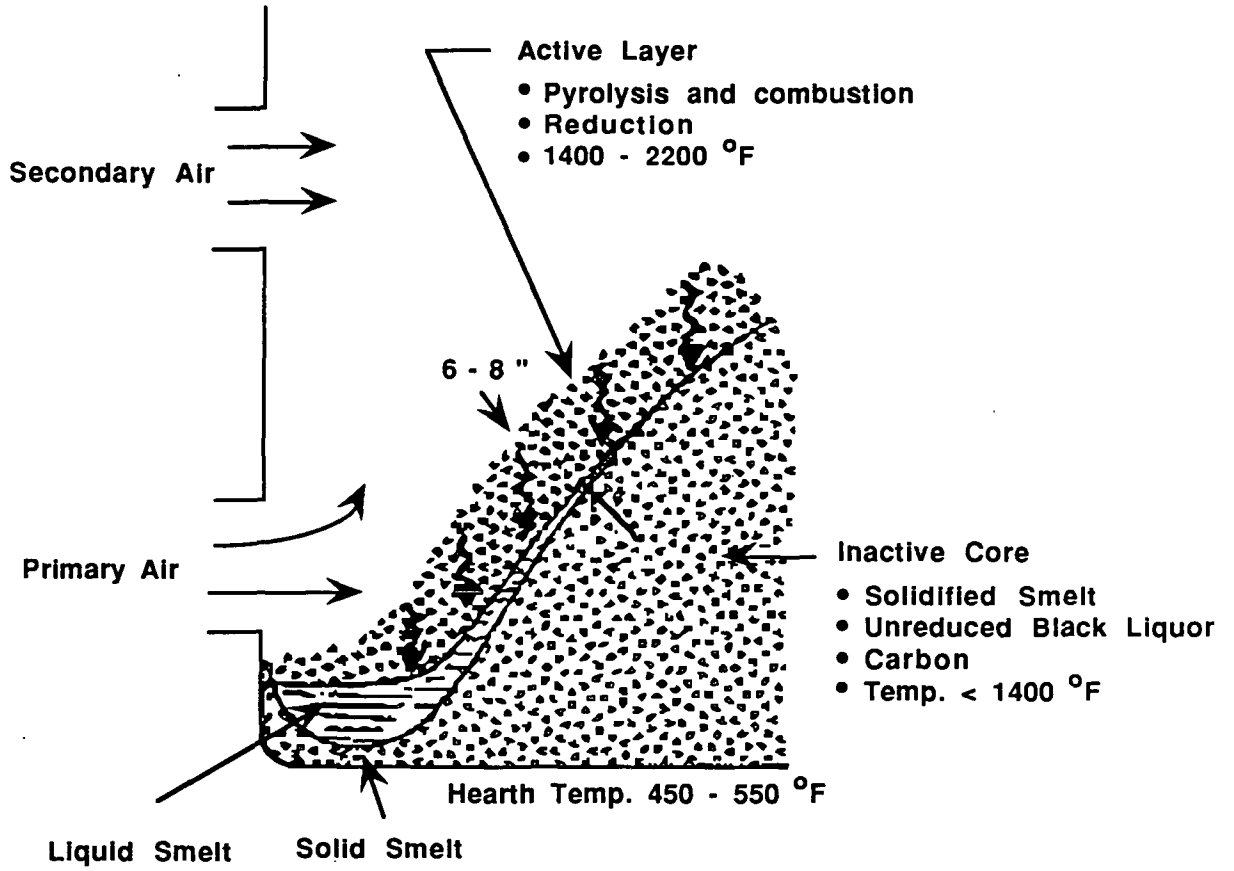

Figure 1. Details of a typical char bed -- B&W boiler.

The depth of the active region was determined by measuring the temperature profile of the bed by thrusting a thermocouple into the bed using a pole inserted through the air port. The zone becomes "inactive" when the measured temperature drops below the melting point of smelt. Several experimental difficulties make the "6 - 8 inch" conclusion only qualitative. Firstly, the path that the thermocouple takes through the bed influences the measurement. If the thermocouple goes through the active zone at an angle, its path will be longer than if it goes straight through. The method of inserting a pole through the air port may be awkward enough to make the path ambiguous. Secondly, air may be introduced to the subsurface when the probe is thrust into the bed. The resulting burning in proximity to the thermocouple would create

a high temperature which is not representative of the subsurface. These difficulties mean that six to eight inches inches is probably an upper limit to the depth of the active zone.

The state of the material reaching the bed depended on the spraying conditions. In the B&W furnaces, black liquor was sprayed in an oscillatory manner on the wall opposite the liquor guns. Some of the drops dried and burned in suspension, but many clung to the wall where they dried and eventually fell to the bed as large chunks of aggregated particles. The primary air tended to redistribute the lighter chunks that fell on the perimeter to other parts of the bed. The material on the hearth contained both frozen smelt and char. The char comes from conditions which existed during the buildup of the bed and the smelt comes from channels formed through the core. The smelt on the floor drains to the spouts.

B&W char beds have a large, porous, inactive core consisting of solidified smelt, unreduced black liquor solids, and carbon. Table 1 lists some of the properties of the inactive core:

Table 1. Properties of the inner core of a B&W char bed.

Temperature	< 1400°F
Conductivity	0.05 BTU/hr-ft-°F
Density	50 - 80 lb/ft^3
Porosity	30 - 40 %

The bed conductivity was measured using the temperature rise history of a sphere which was thrust into the bed. The data were widely scattered, and measured conductivity may be overestimated in some cases due to flowing smelt. A value of 0.55 BTU/hr-ft-°F was measured in one instance, but the conductivity of quiescent smelt is 0.26 BTU/hr-ft-°F . The discrepancy was

never resolved, and the ball probe method for obtaining thermal properties was not validated in a well characterized system. The porosity was estimated by comparing the bed density to smelt. The bed sampling technique may tend to collect more loose material than solidified smelt, perhaps making the density measurements on the low side of real bed densities.

Richardson and Merriam's char bed studies give a qualitative picture of char bed characteristics, but the conclusions are based on measurements affected by difficulties in sampling the furnace cavity. The conductivity measurements are affected by flowing smelt. The accuracy of composition measurements is influenced by sampling techniques. Although the sampler was purged with N_2 to quench oxidation, there is no guarantee that the sample was representative of the region from which it was taken. Surface material may be pushed ahead of the sampler as it is thrust into the bed. If this happens, the sample may contain some surface material and some material from the inactive core. The accuracy of density measurements is also limited by rough sampling methods. Despite these limitations, a qualitative picture of B&W char beds emerges: the beds are dense, have a low porosity, a low thermal conductivity on the same order of magnitude as a refractory material, and a thin active zone on the surface of the bed.

Measurement of the temperature profile in a typical B&W char bed showed that all of the temperatures at a distance greater than six inches into the bed are 1100 to 1300 °F, while the melting point of the smelt is approximately 1400 °F. These low temperatures are consistent with the conclusion that typical B&W char beds contained an inactive core and a thin active zone.

CE Char Beds

CE char beds discussed by Richardson and Merriam are not only different from B&W char beds, but they can vary substantially from one CE furnace to another depending on firing rate, black liquor temperature, and the quantity of primary air. Figure 2 depicts a typical case for CE char beds.

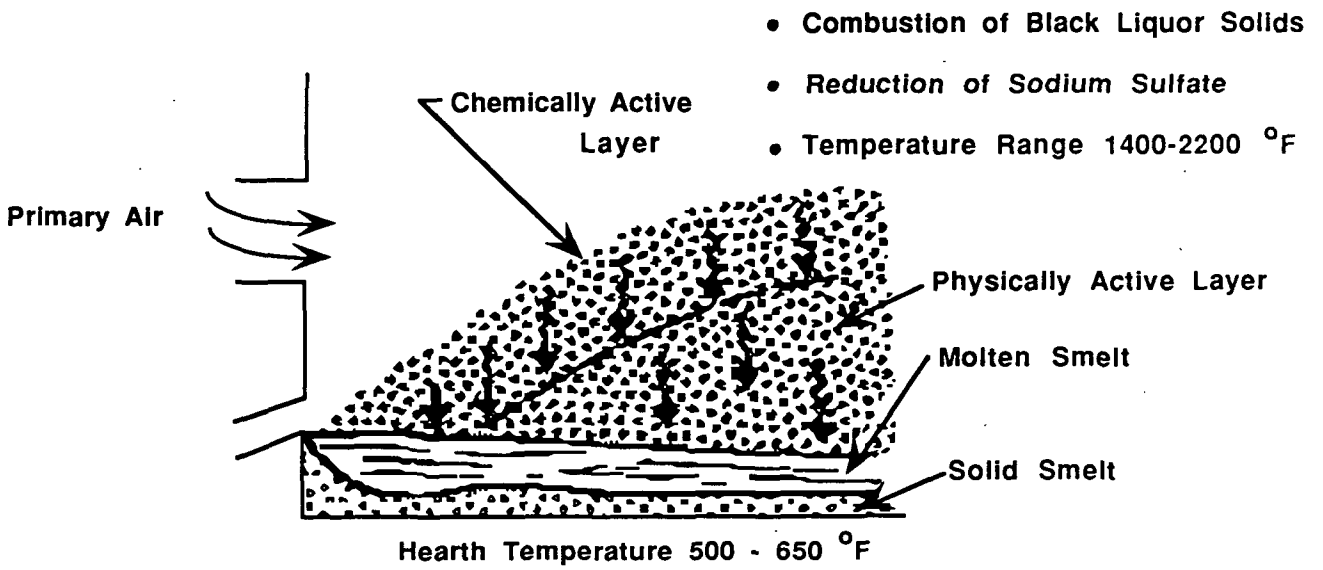

Figure 2. Details of a typical char bed -- CE boiler.

The maximum observed bed height was always relatively low. The bed may partially float on a layer of molten smelt except in the center of the bed where the weight may cause the molten smelt to be displaced.

Table 2 lists some of the properties of CE char beds. The temperature decreases with distance into the bed but usually stays above the melting point. Smelt is thought to move from the active zone by percolating through the bed to the smelt pool. The smelt is able to travel through the core because the temperature is above the melting point of smelt throughout the porous core.

The higher porosity permits radiative heat transfer at high temperatures within the pores to keep the temperature above the melting point -- making it possible for smelt to flow through the bed. CE char beds do not have the same inactive core that B&W beds have; however, the structure of the active region of a B&W char bed is similar to that of a CE char bed.

Table 2. Properties of CE char beds.

Temperature	1400 - 2200 °F
Conductivity	0.16 - 0.22 BTU/hr-ft-°F
Density	18 lb/ft^3
Porosity	87 %

The hearth usually has a 3 - 6 inch layer of frozen smelt. The molten smelt lies on top of the solid layer with the char bed floating on top of the smelt pool. The tube temperatures on the hearth range between 500 and 650 °F depending on the operating pressure of the boiler.

The results from four different tests on a CE char bed showed variable temperature profiles caused by changing conditions, location on the bed, and measurement technique. The temperature reaches a maximum in the combustion zone and then declines with depth into the bed. The temperature usually stays above the melting point of smelt although there are exceptions.

A summary of Richardson and Merriam's thermal property data is listed in Table 3:

Table 3. Thermal properties of char beds [2].

	Smelt		Char Bed	
	Liquid	Solid	Inactive	Active
Density, lb/ft^3	120	132	30-80	18-30
Specific heat, BTU/lb-°F	0.32	0.34	0.3	0.3
Thermal conductivity, BTU/hr-ft-°F	0.26	0.48	0.05	0.16-0.22
Thermal diffusivity, ft^2/hr	0.007	0.011	0.002-0.006	0.02-0.04
Latent heat, BTU/lb	61			

Note that the low char bed density compared to the smelt density indicates a porous bed. The porosity permits radiation to contribute to heat transfer at high temperatures. The loose, porous structure is a good insulator at lower temperatures, but heat transfer is enhanced at higher temperatures due to radiative heat transfer within the pores, making the apparent thermal conductivity higher at high temperatures.

The char bed data in Table 3 are approximate values which can vary substantially depending on conditions. For example, the conductivity was measured as low as 0.045 BTU/hr-ft-°F in the inactive core of a B&W bed, but a value of 0.16 was obtained in a CE char bed sample at 1400°F -- at or slightly below the melting point of smelt. Thus, regions of similar temperature had different conductivities. A high radiative contribution in the more porous CE char bed is one possible explanation for the difference. Another possibility is that the probe was in better contact with liquid smelt than the solid inactive core of the B&W bed.

An empirical correlation for conductivity was presented by Richardson and Merriam which accounts for the radiation component of heat transfer[2]:

$$k = 0.05 + 4 \sigma \phi D_p T^3 \quad (1)$$

where

k = apparent thermal conductivity, BTU/hr-ft-°F

σ = Stefan-Boltzman constant

ϕ = bed porosity

D_p = average pore size

T = absolute temperature

An average pore size was not measured. The ϕD_p term is used to fit the form of the equation to the measured data. The radiation component, the second term in Equation (1), is an adjustment to the lower-temperature conductivity, 0.05 BTU/hr-ft-°F.

CHAR BED CHEMISTRY

Scope of Chemical Reactions

The finding that a thin, high-temperature zone exists on the surface of the char bed means that the combustion reactions will be limited to the bed surface region. The C/Na_2SO_4 reaction is endothermic, so it tends to be self-limiting; as smelt leaves the surface, the endothermic reaction becomes farther away from the source of heat needed to sustain the reaction. Cameron and Grace measured a high activation energy for the C/Na_2SO_4 rate[4]. They concluded that the combination of an endothermic reaction and strongly temperature-sensitive kinetics causes the reaction to become self-limiting. The extent of reaction is therefore determined by the initial amount of sensible

heat available in the reacting mass and the rate of heat transfer into the bed. As discussed earlier, the bed has a low conductivity, hindering the amount of heat that can be transferred from the surface into the bed.

Brown et al. found sharp bed-temperature gradients in an experimental char bed apparatus[5]. A 10 x 20 cm char bed with three imbedded thermocouples was raised into the path of a slot jet at a rate which kept the char surface level with the jet. A rapid temperature rise was measured as the surface of the char bed burned passed each thermocouple. The active region was between three and seven centimeters based on the known vertical speed of the bed and the measured temperature rise.

The discussion on the depth of the active region has so far been based on temperature measurement. The 15 - 20 cm zone reported by Richardson and Merriam and the 3 - 7 cm thickness measured by Brown represent thermally active regions which are not necessarily the same as the chemically active thickness for all reactions. Solid carbon reacts with liquid Na_2SO_4, but the other reactions occur between the gases above the bed and the char surface. Thus, the reactions which involve gases above the bed are limited by the extent to which gases can penetrate the char surface.

Experimental studies suggest that gases penetrate the char surface to a very limited extent. Aiken measured the products of char combustion in a char pile reactor[6]. A small amount of crushed char was contacted with an impinging, laminar jet. His main findings from the char pile studies are as follows:

1) CO is the principle product for all experimental conditions, with the molar $CO/(CO + CO_2)$ ratio ranging from 0.80 to 0.96;

2) the molar $CO/(CO + CO_2)$ ratio is not dependent on temperature, time, or supply gas oxygen concentration for the conditions studied;

3) gas-phase oxidation of CO is significant close to the char pile.

The morphology of Aiken's char surface after reaction and post-experiment char analyses indicate that the impinging jet did not penetrate the char surface more than a few millimeters. Smelt covered the char surface to varying degrees depending on the reactor temperature. The coverage ranged from a few small smelt beads at 1039 K to a large smelt bead in a burned-out pit at 1590 K. The post-experiment mass was separated into smelt, surface, and subsurface samples. Analysis of subsurface samples showed that little reaction occurred. Thus, an impinging jet was unable to penetrate a crushed char surface more than a few millimeters. Char particles on the char bed surface are coarser, so it may be possible to transport gases convectively between the larger spaces resulting from coarser particles.

Li studied the C/CO_2 reaction using a thermogravimetric technique[7]. In the process of determining a kinetic rate expression, he investigated the magnitude of the external, interparticle, and intraparticle mass transfer resistances. Li found that the inter-particle mass transfer resistance became important when the char layer was larger than a few millimeters. The increased gasification rate at higher temperatures in the char bed will lead to even stronger mass transfer limitations. Thus, the penetration of gas species into the char bed will be confined to a thin layer at the top of the bed. Li used char passed through a 500 mesh screen; char particles on the bed will be larger, but the conclusion that gas species will not penetrate the bed deeply still applies.

The previous discussion suggests that the char bed combustion reactions can be adequately modeled by considering a thin zone on the char bed surface. The exact depth of this reaction zone is unclear. Aiken used crushed char, and a depth on the order of a few millimeters can be inferred

from his results. This depth would not be representative of the coarser morphology expected on a char bed. The depth based on temperature measurement can give an upper limit to the reactive zone, but it is not representative of the depth to which gases can penetrate the surface. The depth of the reactive zone is not likely to be more than a few centimeters, but the exact depth will depend on the local morphology. If char surface consists of packed particles, it may be expected that interparticle diffusion or convection could carry gases into the bed a few particle widths. If the surface is more molten and fused, less penetration would be expected. Lacking a way of predicting local surface morphology rigorously, physical arguments can be used to estimate the depth of the reactive zone. A depth of two centimeters is used later based on assuming that the gases can penetrate only to a few char particle widths.

Composition

Table 4 is a compilation of average char bed data from Richardson and Merriam[3]. An inerting sampler was used to minimize oxidation of the samples after they were taken. Some samples were taken of the material landing on the bed (fines) in addition to samples of bed material. These data indicate that most of the bed material is inorganic sodium salts -- mainly sodium carbonate (Na_2CO_3). Most of the sulfur is contained in inorganic compounds of various oxidation states. The carbon content is only about 5 to 8 % by weight. The carbon contents of the "fines" tended to be higher than those of bed samples, ranging up to 15 wt. %. The average oxidation state of sulfur compounds was higher in the "fines" than in bed samples. There was considerable variability in sulfur oxidation state from sample to sample. Most of the bed samples were

highly reduced, over 90 % reduction, although one sample had a reduction efficiency of 46%.

Table 4. Average values of sample analyses from three mills (wt. %).

	Bed	Smelt	Fines
Samples	14	4	7
Na_2CO_3	65.8 ± 11.9	68.2 ± 9.7	67.3 ± 12.8
Na_2S	11.0 ± 6.4	18.0 ± 3.9	5.0 ± 4.7
Na_2SO4	2.4 ± 2.1	3.1 ± 2.2	7.2 ± 1.9
$Na_2S_2O_3$	4.5 ± 3.1	0.2 ± 0.3	4.2 ± 3.0
Na_2SO_3	2.2 ± 3.3	0.1 ± 0.1	0.3 ± 0.3
NaOH	8.2 ± 2.1*	--	--
C	5.8 ± 3.2	0.2 ± 0.3	7.6 ± 4.7
S	7.0 ± 2.4	7.4 ± 2.0	6.2 ± 3.1
Reduction, % ‡	84.4 ± 16.3	91.8 ± 4.2	54.2 ± 22.5

note: ± indicates standard deviation
* four samples
‡ Reduction efficiency is defined as the molar $Na_2S/(Na_2S + Na_2SO_4)$ ratio.

Grace et al. has also published data on char composition[8]. A simplified char composition was developed based on interpretation of several char analyses. The following assumptions were made to arrive at a simplified composition:

1. All sodium and sulfur are present as three inorganic compounds: carbonate, sulfate, and sulfide;

2. The relative amounts of sulfate and sulfide define the average oxidation state of the sulfur;

3. Hydrogen present as condensed aromatics is treated as "bound" hydrogen;

4. Carbon not present as sodium carbonate is treated as solid carbon;

5. All oxygen is accounted for by the inorganics;

6. The S/Na_2 ratio is 1 to 3 and the initial state of reduction is equivalent to 50% reduction efficiency ($Na_2S/(Na_2S + Na_2SO_4)$);

7. The relative amounts of carbon, hydrogen, and alkali are close to those found in the actual char samples.

These assumptions lead to the char composition shown in Table 5 before burning. The expected composition after burning is also shown in Table 5. The assumed char components in this thesis will be Na_2S, Na_2SO_4, Na_2CO_3 , and carbon.

Table 5. Simplified char composition before and after char burning.

	Before		After	
	mole/mole Na_2	wt. %	mole/mole Na_2	wt. %
Na_2S	1/6	9.0	19/60	25.0
Na_2SO_4	1/6	16.4	1/60	2.4
Na_2CO_3	2/3	49.0	2/3	71.6
C	3	24.9	1/12	1.0
H	1	0.7	0	0

Chemical Reactions

The previous discussion gives some idea of the chemical and morphological characteristics of char and char beds. This section discusses important combustion reactions occurring during char burning, which may or

may not take place on the char bed.

The simultaneous oxidation of char carbon and reduction of Na_2SO_4 is described by the sulfate/sulfide cycle theory of char burning. The sulfate/sulfide cycle was first identified in molten sodium carbonate melts by Gehri and Oldenkamp [9] and later applied to kraft char burning by Grace et al.[10] The cycle is depicted in Fig. 3. Oxygen reacts with sodium sulfide (Na_2S) to produce sodium sulfate (Na_2SO_4) which in turn reacts with carbon to produce a mixture of carbon monoxide (CO) and carbon dioxide (CO_2); sodium sulfide is regenerated in the reaction between carbon and sodium sulfate. In the sulfate/sulfide cycle, the only pathway for carbon consumption is the C/Na_2SO_4 reaction, and the only source of oxygen for the Na_2S/O_2 reaction is oxygen from the combustion air. The relative amounts of sulfide and sulfate depend on the relative rates of the Na_2S/O_2 and C/Na_2SO_4 reactions. Sulfide predominates over sulfate while carbon is burned if the rate-limiting step is the Na_2S/O_2 reaction or oxygen mass transfer; it is therefore possible to have sulfide be the dominant sulfur species as char carbon is burned in air.

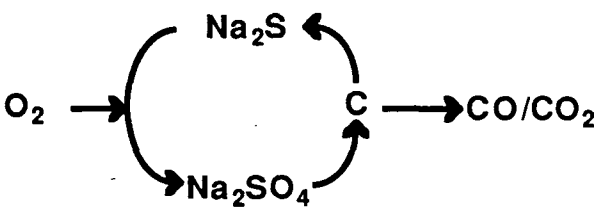

Figure 3. Sulfate - Sulfide Cycle.

Rate expressions have been developed for the C/Na_2SO_4 reaction in a molten carbonate melt for different types of carbon. A smelt pool reactor was used by Grace et al.[8] which consists of a crucible heated to a set temperature by an induction furnace. Small quantities of char are placed in a smelt, and the

sulfate/sulfide cycle is active when an oxygen-containing gas is bubbled through the smelt. The system relies on the bubbling action for mixing the char/smelt mixture. The sulfide oxidation was found to be a very fast, mass-transfer-controlled reaction in this system. The rate expression for the C/Na_2SO_4 reaction takes the following form:

$$R_{CS} = -k_1 \left\{ \frac{[SO_4]}{k_2 + [SO_4]} \right\} [C]\, e^{\frac{-E}{RT}} = -k_1 \left\{ \frac{(1-r)\,s}{k_2 + (1-r)\,s} \right\} [C]\, e^{\frac{-E}{RT}} \qquad (2)$$

where

$[SO_4]$ = sulfate concentration, mole sulfate/mole Na_2
$[C]$ = carbon concentration, mole C/mole Na_2
k_1, k_2 = rate constants
E = activation energy
R = gas constant
T = absolute temperature
r = reduction efficiency, $(Na_2S/(Na_2S + Na_2SO_4))$
s = sulfidity, mole S/ mole Na_2

Table 6 contains the rate constants for different types of carbon in batch experiments with great excess of molten salt.

Table 6. Rate parameters for the carbon-sulfate equation of Grace et al.

Carbon type	k_1, sec^{-1}	k_2, $\frac{\text{mole } SO_4}{\text{mole } Na_2}$	E, $\frac{cal}{mole}$
Kraft char	$1.31 \pm 0.41 \times 10^3$	0.0011 ± 0.0004	$29{,}200 \pm 1{,}000$
Pulverized graphite	$4.94 \pm 0.82 \times 10^4$	0.0013 ± 0.0003	$44{,}000 \pm 1{,}200$
Soda char	$3.04 \pm 0.73 \times 10^5$	0.0020 ± 0.0006	$39{,}850 \pm 1{,}500$

The C/Na_2SO_4 reaction was also studied by Thorman and Macur using activated carbon[11]. They also used a molten-salt reactor, but mixing was performed using a turbine blade agitator rather than relying on the mixing action of the bubbles. The turbine allowed them to investigate higher carbon

loadings than Grace et al. could. Thorman and Macur's rate expression takes the following form:

$$-\frac{d[SO_4]}{dt} = A[C]^n e^{\frac{-E}{RT}} \qquad (3)$$

where

$A = 1.67 \pm 0.15 \times 10^8$ $g^{0.69}$ min^{-1} 100 g $solution^{-0.69}$

E = activation energy = $2.04 \pm 0.15 \times 10^5$ J/gmole

n = reaction order = 0.31 ± 0.02

Thorman and Macur investigated the reaction in the temperature range of 1200 - 1300 K and carbon concentrations in the range of 1 - 3.6 mole C/mole Na_2. The data of Grace et al. were obtained at temperatures between 1060 - 1230 K and carbon concentrations on the order of 0.02 mole C/mole Na_2.

The rates are compared in Table 7 at various conditions. The rate of Grace et al. for kraft char is predicted to be substantially greater than Thorman and Macur's (T&M) rate using activated carbon. On the other hand, Grace et al.'s rate for pulverized graphite is much closer to the T&M rate using activated carbon. The difference in rates between kraft char and T&M activated carbon may possibly be explained by the difference between the structures of activated carbon and char. The expression of Grace et al. for kraft char is most applicable to this thesis since the source of carbon used for the rate expression was kraft char.

Table 7. Relative rate for the carbon/sulfate reaction.

T K	[C] $\frac{\text{mole C}}{\text{mole } Na_2}$	$\frac{\text{Grace et al. kraft rate}}{\text{T\&M rate}}$	$\frac{\text{Grace et al. graphite rate}}{\text{T\&M rate}}$
1200	0.03	10	0.73
1200	0.3	46	3.5
1200	3	190	14
1600	0.03	1	0.45
1600	0.3	6	2.2
1600	3	25	8.9

An appropriate rate equation for the carbon/oxygen reaction must be chosen. There are weight loss data for combustion of soda char particles, but a rate equation has not been developed. Note that soda char data are used rather than kraft char to avoid the contribution of the sulfate/sulfide cycle to the rate. It is possible, however, to borrow the mathematical form of the rate equation from the coal literature, and match the soda char rate to the coal char rate. The coal literature has data for coal of varying reactivities. A rate expression from the coal literature was chosen to match the observed rate of the carbon/oxygen reaction in soda char. The selection of an appropriate rate expression is discussed further in Appendix I.

The C/CO_2 reaction was studied by Li [13] at high carbon concentration and by Goerg [14] at very low carbon concentration. Li's data span the range of 1.2 - 5.8 mole C/mole Na_2 while Goerg's data span the range of 0.015 - 0.062 mole C/mole Na_2 . Li's data were taken in the temperature range of 973 - 1048 K to avoid mass-transfer interferences such as inter- and intra- particle diffusion. Goerg's data were taken in the range of 1200 - 1283 K. Thus, Li's equation must be extrapolated to higher temperature while Goerg's equation must be extrapolated to higher carbon content to match the conditions found during char burning in the recovery furnace. Their rate expressions take the

following form:

$$R_{CO_2} = \frac{-k_1 P_{CO_2}[C]}{1 + k_2 P_{CO_2} + k_3 P_{CO}} e^{\frac{-E}{RT}} \quad (4)$$

The values of the constants are found in Table 8. Li's original equation had to be converted to the form found in Equation (4) (See Appendix II).

Table 8. Values for C/CO_2 rate equation.

Parameter	Goerg	Li
k_1	1.043×10^8 (atm-sec)$^{-1}$	9.53×10^7 (atm-sec)$^{-1}$
k_2	28.99 atm^{-1}	10.8 atm^{-1}
k_3	45.6 atm^{-1}	6.3 atm^{-1}
E	227,300 J/mole	187,000 J/mole

The inhibitory effect of CO and CO_2 is stronger in Goerg's data than Li's. This may be partly due to the different temperatures at which the experiments were performed. The different activation energies have the biggest effect on the calculated rate. Goerg's activation energy is 21% greater than Li's, which causes Li's exponential term to be 40 times greater at 1300 K.

The rate equations were developed under very different conditions, but the rates can be put on a common basis for comparison. A temperature of 1300 K, partial pressures of 0.2 for both CO and CO_2, and a carbon concentration of 3 mole C/mole Na_2 were assumed. Goerg's equation predicts a rate of 0.00289 mole C/mole Na_2 - sec at the specified conditions. Li's equation predicts a rate of 0.124 sec^{-1}. Li's rate was obtained (shortly after CO_2 is introduced into the initially-inert gas) by dividing the maximum weight loss rate by the difference between the initial weight and the final weight. A rate of 0.124 sec^{-1} is converted to Goerg's units by multiplying by the carbon concentration. The rate is [3] x 0.124 sec^{-1} or 0.372 mole C/mole Na_2 - sec. Li's reaction rate is 129 times greater than Goerg's at the specified conditions. For comparison, the C/Na_2SO_4 reaction at 1300 K with CO as the product and

[C] = 3 mole C/mole Na_2 is 0.194 mole C/mole Na_2 - sec. Thus, Li's rate equation predicts a rate for the C/CO_2 reaction which is similar to that of the sulfate/sulfide cycle.

The coal literature provides some insight into the relative importance of different pathways for carbon consumption. The following passage is found in Smoot[12]:

> "The rates of carbon oxidation by steam and carbon dioxide are of the same order of magnitude, and are generally much lower than the reaction of carbon with oxygen, while the hydrogenation reaction (i.e. H_2 + char) is several orders of magnitude slower than the steam-char and CO_2-char reactions. For example, Walker et al. (1959) estimated the relative rates of the reactions at 1073 K and 10 kPa pressure as being 3 x 10^{-3} H_2, 1 for CO_2, 3 for H_2O, and 10^5 for O_2. At higher temperatures, the differences in rates will not be so extreme, but rates for H_2, CO_2, and H_2O will still remain relatively unimportant as long as comparable concentrations of oxygen are present."

Then later:

> "In coal gasifiers, however, the reactions with steam and CO_2 can be quite important especially after rapid depletion of oxygen."

The gasification reactions are relatively unimportant in common coal combustion systems, but the C/CO_2 and C/H_2O reactions would be expected to play a larger role in kraft recovery boilers for two reasons. Firstly, kraft char contains a much higher alkali salt content than coal char; alkali salts are known to catalyze carbon gasification reactions[13], making the gasification reactions significant in kraft char at a lower temperature than they would be in coal char.

Secondly, parts of the lower recovery furnace are expected to be oxygen deficient, so less oxygen is available to react with the char bed surface. The atmosphere may be similar to a coal gasifier.

Different mechanisms may be operating in the different regimes in which Li's and Goerg's experiments were performed. The task is to determine which regime is most applicable to bed burning. There are certainly molten regions in the char bed, but the surface area of the bed would also have char particles in various stages of combustion. Thus, important reactions in each environment must be modeled. Li's data indicate that the C/CO_2 reaction is important for direct gas/solid contact while Goerg's data demonstrate the insignificance of the reaction in molten regions.

Li's measured rate is twenty times higher than the rate for coal char mixed with sodium carbonate. The thermogravimetric technique Li used makes rates appear higher than they actually are since all weight loss is attributed to the C/CO_2 reaction. In the thermogravimetric technique, the gas contacts the char which is suspended from a microbalance. The CO_2 is introduced into the inert gas stream after the reactor is ramped to 750 $^{\circ}$C over a 30 minute period. The reaction rate is measured by taking the slope of the weight loss curve shortly after CO_2 is injected. Pyrolysis is assumed to be complete by the time CO_2 is injected, and Li showed that CO or CO_2 suppressed weight loss due to sodium emission.

The thermogravimetric method, however, exaggerates the measured rate since any residual pyrolysis or sodium emission would be occurring simultaneously. The slope of the weight loss curve before CO_2 is introduced is about 1/3 the slope after CO_2 is introduced. It is possible that volatilization of organics or sodium is superimposed on the C/CO_2 rate. If this is the case, the measured rate would be in error by as much as 50%. Measurements on a single

particle reactor found that most pyrolysis stops at 600 ° C[15]. Aiken found that a pyrolysis time of 950 ° C for ten minutes was necessary to completely pyrolyze the char[6]. Li pyrolyzed for thirty minutes, reaching a temperature of 750 °C at the end of the heating period. Most of the pyrolysis should be complete at 750 °C.

Li's elemental char composition has a higher carbon content than other chars. A lower heating rate results in a higher carbon content of the resulting char. A comparison of carbon contents for different chars is shown in Table 9.

Table 9. Comparison of char carbon contents.

Source	wt. % C	Yield %
IPC(soda)[8]	33.4	69
IPC(kraft)[8]	29.4	69
Weyerhauser[8]	27.5	64
Aiken[6]	23.4	--
Li[13]	38	66

Li's high carbon content is consistent with char that is produced by a slower heating rate.

The coal literature gives insight to black liquor char combustion since the same reactions are occurring. The coal literature indicates that the C/O_2 reaction is two to four orders of magnitude greater than the C/CO_2 reaction in the temperature range of 1200 - 1600 K[12]. The C/H_20 reaction is slightly greater than the C/CO_2 reaction. Alkali salts are known to catalyze combustion reactions so it is reasonable to assume that char burning rates may be faster than the coal burning rates for the same reaction. Li's rate is twenty times greater than the rate for the same conditions using coal char mixed with 10%

or 20% Na_2CO_3 . He explained the larger rate as being due to a large number of small catalytic sites in intimate with the carbon surface in black liquor char in contrast to the physical mixing of coal chars with the alkali salt. Kraft black liquor char is very reactive relative to coal char.

In summary, Li's rate expression predicts gasification rates which would make the C/CO_2 reaction a significant contributor to bed burning. The thermogravimetric technique Li used attributes all weight loss to the C/CO_2 reaction, but the error caused by continued volatilization of organic material or sodium emission would be at most 50%. Li and Goerg found that weight loss stopped after CO_2 or CO was introduced, and most of the pyrolysis would occur before the temperature reaches 750 °C. Thus, Li's rate expression predicts a C/CO_2 rate which is representative of kraft char.

An experiment performed on a single particle reactor provides an independent confirmation of Li's rate expression[16]. A char particle was contacted with CO_2 at 885 °C, and the CO in the gas stream was measured. The measured rate is very comparable to the rate predicted using Li's rate equation. Detailed calculations are shown in Appendix III. The rate predicted using Li's equation is 1.53×10^{-5} mole/s compared with a measured rate of 1.4×10^{-5} mole/s in the single particle reactor. These reaction rates are very comparable and are certainly within the range of possible error introduced in making the assumptions for the calculations. The point of this comparison is to demonstrate that Li's rate equation is quite comparable to data obtained on a different system. Li's rate equation is independently confirmed although with only one experiment. The use of Li's rate expression in the char bed model is therefore reasonable.

The C/CO_2 reaction will be an important reaction on the char bed. The

C/H_2O reaction should also be important since these two reactions are on the same order of magnitude for coal. Concerns about experimental techniques which result in a high kinetic rate expression are decreased when the mass transfer resistance is taken into account. Mass transfer controls the rate at higher temperatures, eliminating the contribution of the kinetic rate expression to the gasification rate. The result of using an unrealistically high kinetic rate expression is a decrease in the temperature at which mass transfer resistance becomes dominant. The error in burning rate caused by using a kinetic expression which overestimates the gasification rate will diminish at higher temperatures where mass transfer becomes the limiting factor.

Grace et al. discussed other potential reactions during char burning[8]. The reduction of sodium sulfate by either CO or H_2 is insignificant. The formation rate of Na_2S by adsorption of H_2S or thiosulfate decomposition is insignificant when compared to the rate of sulfide formation from the C/Na_2SO_4 reaction. Direct oxidation of char carbon in smelt is a relatively slow reaction.

PREVIOUS CHAR BED MODELS

Purdue Model

Williams and Galtung constructed a furnace model used to design a control system to operate the recovery boiler.[17] The approach was to develop a mathematical model based on physical principles and then adjust it to available operating data. The entire recovery furnace was modeled with emphasis on dynamics and control. Equations were based on material and energy balances and were supplemented heavily by empirical functions where exact models could not be formulated.

The bed portion of the model was simplistic and empirical. Some of the assumptions made include:

1. water evaporates instantaneously on the bed

2. no Na or sulfur emission

3. the bed consists of one homogeneous reaction zone

4. the carbon reaction rate is proportional to the mass fraction of carbon and an exponential temperature term

5. reduction efficiency is determined by an equilibrium calculation

6. constant bed density

Water does not evaporate instantaneously, and the char bed will be a significant contributor to fuming. The bed is certainly not homogeneous; conditions near the primary air ports will be very different from those near the center of the furnace. The coefficients for the carbon reaction rate were chosen empirically to get the bed dynamics to respond to changes in the black liquor changes; the reaction rate is not based on fundamental process chemistry. The reduction efficiency is based on a model which uses the excess or deficiency of oxygen; however, as discussed in the literature review, the reduction efficiency is determined by the balance between the sulfide oxidation rate and the sulfate reduction rate. Sulfide oxidation is generally mass transfer controlled and sulfate reduction is kinetically limited: neither reaction involves equilibrium considerations. The bed processes in the Purdue model are based primarily on empiricism rather than fundamental processes. In summary, almost no useful information on char beds can be obtained from the Purdue model.

ADL Model

Merriam developed a computer model which dealt with the chemical, mass transfer, and energy processes in the lower furnace.[18] The so-called "Arthur D. Little" model is a one-dimensional zonal model of the recovery boiler which takes the furnace dimensions into account for the radiation calculations. The furnace is divided into seven zones; three of these zones make up the char bed as shown in Fig. 4.

Zone one is the inactive region of the char bed. No chemical reactions occur, and heat is transferred by radiation and conduction. The correlation for apparent conductivity developed by Richardson and Merriam was used for heat transfer calculations.

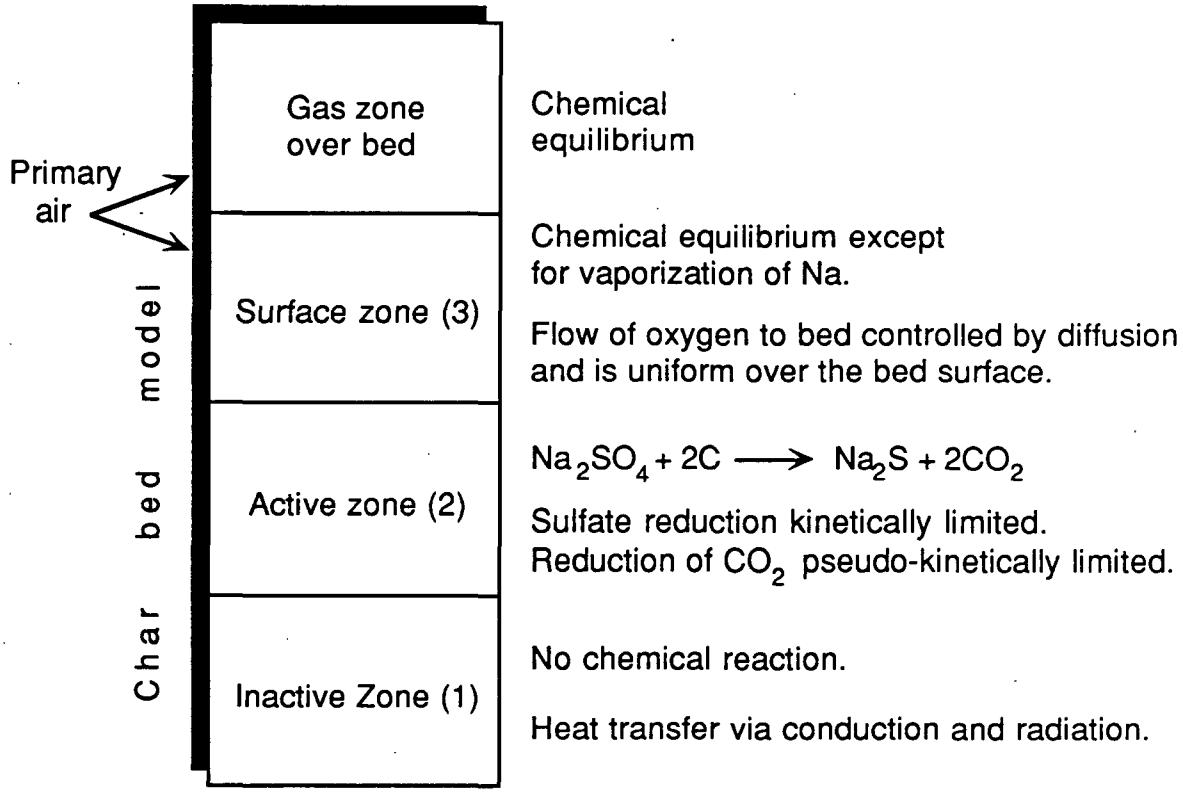

Figure 4. Overview of char bed portion of ADL model.

Zone two is the active region of the char bed. Oxidized sulfur salts in the smelt are reduced, the endothermic reactions being driven by sensible heat from the smelt and conduction and radiation through the porous char. The reduction of sodium sulfate is described by a kinetic rate expression developed by Zhitkov[19]; CO_2 is assumed to be the primary gas product. The reduction reactions assumed to occur are as follows:

$$Na_2SO_4 + 2C \rightarrow Na_2S + 2CO_2 \quad (5)$$

$$Na_2SO_3 + 2C \rightarrow Na_2S + CO + 2CO_2 \quad (6)$$

$$Na_2S_2O_3 + Na_2CO_3 + 2C \rightarrow 2Na_2S + 3CO_2 \quad (7)$$

The kinetic description for sulfate reduction was arbitrarily assumed to apply to the other two reactions. There is no theoretical or experimental basis given to justify this assumption. The final reduction efficiency is determined by the kinetic rate for the sulfate/carbon reaction and the residence time in the active zone:

$$\text{Reduction efficiency} = 1 - e^{-k_f \tau} \quad (8)$$

where

$k_f = 8.28 \times 10^9\ hr^{-1}\ e^{-\frac{E_a}{RT}}$
R = universal gas constant
T = absolute temperature of zone 2
E_a = activation energy = 47.4 kcal/gmole
τ = residence time of smelt in zone 2 = $\Delta z/u$
Δz = zone 2 thickness
u = local velocity

The velocity of the smelt through the porous char is assumed to follow Darcy's law for flow through a porous medium:

$$\left(\frac{\mu}{\kappa}\right) u = \rho g \quad (9)$$

where

u = local velocity
g = gravitational constant
κ = permeability of medium
μ = dynamic viscosity

The viscosity of the smelt was based on data for carbonate/sulfide mixtures. The permeability of the bed was estimated using physical reasoning. As the smelt flows deeper into the bed, its temperature decreases due to the endothermic reactions, with a subsequent decrease in smelt velocity. As the velocity decreases the fraction of the bed saturated by smelt is assumed to increase. Based on an assumed bed porosity, smelt temperature, saturation factor, residence time, and smelt composition, the permeability is 4×10^{-10} ft^2.

The C/CO_2 reaction can also occur in the active zone. The gas leaving the bed is thus a combination of CO and CO_2. The relative amounts of each gas are established by equilibrium relationships and an arbitrary parameter which specifies the percentage achievement of equilibrium. CO would be the dominant product under equilibrium conditions; but the developers of the model recognized that the gases leaving the bed are not in equilibrium, so a "percent completion factor" was introduced as follows:

$$(CO)_f = (CO)_i + \left(\frac{PCF}{100}\right)(\Delta CO)_{equil.} \qquad (10)$$

where

$(CO)_f$ = net CO gas leaving zone 2

$(CO)_i$ = CO gas entering subzone form subzone below it

(ΔCO) = change in CO gas predicted by reduction of CO_2 under chemical equilibrium excluding the CO formed directly from the reduction of sodium sulfite

PCF = "percent completion factor"

Zone three is the bed surface. Transfer of primary air from the gas to the bed occurs in this region, and the gas phase is treated as an equilibrium zone. The flux of oxygen to the bed is calculated as follows:

$$N_{O2} = \left(\frac{c\,D}{\delta}\right) X_{O2,\infty} \qquad (11)$$

where

N_{O2} = oxygen flux
c = molar gas concentration
D = diffusivity
δ = film thickness
$X_{O2,\infty}$

The model adjusts the oxygen diffusion film thickness to account for the increased velocity of the combustion air in the vicinity of the bed. The film thickness is assumed to vary as the -0.8 power of the air input:

$$\delta = \frac{\text{const}}{(M_p)^{0.8}} \qquad (12)$$

where

M_p = primary air input

The evolution of elemental sodium is modeled assuming the following reaction:

$$Na_2CO_3 + CO \Leftrightarrow 2Na(g) + 2CO_2 \qquad (13)$$

The decomposition of sodium carbonate and subsequent evolution of elemental sodium is assumed to be pseudo-kinetically limited, similar to the CO_2/C reaction in zone 2. The sodium generated by the bed is:

$$Na = f\,(Na)_{equil.} \qquad (14)$$

where

f = fractional approach to equilibrium
Na = calculated sodium gas leaving the char bed
$(Na)_{equil.}$ = sodium gas leaving the bed if the above reaction goes to equilibrium

The ADL model correctly identifies fundamental processes occurring on the bed such as fuming, the self-limiting behavior of the sulfate reaction, oxygen diffusion to the char surface, and the CO_2/C reaction; however, the model tends to over-rely on arbitrary parameters which are chosen to obtain an answer which matches real experience. Terms like "pseudo-kinetic" and "percent completion factor" recognize that some reactions do not reach equilibrium, but fail to treat the process properly. The gasification reaction is arbitrarily stopped at some point which gives a reasonable split of carbon monoxide and carbon dioxide leaving the bed. The problem with this type of approach is that the appearance of a fundamental treatment is given without substance. Computational effort could have been saved if the split was a user-defined parameter. The treatment of sodium evolution suffers the same flaws with its pseudo-kinetic factor f specifying how close Na evolution is allowed to approach equilibrium. This method can give erroneous results when strongly endothermic reactions are involved.

The description of oxygen transfer to the bed is limited by the one-dimensionality of the model, and there is an undesirable degree of arbitrariness. The film thickness is calculated based on analogy between heat and mass transfer. A typical convective heat transfer coefficient of 10 BTU/hr-ft^2-°F gives a film thickness of 1.0 mm, and it is assumed to vary as the -0.8 power. The -0.8 power applies to turbulent boundary layers, which is probably a reasonable assumption. The one-dimensionality of the model, however, prevents the description of the three-dimensional distribution of gas concentration, velocity, and temperature which occurs around a real bed.

Using Darcy's law to model smelt flow is ultimately arbitrary and misleading. Firstly, Darcy's law applies to simple systems where the liquid saturates the porous medium. The ADL model recognizes that the bed is not entirely saturated since it calculates a saturation factor. The flow of smelt is much more likely to be a trickling or runoff process rather than a process of smelt "filtering" through a porous medium. Secondly, parameters such as permeability are extremely difficult to characterize and would certainly not be isotropic as assumed. Darcy's law applies to single-phase flow through a porous medium, but smelt flow through a char bed is three-phase flow through a poorly characterized porous medium with simultaneous heat transfer, phase change, and chemical reaction between the fluid and medium. The Darcy's law treatment of smelt flow through the char bed can be reduced to the following scenario: choose a permeability which gives a velocity which gives a residence time which gives a reduction efficiency that appears reasonable. Thus, the Darcy's law description is incorrect and subject to selecting parameters which give reasonable answers.

In summary, several aspects of the ADL treatment of the char bed are inadequate. Equilibrium is a limiting condition, and the factor which specifies the percentage completion of equilibrium is an incorrect way of simulating the actual reactions. The "pseudo-kinetic" treatment of fuming is similarly flawed. The thickness of the active zone is arbitrarily specified and the flow of the smelt through the active zone is based on many empirical and some incorrect assumptions; the residence time and therefore the reduction efficiency is arbitrary. The ADL model cannot predict the combustion rate or reduction efficiency based on fundamental processes, and does not take into account the three-dimensional distribution of conditions around the char bed.

GEMS Model

Shiang has written a recovery boiler model using the GEMS program[20,21]. GEMS is a modular, steady-state simulation program designed for mill simulations. Shiang constructed a series of GEMS modules which simulate processes occurring in different parts of the furnace. The modular, steady-state, one-dimensional model predicts the temperature distribution and pressure drops throughout the furnace and heat transfer sections for both simulation and design calculations. The effect of gas recirculation, wall emissivity, and dust deposits on the tubes were included, but the chemical processes occurring on the char bed were handled superficially.

The char bed behavior is simulated by a one-dimensional heat transfer model with chemical reaction. The GEMS combustion module COMB calculates the surface combustion of black liquor solids based on equilibrium calculations. The char bed model is comprised of two GEMS modules, CBED and HSMEL[22]. CBED calculates the reduction efficiency and carbon in the smelt while HSMEL simulates the removal of heat from the smelt by the floor tubes and the wall tubes surrounding the smelt. The treatment of smelt flow and sulfate reduction is similar to that in the ADL model. The following assumptions are made:

1) the flow of smelt through the char bed follows Darcy's law;

2) the conductive heat transfer term can be neglected due to order-of-magnitude analysis;

3) the rate of sodium sulfate reduction in the bed follows the kinetic model of Zhitkov[19].

The two differential equations resulting from the mass and energy balance are solved using a fourth-order Runge-Kutta method:

$$\frac{dX_S}{dZ} = \frac{k_0 \exp\left(\frac{-E}{RT}\right) * (1 - X_s)}{U} \quad (15)$$

$$\frac{dT}{dZ} = \frac{-\Delta H_r * k_0 \exp\left(\frac{-E}{RT}\right) * W_S * (1 - X_s)}{C_p * U} \quad (16)$$

where

ΔH_r = heat of reaction which depends on a user-specified CO fraction
X_S = sulfate conversion
Z = distance beneath the char bed surface
U = smelt velocity
W_S = weight fraction of sulfate initially in smelt

The surface temperature of the char bed, the depth of the active zone, the unburned carbon reaching the bed, and the fraction of the carbon gases that is carbon monoxide are arbitrarily specified. The reduction efficiency is calculated using a method which is similar to the ADL model. The reduction efficiency is based on a kinetic expression and the residence time in the active zone. The temperature profile in the active zone is calculated, and the reactions are stopped if the temperature drops below the melting point of smelt.

The GEMS char bed model is necessarily brief since calculations must be simple enough avoid slowing full-mill simulations. It has the flavor of a stripped-down version of the ADL model. Many parameters need to be specified, making the calculations arbitrarily result in numbers which are close to reality. The same limitations of the Darcy's law treatment discussed earlier also apply to Shiang's model.

The review of the Purdue, ADL, and GEMS models reveals a lack of an adequate char bed model. The Purdue model is almost entirely empirical, and

the ADL and GEMS models rely too much on arbitrary parameters which are chosen to give results close to what is found in real experience. The complexity of char bed processes requires some arbitrariness in choosing parameters, but the confidence in model predictions is eroded when the model itself does not describe the actual processes occurring. The models all are one dimensional and do not account for the variation of oxygen concentration, temperature, and gas velocity across the surface of the char bed. None of the models calculate a bed burning rate, and the calculation of reduction efficiency can be improved.

OBJECTIVES

The first objective of this thesis is to develop a mathematical model of the kraft char bed that is a component of a three-dimensional recovery furnace. The model will have the following characteristics:

1) the bed model interfaces with the recovery furnace model called FLUENT/RFM;

2) all significant combustion reactions are modeled with the best available information;

3) it is flexible enough to incorporate new data as it becomes available;

4) an arbitrary bed shape can be specified;

5) the three-dimensional distribution of temperature, velocity, and gas concentration is handled;

6) the bed combustion rate and reduction efficiency are calculated;

7) the reactions occur in a thin zone on the bed surface.

The second objective is to examine issues related to interfacing a char bed model with the above-bed model of the recovery furnace. The overall model uses a computational fluid dynamics program called FLUENT/RFM to perform gas phase and particle calculations, so the bed model must necessarily use the methodology of FLUENT/RFM. Choosing to develop a bed model in the context of a FLUENT-based model restricts the form that the bed model can take. Issues such as interfacing between the bed and gas phase, gas-phase mixing above the bed, and bed dynamics will be examined.

The third objective is to use the model to gain understanding of the beds impact in recovery boiler operation. The relative contribution of reactions to bed burning and the influence of bed shape will be examined.

CHAR BED MODEL

SCOPE

The char bed model will be developed by considering only a thin region on the surface of the bed. There are two reasons for this treatment. One reason is related to the overall model. The bed is a boundary in the recovery furnace model for the purposes of the gas phase and particle calculations. A bed surface model which interacts with the gas phase and particles is most appropriate in this context. A subsurface model may be computationally expensive and consume computer time out of proportion to the usefulness of the information gained.

A second and more important reason for adopting a surface combustion approach is that the important combustion reactions on the char bed occur within a short distance from the surface of the bed. Evidence was presented in the literature review which showed that large temperature gradients exist near the bed surface. The temperature decreases rapidly as the distance into the bed increases. The endothermic subsurface reactions become self-limiting since the source of heat needed to sustain the reaction, the hot surface, becomes farther away. The literature review also discussed the importance of resistance to mass transfer into the bed. The gases which react with char will not penetrate below the bed surface more than several centimeters. Thus, treating the bed as a surface reaction zone will result in a bed model that includes the important combustion phenomena occurring on the char bed.

The bed surface interacts with the above-bed model in several ways. External mass transfer and chemical kinetic rates are modeled for each reaction. Oxygen, carbon dioxide, and water vapor in the gas phase above the bed are allowed to react with the char bed surface. The local velocity and

temperature are used to calculate a local mass transfer coefficient. The local mass transfer coefficient and kinetic rate are combined as "resistances" to determine the local reaction rate. An energy balance is performed over the char surface to calculate a surface temperature. The details of the interactions between the bed and above-bed models will be discussed in the following sections.

Char is assumed to be comprised of char carbon, sodium carbonate, sodium sulfate, and sodium sulfide. The bed receives a flux of particles in various stages of the combustion process. Sodium sulfate in burned-out particles can be a source of oxygen to the bed. Parts of the bed may grow or shrink depending on the local balance between incoming particles and the combustion rate on the bed. The char carbon reacts through reactions which will now be discussed.

REACTIONS MODELED

The following combustion reactions are included in the char bed model:

$$C + 1/2\ O_2 \rightarrow CO \quad (17)$$

$$C + O_2 \rightarrow CO_2 \quad (18)$$

$$C + CO_2 \rightarrow 2CO \quad (19)$$

$$C + H_2O \rightarrow CO + H_2 \quad (20)$$

$$4C + Na_2SO_4 \rightarrow 4CO + Na_2S \quad (21)$$

$$2C + Na_2SO_4 \rightarrow 2CO_2 + Na_2S \quad (22)$$

$$Na_2S + O_2 \rightarrow Na_2SO_4 \quad (23)$$

The rationale for the list of reactions, the development of a char burning model, and the selection of rate expressions for each reaction are discussed in Appendix I.

Figure 5 depicts the char bed reactions that are modeled. There are two ways that oxygen from the gas phase can react with the char to produce either carbon monoxide or carbon dioxide. Oxygen can react directly with char carbon, or it can oxidize sodium sulfide to sodium sulfate which then reacts with carbon. This second path is the sulfate/sulfide cycle which was discussed in the literature review. The products of the char carbon reactions are CO and CO_2. Aiken found that the relative fraction of CO, f, ranged between 0.80 and 0.96 for char pile combustion[6]. The value (1-f) is the fraction of the carbon which becomes CO_2. The oxygen can also react with H_2 or CO in the gas phase as shown by the lighter arrows on Fig. 5. Thus there are several competing reactions for oxygen in the vicinity of the bed surface.

The CO_2 and H_2O in the gas phase can react with the char bed surface. The CO_2/char reaction produces CO while the H_2O/char reaction produces CO and H_2.

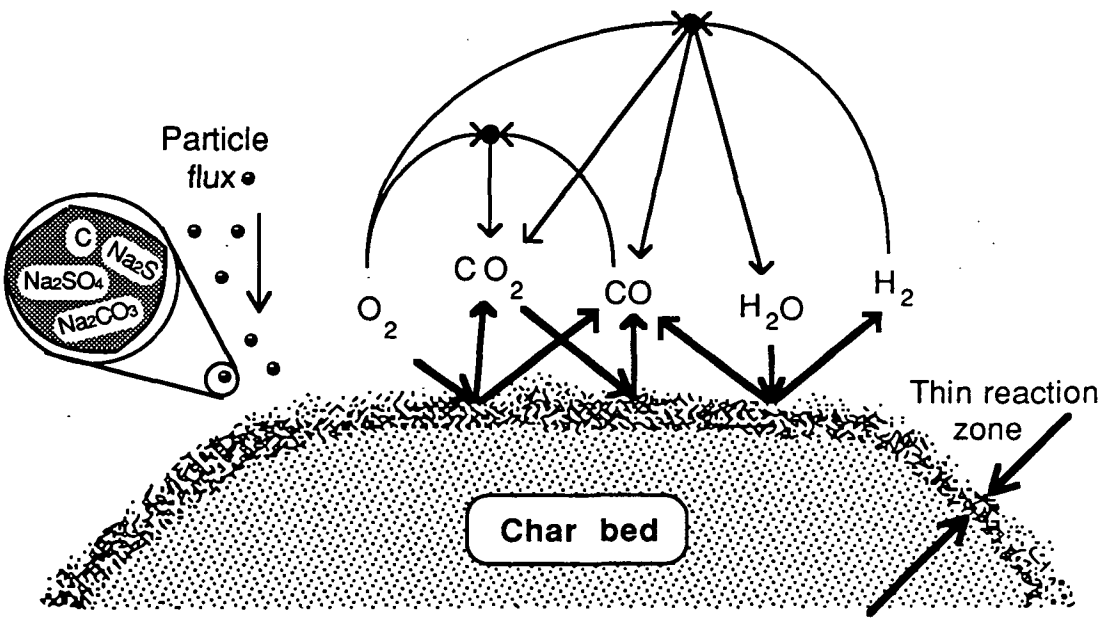

Figure 5. Char bed reactions.

Na_2SO_4 in burned-out smelt droplets can react with char carbon on the bed in an endothermic reaction. Oxygen in the form of Na_2SO_4 may be a significant contributor to carbon depletion on the bed.

The kinetic reaction rate for the C/Na_2SO_4 reaction is calculated using Equation (2) cited earlier[10]:

$$R_{CS} = -\frac{4 * k_1}{2 - f}\left\{\frac{[SO_4]}{k_2 + [SO_4]}\right\}[C]\, e^{\frac{-E}{RT}} = -\frac{4 * k_1}{2 - f}\left\{\frac{(1 - r)\, s}{k_2 + (1 - r)\, s}\right\}[C]\, e^{\frac{-E}{RT}} \qquad (2)$$

where

$[SO_4]$ = sulfate concentration, mole sulfate/mole Na_2
$[C]$ = carbon concentration, mole C/mole Na_2
k_1 = 1310 sec^{-1}
k_2 = 0.0011 mole Na_2SO_4/mole Na_2
s = sulfidity
r = reduction efficiency
f = $CO/(CO + CO_2)$ in combustion product
E = activation energy, 29,200 cal/mole
R = gas constant, 1.987 cal/mole
T = absolute temperature

The kinetic reaction rate for the C/O_2 reaction is calculated using Equation (24)[12]:

$$k_r[=]\frac{cm}{s} = 236\, T_g\, e^{\left(\frac{-11022}{T_p}\right)} \qquad (24)$$

where

T_g = gas temperature
T_p = particle temperature

For an irreversible heterogeneous reaction which is first order in oxygen concentration, the rate of oxygen consumption is $K*C_{BO}$ where the reaction constant K is comprised of the mass-transfer resistance and chemical reaction resistance in series [23]. The mass-transfer coefficient, k_m, and

chemical reaction constant, k_r, make up K as follows:

$$K = \frac{1}{\frac{1}{k_m} + \frac{1}{k_r}} \tag{25}$$

Equation (25) is used to calculated the overall reaction constant (K_{COX}) for the C/O_2 reaction.

The following expression is used for the C/CO_2 and C/H_2O reaction rate based on experiments performed by Li[13]:

$$R_{CO_2} = \frac{-k_1 P_{CO_2}[C]}{1 + k_2 P_{CO_2} + k_3 P_{CO}} e^{\frac{-E}{RT}} \tag{26}$$

where

$k_1 = 9.53 \times 10^7$ (atm-sec)$^{-1}$
$k_2 = 10.8$ atm^{-1}
$k_3 = 6.3$ atm^{-1}
$E = 187{,}000$ J/mole
P_i = partial pressure
$R = 8.314$ J/mole

Equation (26) was determined for the C/CO_2 reaction but is assumed in this thesis to be applicable to the C/H_2O reaction. The coal literature indicates that these two reactions are expected to be on the same order of magnitude. In the absence of data for the C/H_2O reaction, the kinetic rate will be assumed to be adequately represented by Li's expression for the C/CO_2 reaction.

Grace et al. found that the kinetic rate of sulfide oxidation is extremely fast relative to mass transfer based on experiments in which sulfide oxidation in molten smelt was measured.[10] The reaction rate for sulfide oxidation is

therefore assumed to be describable by an appropriate expression for mass transfer.

The oxygen from the combustion air is split between the Na_2S/O_2 reaction and direct carbon oxidation. A partition parameter, P, determines the fraction of oxygen which reacts directly with char carbon. The development of the expression used to calculate P is discussed in Appendix I.

MASS TRANSFER TO THE CHAR BED

All combustion reactions on the char bed can be limited by the rate of mass transfer. The accurate modeling of mass transfer to the bed is therefore important. This section discusses the modeling of mass transfer to the char bed. The mass transfer model is based on boundary layer theory; the commonly-used analogy is made between momentum, heat, and mass transfer. A mass transfer correlation can then be obtained from correlations developed using idealized systems for momentum or heat transfer.

Predictive equations for momentum or heat transfer have been developed for simple experimental systems by correlating transport data with dimensionless transport groups. In order to use one of these correlations to predict mass transfer, the appropriate dimensionless group for mass transfer (Schmidt number) needs to be substituted into its analogous dimensionless group for heat transfer (Prandtl number). The resulting mass transfer coefficient can then be used over the range of conditions for which the heat transfer coefficient was determined. The challenge in modeling mass transfer to the char bed surface is to find a simple system which is similar to the gas/char interface; the mass transfer correlation developed for the simple

system can then be applied to the char bed surface. Two simple systems which are considered in this section are parallel flow past a flat plate and unidirectional flow past a sphere.

The gas flows around the char bed are strongly influenced by the flow from the primary air ports and the secondary air ports to a lesser extent for low char beds. The flows from the air ports will be turbulent, and the thickness of the boundary layer on the char bed surface will depend on local conditions such as temperature, velocity, and the roughness of the char bed surface. The appropriate mass transfer correlation depends on whether or not the boundary layer is turbulent.

It is possible to have a laminar boundary layer even though the external flow is turbulent. A correlation for a laminar boundary layer is appropriate in such a case. There is a distinction between turbulent flow external to the boundary layer and turbulence inside the boundary layer. Schlichting states that the influence of the free-stream turbulence on the boundary layer appears to be small[24]. On the other hand, certain nonidealities of the char surface such as roughness promote transition from a laminar to a turbulent boundary layer. A mass transfer correlation for a turbulent boundary layer would be more appropriate in this later case. The following discussion considers the merits of the flat plate system with a laminar boundary layer, the flat plate system with a turbulent boundary layer, and unidirectional flow past spheres.

The Char Surface as a Flat Plate

Figure 6 shows a comparison between the gas/char system and the simple flat-plate system. In the recovery boiler, the turbulent primary air flows essentially parallel to the coarse, undulating char bed surface. The velocity and

turbulence decay with distance into the furnace. On the other hand, the flow in the smooth flat-plate system is uniform and disturbance-free. Despite the obvious differences such as turbulence and roughness, the parallel flow past the char bed surface is a similar system to uniform flow past a flat plate; thus, the form of the mass transfer correlation for flow past a flat plate may be applicable to the gas/char interface.

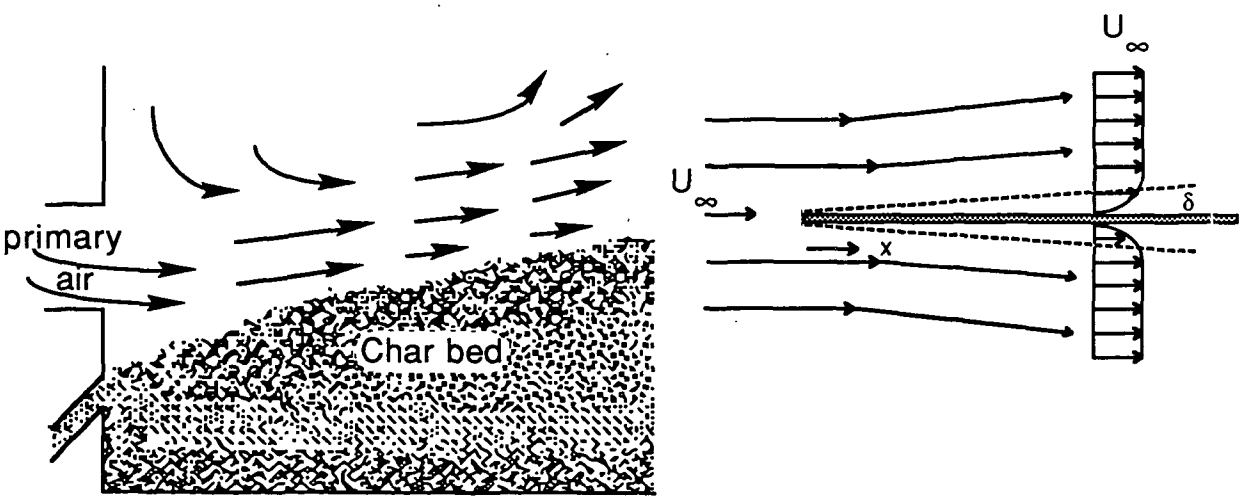

Figure 6. Treating the char surface as a flat plate.

Solution of the Navier-Stokes equations provides the laminar boundary layer thickness for the smooth flat plate which has a uniform velocity parallel to the plate:

$$\delta \approx 5\sqrt{\frac{\nu x}{U_\infty}} \tag{27}$$

where

δ = boundary layer thickness
ν = kinematic viscosity
x = distance along the plate
U_∞ = bulk velocity

The Reynold's number range that the char bed will see is one factor in determining whether to use a correlation for a laminar boundary layer or one for a turbulent boundary layer. The Re number is based on the length of the plate:

$$Re = l\langle v\rangle/\nu \tag{28}$$

where

l = plate length
<v> = bulk velocity
ν = kinematic viscosity

For flow along a flat plate, a Reynolds (Re) number of 320,000 is the value where the transition occurs between a laminar boundary layer and a turbulent boundary layer [25]. This is regarded as the minimum Re number where transition occurs. It can occur at Re numbers as high as 10^6 with exceptionally disturbance-free external flow, but this condition would not apply to the surface of a char bed. An upper limit for velocity in a furnace near the bed is 55 m/s[26]. Thus, the minimum length at which transition occurs at 1200 K is:

$$l = Re*\nu/\langle v\rangle = 320{,}000*1.6\ cm^2/s/5500\ cm/s = 93\ cm \tag{29}$$

For lengths less than 93 cm, the boundary layer on a flat plate will be predicted to be laminar at these conditions. The predicted boundary layer in the furnace is therefore laminar for lengths less than 93 cm. At lengths greater than 93 cm, the velocity would be less than than at the ports, so Re would decrease. The Re number for the gas/char system will always be in the range where the correlation for a laminar boundary layer is applicable.

The value to use for the characteristic length in the furnace is

ambiguous since the char bed is not a flat plate with a well-defined length. For flat plates, the length of the plate is chosen as the characteristic length used in Re number calculations. There are several possibilities for the characteristic length in the furnace: the width of the furnace, an intermediate distance such as 1 m, or the approximate diameter of the particles on the char bed (ca. 1 cm). The width of the furnace is almost certainly too long and would cause a substantial underprediction of mass-transfer coefficients. An arbitrary length of 1 m is used in later calculations. Another alternative for the characteristic length is the approximate particle diameter (1 cm). The predicted mass transfer coefficient using a characteristic length of 1 cm will be ten times greater than that using 1 m. Thus, the characteristic length is important, but the correct value to use for furnace calculations is not known.

Equation (30) is the mass transfer correlation for uniform flow over flat plates with laminar boundary layers[27]:

$$Sh_l = K_l l/D = 0.664\ Re_l^{0.5} Sc^{0.33} \qquad (30)$$

where

K_l = average mass transfer coefficient over the length of the plate
D = diffusivity
ν = kinematic viscosity
Re = Reynolds number = $\langle v \rangle l/\nu$
Sc = Schmidt number = ν/D

The mass transfer correlation is based on the assumption that momentum transport and mass transport are analogous. Bird lists the following limitations on the applicability of the analogy: 1) the Schmidt number (Sc) must be greater than 0.5, 2) the boundaries cannot be strongly curved, 3) the mass transfer rate must be low enough that diffusion does not create a net bulk flow, and 4) the interfacial composition must be uniform[25]. Calculations show that Sc remains constant at about 0.66 over the temperature range 1100-1400 K

which is the approximate range seen in the furnace. The char bed surface may have curves which may cause boundary layer separation; the flat-plate correlation is no longer applicable if boundary layer separation occurs. A constant interfacial gas concentration is another limit to applicability of the correlation. It may be reasonable to assume $x_{O2} \approx 0$ at the interface since oxygen is rapidly consumed. The gas/char system meets some of the limitations, but there are also some limitations that may be violated.

The roughness of the char surface will have an important influence on the mass-transfer coefficient. Schlichting reported that the surface roughness would have no effect on the transition to turbulence if the surface conforms to the following equation[24]:

$$\frac{U k_s}{\nu} < 120 \qquad (31)$$

where

U = velocity of gas stream
k_s = surface roughness
ν = kinematic viscosity

In the temperature range of 1100 - 1400 K, ν will be in the range of 1.4 - 2.1 cm^2/sec. Gas velocities around the bed may be in the range of 5 - 50 m/sec. Thus, the acceptable surface roughness would be between 0.03 and 0.5 cm. Char particles may be on the order of 1 cm, so the surface roughness definitely affects the transition to turbulence.

The correlation for laminar flow over flat plates predicts mass-transfer coefficients that are generally so low that little mass transfer and bed burning is possible. Calculations which use approximate furnace conditions demonstrate the range of oxygen fluxes which the correlation predicts. Let the characteristic lengths be 1 and 100 cm; $\langle v \rangle$ = 300 and 3000 cm/s; X_{O2} = 0.01

and 0.20. Table 10 lists the predicted oxygen flux in units of moles O_2/cm^2-sec x 10^{-6}. The first number is for 1% oxygen and the second number is for 20% oxygen.

Table 10. Predicted oxygen flux for laminar flow over a flat plate, moles O_2/cm^2-sec x 10^{-6}.

l(cm)	<v>(cm/s)	1100 K	1200 K	1300 K	1400 K
1	300	2.0, 40	1.9, 39	1.9, 38	1.9, 38
	3000	6.2, 120	6.1, 120	6.0, 120	5.9, 120
100	300	0.20, 4.0	0.19, 3.9	0.19, 3.9	0.19, 3.8
	3000	0.62, 12	0.61, 12	0.60, 12	0.59, 12

The carbon flux to the bed can be estimated in order to compare the carbon flux with the estimated oxygen fluxes in Table 10. A typical design parameter for recovery furnaces is 2 lb solids/ft^2-min. If 60% of the black liquor solids reaches the bed with a carbon content of 25%, the flux is:

$$N_C = 2 \text{ lb/ft}^2\text{-min} * 3 \text{ mole C/144 lb char} * 0.60 * \text{ft}^2/30.48^2 \text{ cm}^2 * \text{min/60sec} * 454 \text{ gmole/lbmole} = 200 \times 10^{-6} \text{ mole/cm}^2\text{-sec}$$

If the carbon content was only 10% carbon, the carbon flux to the bed would be 80 x 10^{-6} mole C/cm^2-sec. The oxygen flux does not have to be quite as high as the carbon flux to burn all the char reaching the bed since some oxygen is supplied by the char itself. The flat plate correlation does predict a greater oxygen supply than the carbon supply under some circumstances; but, in

general, the flat-plate correlation predicts insufficient oxygen to burn the carbon landing on the char bed.

The flat-plate correlation for a laminar boundary layer is inadequate for several reasons. The boundary layer for flow across the char bed surface will always be calculated as being in the laminar range, but the surface roughness will be a very important influence which affects the transition to a turbulent boundary layer. The choice of a characteristic length is important, but the correct value to use for the char bed surface is uncertain. The correlation for smooth, flat plates will most likely underpredict mass-transfer coefficients on the rough, undulating bed. In summary, the laminar flat-plate correlation is not applicable to the char bed mass transfer model although it may supply the form of an applicable correlation.

The use of a correlation for a turbulent boundary layer on a flat plate suffers some of the same weaknesses as the correlation for a laminar boundary layer. The characteristic length is still unknown, and the Re number for the char bed surface is outside the range of applicability for the correlation. In the case of the correlation for a laminar boundary layer, the Re number was in the laminar range for furnace conditions, but the surface roughness promotes transition to a turbulent boundary layer. On the other hand, the Re numbers for the char bed lay outside the applicable range for the correlation for a turbulent boundary layer on a flat plate.

A heat transfer correlation for a turbulent boundary layer on flat plates is as follows[28]:

$$Nu_x = 0.037\, Re_x^{0.8}\, Pr_0^{0.43} \left(\frac{Pr_0}{Pr_i}\right)^{0.25} \qquad (32)$$

where

Nu = Nusselt number = h x/ k
h = heat transfer coefficient
x = distance along plate
k = thermal conductivity
Pr = Prandtl number = $C_p \mu/k$
C_p = heat capacity
μ = viscosity

The subscripts 0 and i denote approach conditions and interface conditions, respectively. The correlation is applicable for Pr between 0.7 and 380, and Re between 5×10^5 and 3×10^7. The correlation for the average mass transfer coefficient is obtained by substituting the analogous dimensionless groups into the correlation and integrating over the plate length. The Pr correction term is neglected in the transformation. The resulting mass transfer correlation is:

$$Sh_l = 0.04625\ Re_l^{0.8}\ Sc^{0.43} \qquad (33)$$

The primary difference between the correlations for laminar and turbulent boundary layers is the dependence on velocity. The laminar mass transfer coefficient is proportional to $V^{0.5}$ while the turbulent correlation has a 0.8-power velocity dependence.

The minimum Re number for which this correlation is applicable is never obtained on the char bed. A velocity of 80 m/s is required to get a Re number of 5×10^5 at 1200 K assuming a length of 100 cm. Thus, even though the boundary layer may be turbulent due to surface roughness or other factors, correlations for a turbulent boundary layer cannot be used to model mass transfer to the char bed; the Re numbers on the char bed are outside the range where the correlations are applicable.

The Char Surface as a Collection of Spherical Particles

As discussed in the last section, two main objections to the flat-plate model are the large surface roughness and the ambiguity of the characteristic length. Treating the char bed surface as a collection of spheres addresses some of the weaknesses of the flat-plate model. The problem of surface roughness is addressed because the particles are treated individually. The problem of characteristic length is solved by using an appropriate particle diameter.

The mass-transfer coefficient is calculated using the Ranz correlation for unidirectional flow past spheres[29]. The idealized system is shown in Fig. 7 along with the conceptualization of the char surface.

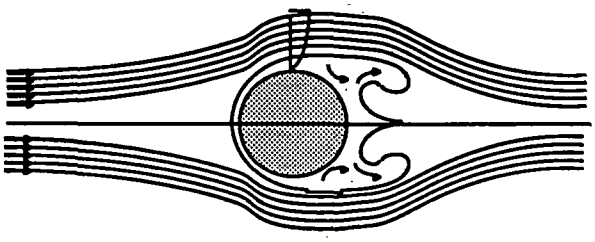

a. System for Ranz correlation.

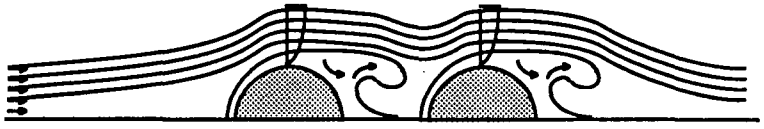

b. Conceptualization of char bed surface.

Figure 7. Treating the char surface as spheres.

In the system which was used to develop the correlation, there is a single particle in a unidirectional flow stream. The char bed surface is here thought to be comprised of spherical char particles. The main weakness of this treatment of the surface is that the char particles will be influenced by the wakes of the upstream particles; however, the Ranz correlation may still apply

since external disturbances tend not to affect the formation of the boundary layer[24]. The Ranz correlation with a particle diameter of 1 cm is one form of the mass transfer coefficient used in the model:

$$Sh = \frac{k_m d}{D} = 2.0 + 0.6\, Re^{\frac{1}{2}}\, Sc^{\frac{1}{3}} \qquad (34)$$

where

d = particle diameter
D = diffusivity
ν = kinematic viscosity
Re = Reynolds number = $\langle v \rangle d/\nu$
Sc = Schmidt number = ν/D.

The reason for choosing 1 cm is explained in Appendix IV. The other mass transfer coefficient used in the model is based on experimental mass transfer coefficients.

Experimental Mass Transfer Coefficients

The discussion about the flat plate system raised objections to the direct application of a flat-plate correlation to the gas/char system, but there are enough similarities between the two systems to suggest that the form of the correlations for each system should be similar. The expected Re number range on the char bed would be in the laminar regime, but the surface roughness promotes turbulent boundary layers. The correlation would therefore have a velocity dependence which is at least 0.5 (laminar) and more likely on the order of 0.8 (turbulent).

The best way to resolve the issue of an appropriate char bed mass transfer coefficient is to measure it. Brown et al. measured experimental mass transfer coefficients as part of project co-sponsored by The Institute of Paper

Chemistry (IPC) and the Department of Energy (DOE)[30]. The experimental system shown in Fig. 8 is designed to represent conditions in the proximity of the primary air ports of the recovery boiler. Char beds were formed by collecting particles from a reactor located above the char bed reactor. Drying and pyrolysis were completed before the mass transfer coefficient was measured. The preformed char bed was raised at a rate that kept the surface of the char bed in contact with an injected jet. Air/nitrogen mixtures were injected across the char bed through a thin horizontal slot. The combustion rate was calculated using information on off-gas composition and flow rate. The oxygen flux was calculated based on the combustion rate and the projected area of the char bed surface. The mass transfer coefficient was calculated by assuming mass-transfer control and estimating the average oxygen concentration across the surface.

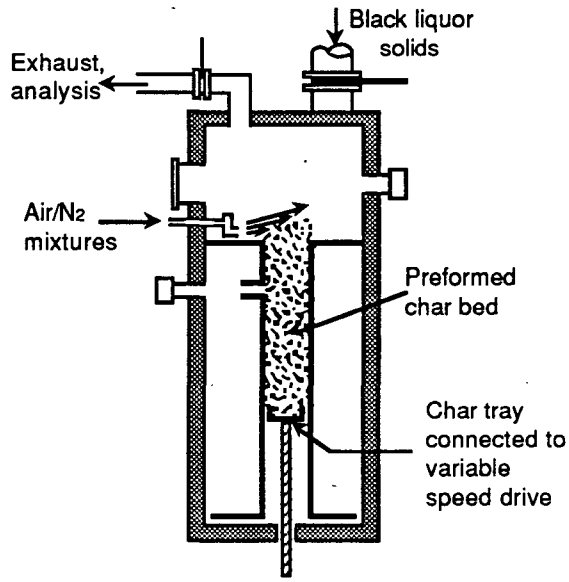

Figure 8. Char bed reactor.

Figure 9 shows several features about Brown's mass transfer correlation. The data shown in the foreground graph were obtained for velocities in the range of 1 - 6 m/s, but the background graph shows that velocities across the

char bed surface extend well beyond the range of the experiments. The power dependence of velocity becomes very important when the correlation is extrapolated beyond 6 m/s. The four curves shown from bottom to top are the

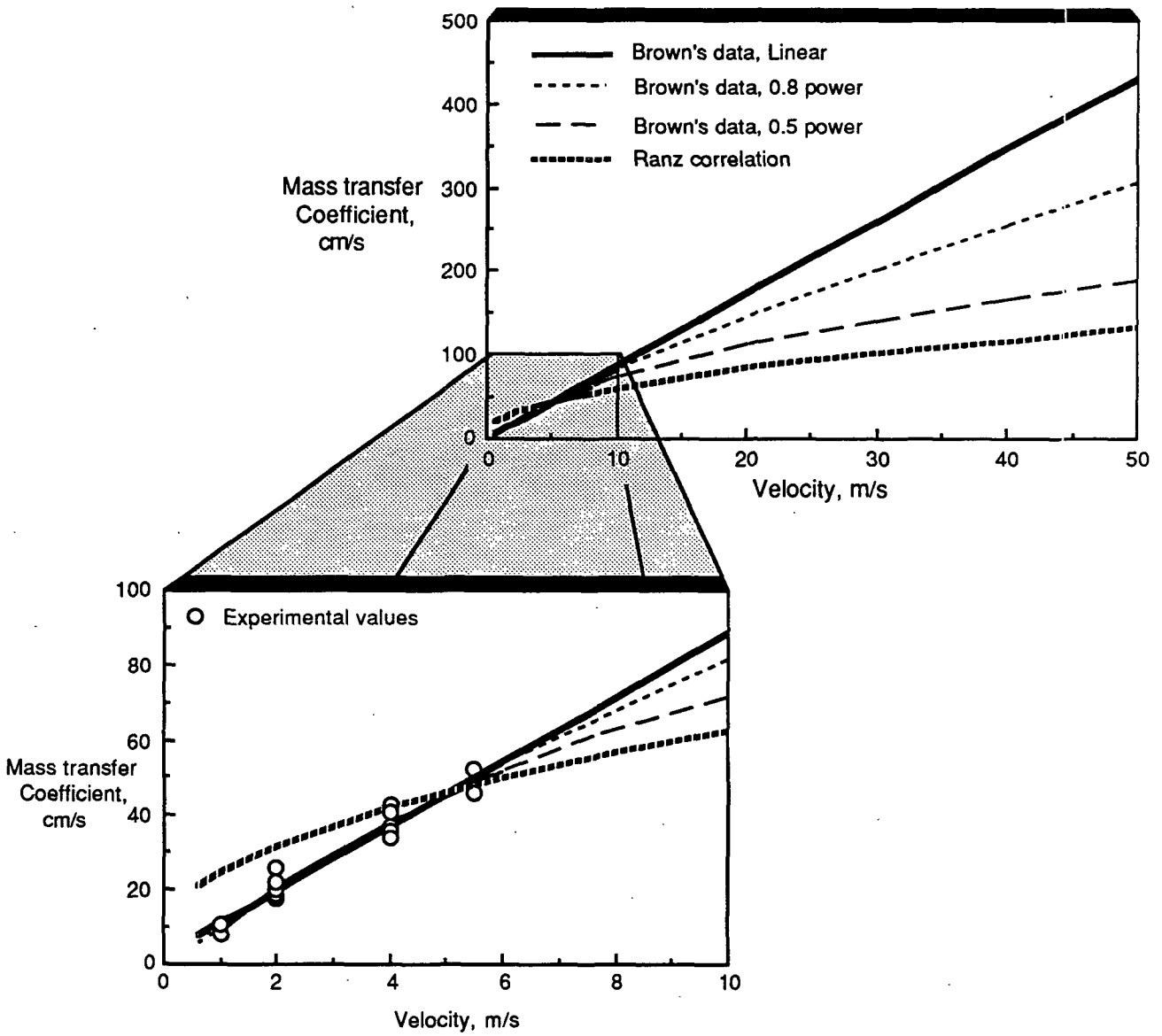

Figure 9. Experimental mass transfer coefficients.

Ranz correlation with a particle diameter of 1.0 cm, and Brown's data correlated with velocity power dependencies of 0.5, 0.8, and 1.0. The foreground graph shows that the data are equally represented with a 0.5, 0.8,

or 1.0 power. The r^2 coefficient was 0.95 for each of the three curve fits. The background graph demonstrates the divergence of the four curves beyond 6 m/s.

The Ranz correlation overpredicts Brown's correlation at velocities under ca. 5 m/s, but Brown's mass transfer coefficient is underpredicted by the Ranz correlation at higher velocities. The square-root dependence of velocity in the Ranz correlation causes a large divergence from the Brown's linear correlation. The divergence between the two correlations will be most important in areas of the bed where high velocities exist, e. g., near the primary air ports.

The form of the mass transfer correlation is more likely to follow the form of the correlation for a turbulent boundary layer primarily because of the roughness of the char surface. The velocity dependence should therefore be on the order of 0.8, but an experimental range of 1 - 6 m/s is too small to determine the power of the velocity dependence with any statistical confidence. Further work is being done to extend the velocity range to get a better estimate of the velocity dependence of the mass-transfer coefficient.

Brown's correlation with a linear velocity dependence and the Ranz correlation with a square-root velocity dependence bracket the range of the expected mass transfer coefficient. Thus, two forms of the mass transfer correlation will be used in this thesis. The first form will be the Ranz correlation with a characteristic length of 1.0 cm. The second form of the mass transfer coefficient is Brown's empirical correlation for char combustion data. Brown's correlation is as follows:

$$k_m = 3.05 + 8.62 * v \qquad (35)$$

where

k_m = average mass transfer coefficient [=] cm/sec

v = average velocity [=] m/sec

This correlation may change form as refinements are made. A better correlation can be substituted in the model at a later date. Brown's linear correlation is sufficient for the purposes of showing the upper boundary for the mass transfer coefficient. It should be noted that neither the Ranz correlation nor the Brown correlation have any dependence on distance away from the wall.

Brown's correlation must be corrected for temperature and gas species. For turbulent flow over flat plates, the Sherwood number is proportional to $Re^{0.8}$ and $Sc^{0.43}$.[28] The mass transfer coefficient is therefore proportional to diffusivity to the 0.57 power and kinematic viscosity to the -0.37 power. Both diffusivity and kinematic viscosity are temperature dependent. The average film temperature for the correlation is estimated to be 800 °C. For the oxygen mass-transfer coefficient at different temperatures, the corrected correlation is:

$$k_{m_{O2}} = (3.05 + 8.62 * v) * \left(\frac{D_T}{D_{800}}\right)^{0.57} * \left(\frac{\nu_T}{\nu_{800}}\right)^{-0.37} \qquad (36)$$

where the subscripts "T" and "800" denote the gas temperature and 800 °C. In order to estimate the mass transfer coefficient for water or carbon dioxide, an additional correction factor is needed. Equation (37) shows the mass transfer coefficient for carbon dioxide, and the correlation for water vapor is analogous:

$$k_{m_{CO2}} = (3.05 + 8.62 * v) * \left(\frac{D_T}{D_{800}}\right)^{0.57} * \left(\frac{\nu_T}{\nu_{800}}\right)^{-0.37} * \left(\frac{D_{CO2/800}}{D_{O2/800}}\right)^{0.57} \qquad (37)$$

BED MODULE DEVELOPMENT

Development of a Recovery Furnace Model

A three-dimensional computer model of the kraft recovery furnace has been developed at The Institute of Paper Chemistry (IPC). The model predicts gas flow patterns, temperature and species distributions, particle interactions with the gas phase, and char bed burning rates. An existing computer code called FLUENT was modified for the unique characteristics of black liquor combustion. FLUENT is a computational fluid dynamics program which contained most of the features necessary to model the furnace. It is a pseudo-steady state, finite difference , computational fluid dynamics program which can solve three-dimensional fields for pressure, velocity, temperature, kinetic energy of turbulence, dissipation rate of turbulence, and several chemical species. The FORTRAN source code was provided through an agreement between IPC and Creare, Inc. Modifications were made which account for the unique aspects of black liquor combustion.

This thesis is one of three theses done at The Institute of Paper Chemistry which resulted in the computer model of the kraft recovery furnace called FLUENT/RFM (Recovery Furnace Model). Jones' thesis discusses the convergence of a base case simulation, modification of an existing combustion model, and inclusion of two additional chemical species into FLUENT[31]. Walsh's thesis describes a black liquor combustion model which handles the combustion of individual particles through exchange of mass, energy, and momentum between the gas phase and the particle phase[32]. This thesis models the char bed reactions through exchange of mass and energy between the char bed surface and the gas phase.

The char bed model is intimately tied to FLUENT's methodology, so a brief orientation to FLUENT is given in this section. A more detailed discussion can be found in the FLUENT Reference Manual[33] and the theses of Jones and Walsh.

The basic equations solved to obtain the gas flow fields are mass and momentum balances for steady state flows in Cartesian coordinates. These equations take the following form when written in tensor notation:

Mass conservation:
$$\frac{\partial}{\partial x_i}(\rho u_i) = 0 \tag{38}$$

Momentum conservation:
$$\frac{\partial}{\partial x_i}(\rho u_i u_j) = \frac{\partial}{\partial x_i}\left(\mu\left[\frac{\partial u_i}{\partial x_i} + \frac{\partial u_j}{\partial x_i}\right]\right) - \frac{\partial p}{\partial x_j} + \rho g_j + F_j \tag{39}$$

convection diffusion pressure gravity phase 2

Turbulence is modeled with the k- ε model which substitutes an "effective" viscosity in the existing equations. The effective viscosity consists of the molecular viscosity augmented by its turbulent counterpart. Transport equations are written and solved for k and ε using five empirical constants.

The governing partial differential equations for the conservation of mass, momentum, energy, and chemical species for the gaseous phase can be arranged into the following general form:

$$\frac{\partial}{\partial x_i}(\rho u_i \phi) = \frac{\partial}{\partial x_i}\left[\Gamma_\phi \frac{\partial \phi}{\partial x_i}\right] + S_\phi \tag{40}$$

The term on the left-hand side is convection, the first term on the right-hand side is diffusion, and S_ϕ represents the source term. ϕ represents a general variable, so this equation applies to momentum, energy, and chemical species.

The three-dimensional domain is divided into finite volumes called cells. The simulation is constructed by specifying the type of cell and the location of the grid point (or node) which lies at the geometric center of the cell. The relationship between the grid points and cells is depicted in Fig. 10.

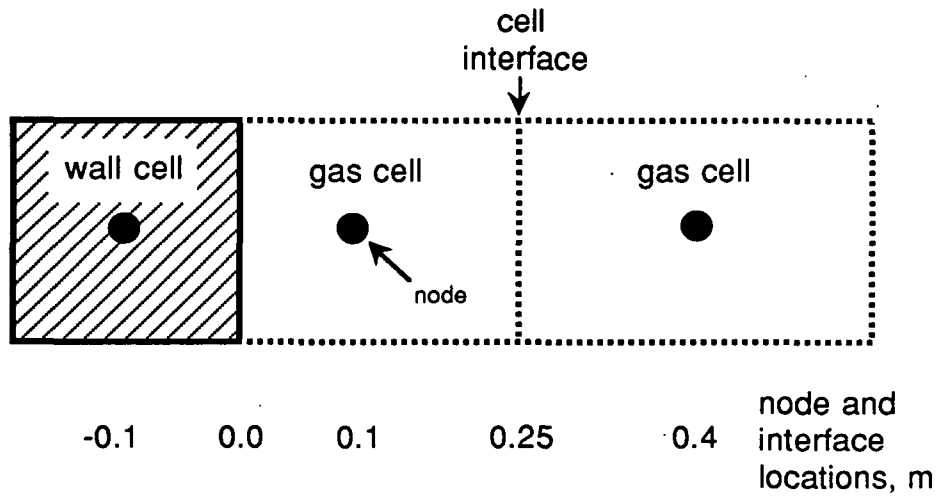

Figure 10. Relationship between nodes and cells.

The interface between two cells lies half way between the two nodes. Thus, the interface between the two gas cells lies halfway between 0.1 and 0.4 m, at 0.25 m. All of the variables except the velocity components are calculated at the nodes; the velocity components are calculated on the cell interfaces for numerical stability.

The equations represented by Equation (40) are reduced to their finite-difference forms by integration over the volume of the computational cells. When Equation (40) is integrated over a finite volume, it becomes an algebraic equation of the following form:

$$\phi_p \sum_i (A_i - S_p) = \sum_i A_i \phi_i - S_c \qquad (41)$$

where the summation is over the six adjacent cells. The A's are coefficients which contain contributions from the convective and diffusive fluxes and S_c and S_p are components of the linearized source term, $S_\phi = S_c + S_p\phi_p$. The set of simultaneous algebraic equations is solved by a semi-implicit iterative scheme which starts from initial conditions and converges to a solution after a number of iterations.

Each iteration in FLUENT's methodology consists of the following steps:

1. The momentum equations for each velocity component are each solved in turn using the best estimate of the pressure field;

2. A pressure-correction equation is solved to obtain corrections to the pressure field and corresponding adjustments to the velocity components;

3. The k and ε equations are solved using the updated velocity field to obtain the distribution of the effective viscosity.

4. Any auxiliary equations such as enthalpy, species, conservation, radiation, and turbulence are solved using the previously updated values of the other variables;

5. The source terms from the second phase are included

6. Iterate until convergence criteria are met.

The particle phase interacts with the gas phase through source and sink terms. The equations of motion and trajectory of a particle are solved for each particle, and the source or sink of mass and energy in each cell is the sum of the sources and sinks of all the particles that have passed through that cell. The particle is tracked in a Lagrangian frame of reference, and its residence time in each cell is broken into a number of time steps. The particle can pass through multiple stages such as drying, devolatilization, and char combustion. When the particle encounters a boundary, it can either be reflected, trapped,

placed back in the gas phase, or allowed to escape the solution domain.

Changes to FLUENT

Gas Phase Model

The changes to the gas phase model to allow a more thorough simulation of the recovery boiler was the subject of a Ph. D. thesis by Jones[31]. The changes include more chemical species and a more complex combustion model.

The original combustion model in FLUENT provided for a fuel, "F", an oxidant, "O", and a combustion product, "C". An inert species makes up the remainder of the gas phase. The following reaction was allowed:

$$F + s\,O \rightarrow (1+s)\,C \qquad (42)$$

where s is the stoichiometric coefficient. The combustion product "C" in the original model was specifically defined to be carbon dioxide.

This model is too simplistic to accurately model a kraft recovery boiler. There was no provision for incomplete combustion of the fuel, and the products of combustion were not differentiated into water and carbon dioxide. The exclusion of water as a separate species has the potential to cause substantial error, particularly with a wet fuel such as black liquor. Water vapor has a heat capacity which is much higher than other combustion gases, so the enthalpy calculations would be in error.

The deficiencies of FLUENT were addressed by adding a more detailed

combustion model and by including more chemical species. The fuel reactions were expanded so that fuel could be combusted to either CO, CO_2, or H_2O. The "fuel" in black liquor comes from pyrolysis gases which contain carbon, hydrogen, and oxygen. The relative amounts of CO, CO_2, and H_2O depend on the assumed composition of the pyrolysis gas. The combustion of fuel is described by Equation (43):

$$\text{Fuel} + s\,O_2 \rightarrow (1+s)\,F_{CO}\,CO + (1+s)\,F_{CO_2}\,CO_2 + (1+s)\,F_{H_2O}\,H_2O \qquad (43)$$

where

s = stoichiometric requirement of O_2 for complete combustion of fuel
F_{CO} = mass fraction of CO formed
F_{CO_2} = mass fraction of CO_2 formed
F_{H_2O} = mass fraction of H_2O formed
note: $F_{CO} + F_{CO_2} + F_{H_2O} = 1$

In addition to the combustion of fuel, provision is made to burn CO to CO_2. The model assumes that all gas phase burning is controlled by turbulent diffusion.

Carbon monoxide and water are two additional species which were added to model incomplete combustion and account for the higher heat capacity of water. The heat capacity in a given cell was made species-dependent.

Particle Phase Model

The particle-phase model in FLUENT was insufficient to handle the unique characteristics of black liquor combustion. The deficiencies included:

1. Evaporated water was given the same physical properties as combusted gases;

2. The reoxidation of sodium sulfide in burned-out smelt was not included;

3. Only 100 droplets could be added, with limited flexibility in describing how they entered the furnace;

4. The drying of black liquor on the wall with it subsequently falling on the bed was not modeled;

5. Only one event (i.e., drying, pyrolysis, char burning, or reoxidation) could take place for a given droplet in a given cell;

6. The mass balance on the drops did not converge;

7. Wet drops could not be described if a description of all other combustion events was desired.

The particle calculations were modified by Walsh.[32] The particle combustion model includes a description of drying, volatile evolution, char combustion, and the oxidation of sodium sulfide in burned-out particles. These reactions were combined with mathematical expressions to describe the distributions of diameters and initial velocities of droplets being sprayed from multiple liquor guns, and the trajectories taken by the particles. A lognormal distribution for droplet diameters was assumed. Black liquor particles which strike the wall while the liquor is still wet are assumed to dry and pyrolyze partially afterwhich they are dropped on the perimeter of the char bed. Particles which are beyond the drying stage are allowed to bounce off the wall.

The modified gas phase and particle models are discussed in more detail in Jones' and Walsh's theses. The modified version of FLUENT plus the char bed model discussed in this thesis comprise FLUENT/RFM.

Subroutine BED

The exchange of mass and energy between the bed and the furnace cavity is modeled within FLUENT/RFM. The char bed model is incorporated into FLUENT/RFM as a subroutine called BED. BED is called after the particle calculations are complete. The bed receives a flux of particles in various states, and material and energy balances are performed over the surface of the bed.

The char bed surface is represented by dividing it into discrete reaction zones referred to hereafter as bed cells. The bed cell is a unique type of wall cell which can exchange mass and energy with the gas phase. There are ten types of wall cells in FLUENT, W0-W9. The wall cell acts as a boundary to fluid flow and is capable of exchanging heat between the fluid phase and wall. A wall cell called W9 has been converted into a bed cell in FLUENT/RFM. The symbol W9 represents a bed cell in the discussion that follows. Figure 11 shows the discretized char bed surface and the interface between the bed cells and the gas cells. Whenever a bed cell is encountered, the mass and energy exchanges for the char bed surface are calculated according to the algorithm in subroutine BED.

FLUENT/RFM solves cases in cartesian coordinates, so the sloped surfaces of the char bed must be discretized into a stair-step representation. This approximation has the potential to create artifacts in the solution, but a finely divided bed surface will act as a "smooth" surface. A coarse char bed surface in a 10,000 node version of FLUENT/RFM caused artificial upward deflection of jets impinging on the bed, while a finer char bed in a 50,000 node version showed no such artifacts. The version of FLUENT/RFM with 50,000 nodes appears to be adequate to describe a reasonable bed shape.

BED uses information from the gas cell immediately above the bed cell

as shown in Fig. 11. The concentrations of CO_2, H_2O, and O_2 are considered to be the "bulk" concentrations for the purposes of calculating mass fluxes to the char surface. The magnitude of the velocity vector in the gas cell is used to calculate the mass transfer coefficient. The radiant flux in the vertical direction in the gas cell is used in the energy balance.

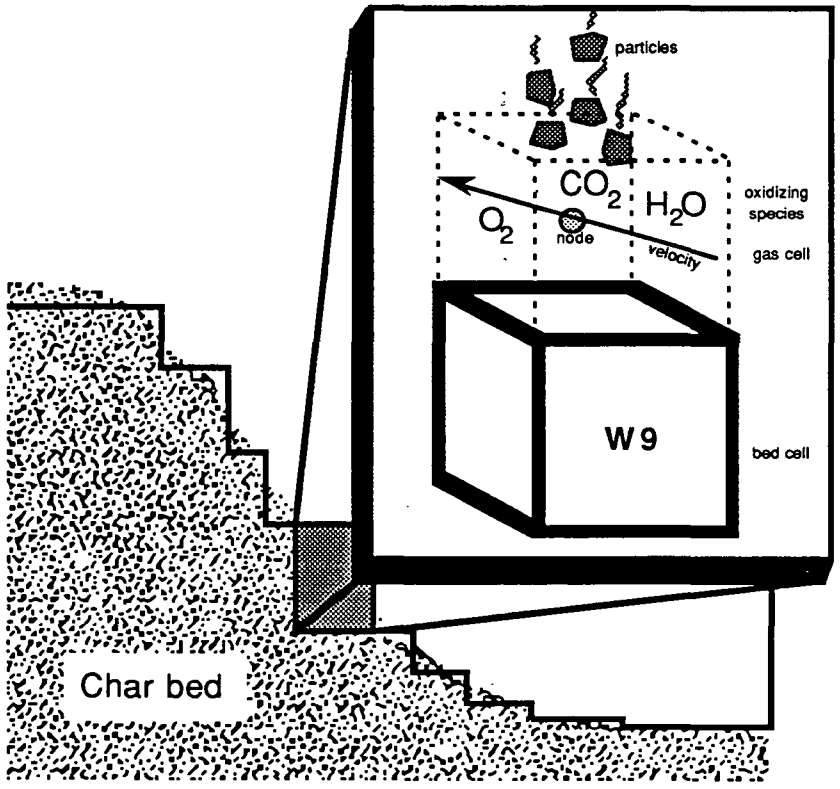

Figure 11. Representation of char bed in FLUENT/RFM.

The temperature in the gas cell is used to calculate needed physical properties. The "film" temperature, defined as the average of the gas and surface temperatures, is used to calculate the diffusivity and kinematic viscosity of the gases. The diffusivities for the oxygen, carbon dioxide, and water are calculated from a second order correlation of values obtained by the method described in Appendix V. The kinematic viscosity is based on correlated values for air and is assumed to be applicable for the gas phase.

The surface area of a cell depends on its location in the bed. If the cell is located in a flat area of the bed, the interfacial area is based on the horizontal face of the cell. If the cell is located in a sloped part of the bed, the area is that of the horizontal and any vertical interfaces. In the version of BED where the Ranz correlation is used, an additional factor of 1.9 is used to account for the fact that the surface is comprised of spheres whose exposed surface area is 1.9 times greater than the flat interfacial area. The factor of 1.9 is derived in Appendix VI.

The hydrogen from the C/H_2O reaction has to be treated as the "fuel" species since hydrogen is not handled as a separate species. A slight inconsistency is introduced by treating hydrogen as fuel. Fuel burns to CO, CO_2, and H_2O in the gas phase, so the hydrogen from the C/H_2O reaction on the bed burns to CO, CO_2, and H_2O. Thus, conservation of mass is violated since carbonaceous gases are created from hydrogen. The error caused by this inconsistency is slight. In a case discussed later, the "fuel" from the C/H_2O reaction on the bed is only 1.8% of the "fuel" entering via the black liquor spray. Treating H_2 as "fuel" is unavoidable since hydrogen is not handled as a separate species and computer memory limitations prevent the addition of another gas species at the present time.

The particle phase calculations affect the char bed since the bed ultimately receives the residual black liquor solids except for carryover. Several assumptions were made regarding the interaction between the in-flight model and the bed model. The droplets that land on the bed while in the drying stage were assumed to dry completely at the location where they landed. The amount of water vapor was entered as a source term in the gas cell immediately above the bed, but the latent heat was assumed to come from the

bed cell beneath the gas cell. Any incompletely volatilized material landing on the bed was allowed to complete volatilization. The volatiles become a source of fuel in the gas cell immediately above the bed.

The FORTRAN source code for subroutine BED is found in Appendix VII.

An iteration in FLUENT/RFM involves the calculation of mass, momentum, and energy balances on a cell-by-cell basis. Each cell has a specific number, L, and a specific three-dimensional coordinate (I,J,K) which specifies its location in the furnace. The number of cells in the three coordinate directions -- NI, NJ, and NK -- are used to make the transformation between L and (I,J,K) as follows:

$$L = I + NI * ((J-1) + (K-1) * NJ) \qquad (44)$$

The I and K coordinates correspond to the two horizontal directions and J is the vertical coordinate. If a cell has a number "L", it can be shown from Equation (44) that the cell immediately above it has a cell number of L + NI; two cells above, L + 2NI; etc.

It was necessary to add an array called BEDCEL to FLUENT/RFM to hold values which BED uses in its calculations. Rather than specifying an array for each variable needed by BED, BEDCEL was used for multiple variables to economize on scarce memory. Each variable needed by BED is stored in a vertical location relative to the bed cell as shown in Fig. 12. The particles that fall on the bed transfer information about composition and temperature into BEDCEL. The char is assumed to be comprised of carbon, sodium carbonate, sodium sulfate, and sodium sulfide. The flux to the bed is segregated into carbon, inorganic, and "burned out drops". This last component contains the inorganic salts in burned out drops including any oxygen picked up from the gas phase through oxidation of sulfide.

The other quantities in BEDCEL are related to the combustion reactions that occur in the cell. The carbon depletion rate is stored for each reaction and the total depletion rate in the cell. The reduction efficiency, relative amount of CO in the gas cell above the bed cell, and oxygen supply to the bed cell are also stored. Each of the values in BEDCEL can be viewed as a contour or color raster plot using the modified graphics routine in FLUENT/RFM.

The oxidant supply is calculated as a function of area, velocity, and gas concentration. Oxygen, carbon dioxide, and water vapor are the three gas phase oxidants of char carbon. An oxidant flux is calculated for every face of the W9 cell that is adjacent to a gas cell. For a cell in a flat part of the bed, the area is that of the horizontal interface. For a cell in a sloped region of the bed, the area is the sum of the horizontal and vertical interfaces between the bed and gas cells. The oxidant concentration and velocity are taken as those in the gas cell above the bed cell. The oxidant supply is calculated in this manner for each cell.

Oxygen comes from two sources: the gas phase and the Na_2SO_4 from particles which have burned out in flight. The oxygen supplied from the gas phase depends on the mass transfer coefficient discussed earlier and the kinetic rates of the Na_2S/O_2 and C/O_2 reactions. The Na_2S/O_2 kinetic rate is assumed to be infinitely fast relative to the mass-transfer coefficient while the C/O_2 kinetic rate is based on Equation (24). The total oxygen transfer from the gas phase is divided between the Na_2S/O_2 and C/O_2 reactions by a partition function. The partition function, P, is based on physical reasoning and represents the fraction of the char surface which is solid carbon. The value (1-P) is the fraction of the char surface which is liquid smelt. Thus, P*100 % of the oxygen supplied from the gas phase reacts with char via the C/O_2 reaction, the remainder reacting via the Na_2S/O_2 reaction. The development of

the expression for P is discussed in the paper in Appendix I.

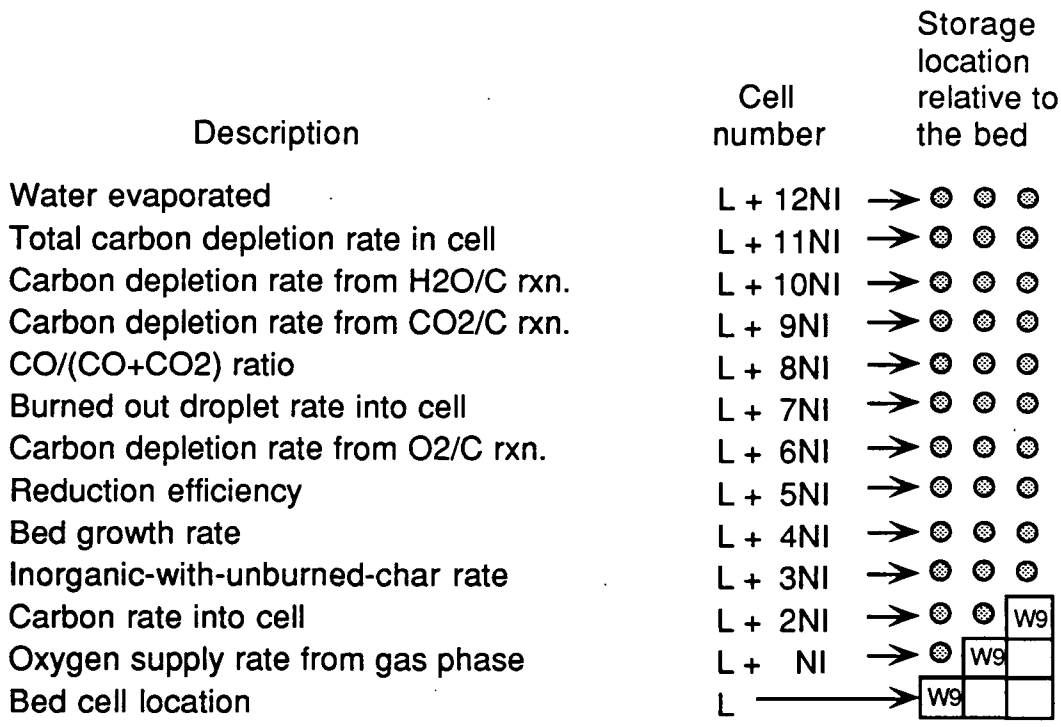

Figure 12. Storage locations in BEDCEL.

A reactor model must be adopted to provide a basis for the mass balances in the bed cell. The gas-phase model is pseudo-steady state; the time derivatives in the gas-phase balances are set to zero. Globally, the system is not at steady state. It is possible for the char bed to grow or shrink depending on the supply from the particles and the bed burning rate. The char supply and depletion rate in individual bed cells will not match in general. The mass balance for the bed must handle the depletion and growth terms.

The three most common chemical reactor models are the batch reactor, the plug flow reactor (PFR), and the continuous stirred tank reactor (CSTR). The batch reactor is not appropriate since the simulation is on a steady state basis. The PFR and CSTR are possible starting points for the

model of the reaction zone.

The PFR model is based on idealized flow and reaction in a plug flow reactor. The reactants are assumed to be perfectly mixed in the radial direction and perfectly segregated in the axial direction. Reactants enter the reactor and flow cocurrently until they exit the reactor.

The surface reactions on the char bed can be simulated with a PFR model. The following variables will be used to develop the PFR model of the char reaction zone:

Q = volumetric flowrate
S = interfacial surface area
G = mass flux to the bed cell
h = depth of the cell
ρ = char density in the cell
V = volume of the cell
t_r = residence time in the cell
C_0 = initial carbon concentration
f = fractional conversion of carbon
R_C = rate of carbon combustion

The mass flux, char density, and depth of the cell below the bed surface define the residence time:

$$t_r = V/Q = hS/GS/\rho = h\rho/G \tag{45}$$

The PFR steady state mass balance over the reaction zone results in the following expression:

$$C_0 \int_0^f \frac{df}{-R_C} = t_r = \frac{h\rho}{G} \tag{46}$$

Equation (46) can be solved in two ways. The residence time can be

specified, leaving f to be determined, or, f can be specified and t_r calculated. The later approach will be used for the purpose of discussion. The product $h\rho$ can be calculated from Equation (46) once t_r is calculated and G is specified; then, a penetration depth, h, is calculated assuming a constant density for char.

The PFR model of the char reaction zone has several deficiencies. Not all of the char components will flow through the reaction zone in a plug flow manner. Smelt drops can flow out of the reaction zone while unburned char remains in the reaction zone. Another objection is that too many arbitrary parameters need to be specified. For example, if a cell does not receive a carbon flux, G would technically be zero, resulting in an infinite residence time. This problem could be fixed by saying that the cell is shrinking and specifying a mass flux G from the subsurface region of the char bed. The specification of G can be chosen to give a physically realistic residence time, but the value of G is still arbitrary. Equation (46) is for a steady state mass balance and does not address the handling of growth or depletion terms. A broad range of residence times and penetration depths may result across the bed which may not be physically realistic. In summary, a PFR model is inadequate for the char bed surface reactions.

The CSTR model cannot be directly applied to the char reaction zone, but a modified CSTR model is more feasible than the PFR model. An ideal CSTR assumes a perfectly mixed reaction zone with the outlet concentrations being equal to the concentrations in the reaction zone. In order to model the char reaction zone, a perfectly mixed control volume must be assumed.

The surface combustion model is based on a thin, perfectly-mixed region on the surface of the char bed. The reaction zone is depicted in Fig. 11 where W9 denotes the bed cell and the sphere denotes the node of the gas cell

adjacent to the bed cell. The model's assumptions are similar to those of a CSTR with some modifications. When a CSTR model is employed, the assumptions are made that the reaction zone is perfectly mixed, the outlet concentration of a species equals that of the reactor concentration, and a steady state exists. Several deviations from this model are made to arrive at the bed model.

One deviation from a CSTR is that the bed cell is not necessarily at steady state. There is no way to guarantee that an individual cell will have the incoming carbon equal to the carbon depletion. Char carbon supply to and consumption by reaction in a bed cell are modeled as totally independent events and normally would not balance. The cell balance must allow for accumulation and depletion terms. The total bed "growth" rate is then the sum of the growths in the individual cells. The growth can be positive or negative. The cell balance for a positive growth is different from that of a negative-growth cell. The calculations are performed on a steady state basis, but there is a growth term. The growth term implies dynamics, but it is really only the excess or deficiency of char in the cell to make the equations balance. A large deviation from zero growth would be an unstable condition.

Another deviation from the CSTR model is that the concentration leaving the reaction zone is not necessarily the concentration within the reaction zone for every species. This condition is caused by the heterogeneous nature of the reaction zone. The smelt does not form from the particle until enough of the carbon matrix is consumed. The smelt is free to flow away from the reaction zone after the particle burns out, and the residual carbon leaving in the smelt will be quite small, probably less than 2%. The CSTR model assumes that the reaction occurs at the concentration in the reaction zone, but employing the CSTR assumption to the bed cell would underestimate the

reaction rate since the representative carbon concentration would certainly be higher than 2%. The problem of determining the most applicable carbon concentration lies in the fact that smelt is free to flow from the reaction zone as soon as it is free from the carbon matrix, but carbon and its associated inorganic compounds can stay in the reaction zone until it is either buried by incoming char or it is burned. It is therefore more accurate to use a carbon concentration which is representative of char on the surface rather than the carbon concentration of the smelt as it leaves the reaction zone. The bed cell assumes that no carbon flows out with the smelt, but rather, it stays in the reaction zone until it is burned or accumulated. A carbon concentration of 2 mole C/mole Na_2 is the assumed carbon concentration in the reaction zone. This is 2/3 of the average carbon concentration before burning shown in Table 5. An average carbon concentration of incoming particles is chosen rather than the carbon concentration of incoming particles because many cells do not have incoming particles. The carbon concentration affects the kinetic rate of the C/Na_2SO_4, C/CO_2, and C/H_2O reactions. In the next section, it is shown that the predicted carbon depletion rate is not sensitive to the assumed carbon concentration for a range of bed temperatures (see Tables 11 and 12).

The Mass Balances

The algorithm for the mass balances will be described in this section. The FORTRAN source code in Appendix VII will be discussed in general terms first, followed by the specific mass balance equations.

The reaction volume is the area of the horizontal interface multiplied by an assumed depth of gas penetration. The value assumed in the model is two centimeters. A small depth is expected based on the experimental work of Aiken[6] and Li[13]. Aiken found that a small circular jet penetrated a crushed char

surface only a few millimeters. Li studied the char/CO_2 reaction and concluded that gases would not penetrate far into the bed. As discussed in the literature review, the depth is less than a few centimeters.

The reaction rate expression for the carbon/sulfate reaction must be transformed to fit into the modified CSTR approach taken to model the reactions in the bed cell. The reactor volume is:

$$V_R = \text{horizontal surface area} * \text{depth} \qquad (47)$$
$$= A * h$$

The depth is assumed to be 2 cm. The units of the carbon/sulfate rate can be converted from mole C/mole Na_2-sec to kg C/sec. R_{CS} in units of mole C/mole Na_2-sec is:

$$R_{CS} = \frac{4(1310)}{2\text{-}f}\left\{\frac{1 - r}{0.0033 + 1 - r}\right\}[C]\, e^{\frac{-14{,}696}{T}} \qquad (48)$$

where

r = reduction efficiency
f = molar $CO/(CO + CO_2)$ ratio
[C] = carbon concentration, mole C/mole Na_2

The transformation to kg C/sec is made by assuming a char composition and density. A "char molecular weight" of 132 g char/mole Na_2 is obtained by adding the weights of the compounds from the simplified char composition in Table 5. A carbon content of 2 mole C/mole Na_2 rather than 3 is assumed in arriving at the value of 132 g char/mole Na_2 . A uniform char density of 0.3 g/cm^3 is assumed. The carbon concentration is converted as follows:

$$\text{kg C} = [C]\frac{\text{mole C}}{\text{mole Na}_2} * 0.012\frac{\text{kg C}}{\text{mole C}} * \frac{\text{mole Na}_2}{0.132\text{ kg char}} * 300\frac{\text{kg char}}{\text{m}^3} * V_R\ \text{m}^3 = 27.27V_R[C] \tag{49}$$

The carbon/sulfate rate in kg C/sec is therefore:

$$R_{CS} = \frac{142900 * V_R}{2 - f}\left(\frac{1 - r}{0.0033 + 1 - r}\right)[C]\, e^{\frac{-14,696}{T}} \tag{50}$$

The depth of the reaction volume, h, and the carbon concentration, [C], are two arbitrary model parameters which, when taken together, determine the residence time in the reactor volume. Values for these variables were chosen based on physical reasoning, but precise values are uncertain. The sensitivity of the overall rate to these variables will now be discussed.

The rate of the C/Na_2SO_4 reaction relative to the mass transfer rate is shown in Table 11 as a function of temperature, h, and [C]. The assumptions that were made are as follows:

1) Equation (50) is used to calculate the C/Na_2SO_4 rate.

2) Brown's mass transfer correlation is used (Equation (35)), giving an optimistic estimate of the mass-transfer coefficient.

3) The velocity for the mass transfer coefficient is 8 m/s. This is the average velocity across the bed calculated for one of the simulations discussed later.

4) An oxygen concentration of 5% is used based on the average concentration across the bed in a later simulation.

Table 11. Ratio of C/Na_2SO_4 rate to mass transfer rate.

	h = 2 cm		h = 4 cm	
	[C] = 2	[C] = 0.75	[C] = 2	[C] = 0.75
1200 K	8.7	2.2	17.4	4.4
1300 K	23.5	6.1	47.0	12.2
1400 K	55.8	14.4	112.0	28.8

[C] [=] mole C/mole Na_2

Table 11 shows that mass transfer controls the reaction rate over most conditions. At lower carbon concentrations and low assumed depths, the kinetic rate is comparable to the mass transfer rate. The bed model prediction will be more sensitive to the kinetic rate, i.e. the values of h and [C], at lower temperatures (1200 K) and lower carbon concentrations (0.75). The more mass transfer controls, the less sensitive the predicted rate will be to the values of h and [C].

The carbon depletion rate due to the gasification reactions is based on a combination of mass transfer- and chemical resistances. The mass transfer rate is equated to the kinetic rate as follows:

$$R_{CO_2} = k_m(C_{CO_2\,B} - C_{CO_2\,S})A = \frac{-k_1 C_{CO_2\,S}[C]}{1 + k_2 C_{CO_2\,S} + k_3 C_{CO}} e^{\frac{-E}{RT}} \qquad (51)$$

The subscripts "B" and "S" refer to the bulk and surface concentrations, respectively. Equation (51) is solved for $C_{CO_2\,S}$. R_{CO_2} is then calculated by substituting $C_{CO_2\,S}$ into one of the expressions in Equation (51). The C/H_2O reaction is handled in an analogous manner by substituting appropriate quantities for water vapor.

A sensitivity study similar to that shown in Table 11 was done for the C/CO_2 reaction. The kinetic rate expression for the gasification also has h and [C] in it when it is transformed in the same manner as Equation (48). The assumptions for the C/CO_2 sensitivity study are the same except that CO and CO_2 concentrations were assumed instead of an oxygen concentration. Values of 10% were assumed for the CO and CO_2 concentrations based on average values across the bed in a later simulation. Table 12 shows that the gasification reactions will be more sensitive to the values of h and [C]. The kinetic rate and mass transfer rate are comparable at low temperatures. A carbon concentration of 2 mole C/mole Na_2 and a reactor depth of 2 cm gives about the same relative rates as a carbon concentration of 0.75 mole C/mole Na_2 and a reactor depth of 4 cm.

Table 12. Ratio of C/CO_2 rate to mass transfer rate.

	h = 2 cm		h = 4 cm	
	[C] = 2	[C] = 0.75	[C] = 2	[C] = 0.75
1200 K	0.9	0.3	1.8	0.7
1300 K	3.9	1.5	7.8	2.9
1400 K	13.0	4.9	25.9	9.7

[C] [=] mole C/mole Na_2

The sensitivity studies just discussed can be summarized in terms whether the reaction is controlled by the kinetic rate or the mass transfer rate. The kinetic rate controls at low temperatures and low carbon concentrations while the mass transfer controls at high temperatures. There is a breakpoint in some temperature range where the kinetic and mass transfer rates are both important. The values of h and [C] determine the breakpoint between kinetic

control and mass transfer control.

The algorithm for determining reduction efficiency and the oxygen balance will now be discussed. In the FORTRAN code in Appendix VII, the following variables are used in the calculation of the C/Na_2SO_4 rate and reduction efficiency:

QBED = f as defined above (Equation (48))

RED = r as defined above (Equation (48))

O2NA2S = oxygen from gas phase which oxidized Na_2S to Na_2SO_4

O2SO4 = oxygen in the form of Na_2SO_4 in burned out drops

FR = function of RED in C/Na_2SO_4 rate equation = $\frac{1 - RED}{0.0033 + 1 - RED}$

Figure 13 shows the algorithm used to determine the C/Na_2SO_4 rate and reduction efficiency. The circled numbers in Fig. 13 refer to the following comments:

(1) The C/Na_2SO_4 rate can be no greater than the sum of the oxygen supplied from the gas and sulfate in burned out drops. The rate is mass transfer controlled to varying degrees if the kinetic rate exceeds the oxygen supply.

(2) The oxygen supply rate in the form of sulfate is greater than the zone's ability to reduce the sulfate to sulfide. RED is set to zero.

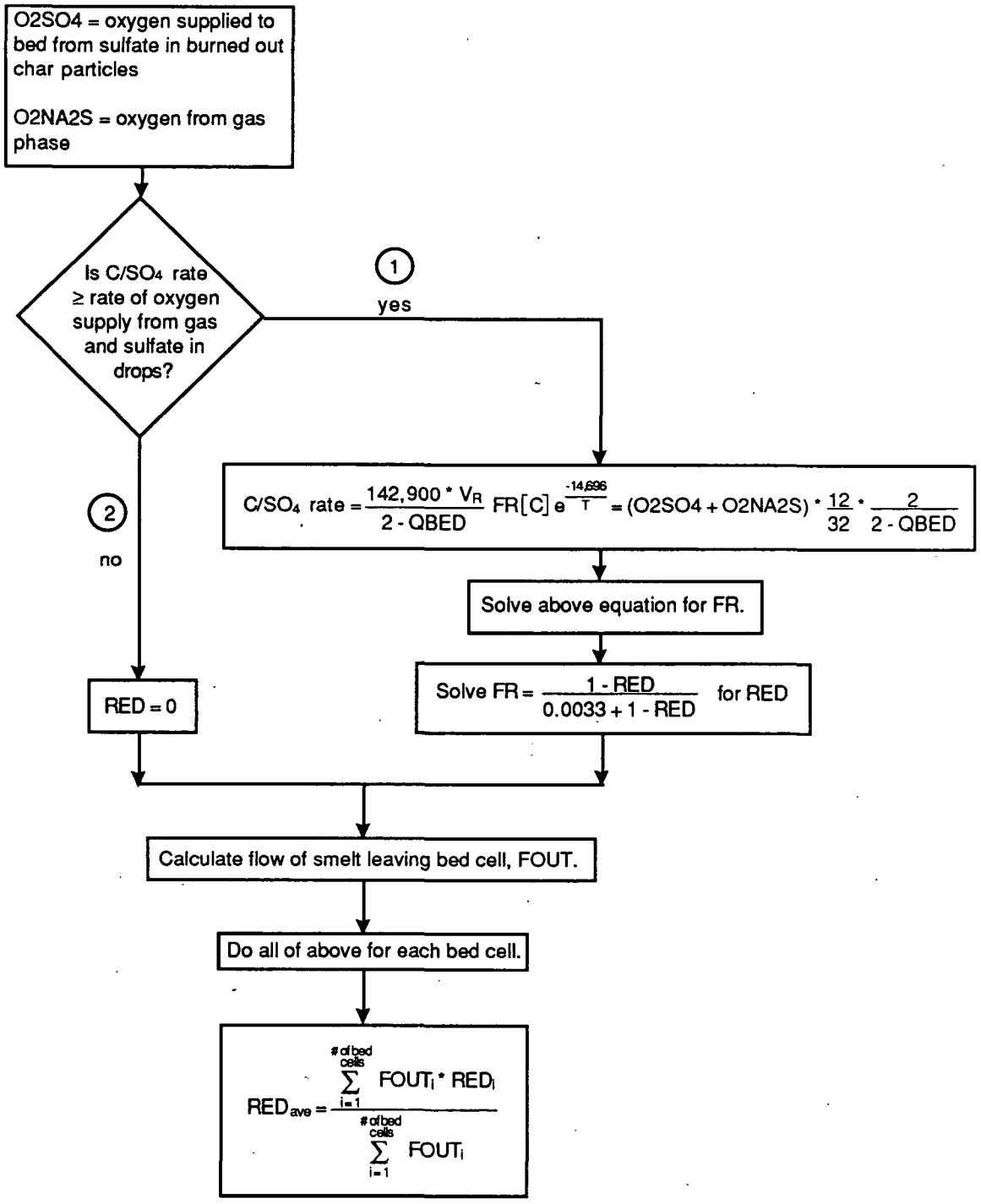

Figure 13. Algorithm for calculating reduction efficiency.

The function FR shown in Fig. 13 is solved for reduction efficiency. FR is plotted as a function of r in Fig. 14. The calculation of r will not be sensitive

to values of h or [C] as long as FR is small. It can be seen from Fig. 14 that r is insensitive to changes in FR at reduction efficiencies close to 1, but r is very sensitive to changes in FR from zero reduction efficiency to about 90% reduction efficiency. If FR is 0.2, cutting the assumed reaction depth in half will double FR to 0.4; however, Fig. 14 shows that going from FR equal to 0.2 to FR equal to 0.4 barely changes the predicted value of r. On the other hand, if

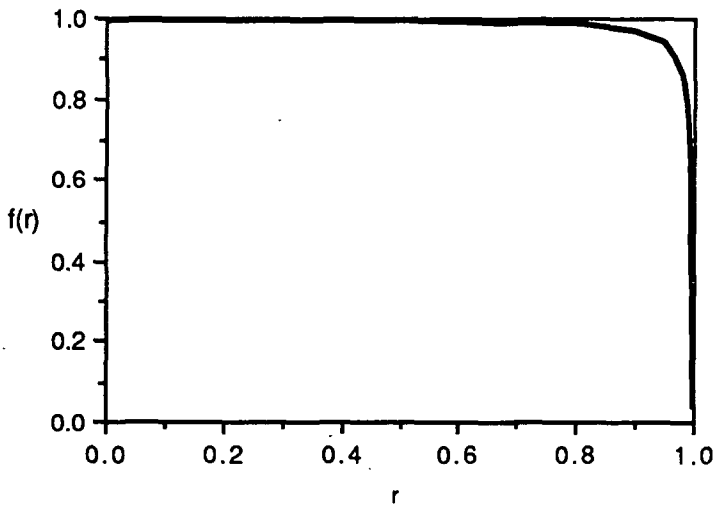

Figure 14. FR as a function of reduction efficiency, r.

FR is 0.49, cutting the assumed reaction depth in half will double FR to 0.98, changing the predicted reduction efficiency from a value close to 1 to a value close to 0.

Table 13 shows values of FR which were computed using the same assumptions used to calculate the numbers in Table 11. Nearly all the values of FR in Table 13 are low enough that the predicted reduction efficiency will not be sensitive to changes in h or [C] except at low temperatures coupled with low carbon concentrations.

Table 13. FR as a function of temperature, depth, and carbon concentration.

	h = 2 cm		h = 4 cm	
	[C] = 2	[C] = 0.75	[C] = 2	[C] = 0.75
1200 K	0.11	0.45	0.06	0.23
1300 K	0.04	0.16	0.02	0.08
1400 K	0.02	0.07	0.01	0.03

[C] [=] mole C/mole Na_2

The sources to the bed in the oxygen balance are oxygen from the gas phase, and oxygen in the form of sulfate in burned-out char particles. The oxygen in the air can react with sulfide or react directly with char carbon. The carbon depletion rate from direct carbon oxidation is assumed to be first order in oxygen concentration. For an irreversible heterogeneous reaction which is first order in oxygen concentration, the rate of oxygen consumption is K^*C_{BO} where the reaction constant K is comprised of the mass-transfer resistance and chemical reaction resistance in series [16]. The mass-transfer coefficient, k_m, and chemical reaction constant, k_r, make up K as follows:

$$K = \frac{1}{\frac{1}{k_m} + \frac{1}{k_r}} \qquad (25)$$

k_r is calculated using Equation (24).

Figure 15 shows the algorithm for the oxygen balance.

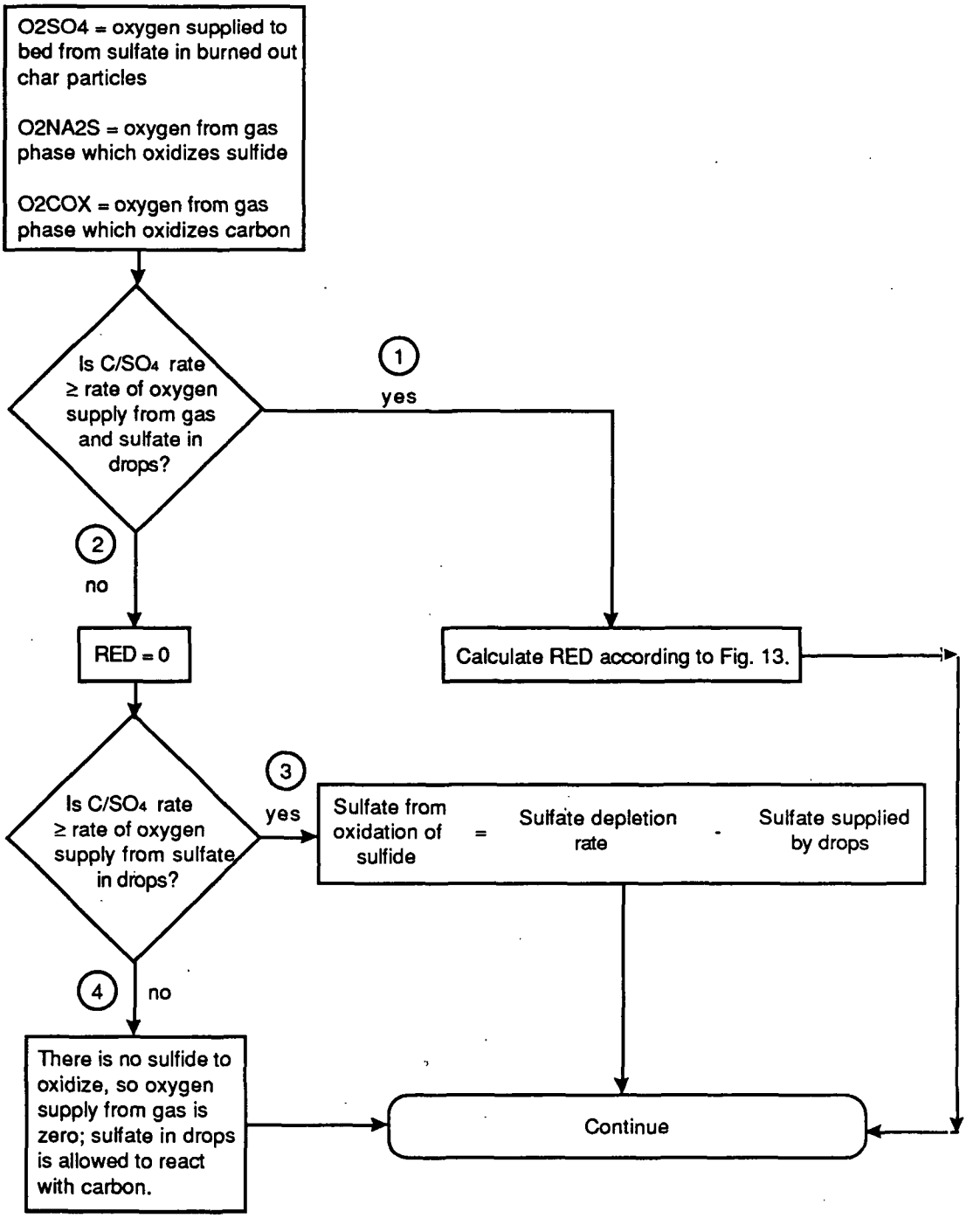

Figure 15. Algorithm for the oxygen balance.

The first part of the algorithm in Fig. 15 is the same as the top of Fig. 13. The following comments apply to the circled numbers in Fig. 15:

① The C/Na_2SO_4 rate can be no greater than the sum of the oxygen supplied from the gas and sulfate in burned out drops. The rate is mass transfer controlled to varying degrees if the kinetic rate exceeds the oxygen supply.

② The oxygen supply rate in the form of sulfate is greater than the zone's ability to reduce the sulfate to sulfide. RED is set to zero.

③ The sulfate reduction is greater than the sulfate supply in the burned out drops. The amount of gas-phase O_2 originally supplied is reduced to make the sulfate balance close.

④ The sulfate supply in burned-out particles exceeds the sulfate reduction rate. No oxygen is transferred from the gas phase since the sulfide is already oxidized. The sulfate in the drops is allowed to react with carbon so there will be no accumulation of sulfate in the bed.

Now the method of calculating the net growth of a cell will be discussed. In the mass balances that follow, the symbols "A", "F", and "R" stand for accumulation, flow rate, and reaction rate. The subscripts "C", and "I" stand for carbon and inorganic.

The growth of an individual cell is calculated based on the carbon balance. The total carbon depletion rate is the sum of the C/Na_2SO_4, C/O_2, C/CO_2, and C/H_2O rates. If a positive growth is calculated, carbon and inorganic accumulate at a rate based on the char composition of the char entering that cell. If a negative growth occurs, an assumed subsurface char composition is

used to calculate the accumulation.

Unburned char is assumed to not flow out of the cell. This assumption is reasonable if it is assumed that the smelt does not flow until the carbon reaches some small value and the fraction that this carbon represents is negligible. If the carbon depletion rate is less than the carbon reaching the bed from unburned particles, the cell will grow. If the reaction rate is greater than the carbon supply, the cell will shrink. A shrinking cell implies that carbon flows into the reaction zone from the the subsurface region at a rate which matches the carbon demand at the surface. The formulation of the balance for a growing cell will be different from that of a depleting cell.

The carbon balance is made up of the rate of carbon accumulation, the unburned particles entering the cell, and the carbon depletion rate:

$$A_C = F_{C\ in} - R_C \tag{52}$$

The total carbon depletion rate, R_C, is the sum of the rates for the C/Na_2SO_4, C/O_2, C/CO_2, and Na_2S/O_2 reactions. If A_C is positive, the cell is growing and char accumulates at a rate which is proportional to the rate of carbon entering the cell:

$$A_{char} = A_C * (F_I + F_C)/F_C \tag{53}$$

If A_C is negative, the cell is shrinking and char must enter the cell from the subsurface region of the bed. Based on the assumed char composition:

$$A_{Char} = 120.7/24 * A_C \tag{54}$$

The flow of smelt out of the cell is based on an overall mass balance on

the char in the cell:

$$F_{out} = F_C + F_I - R_C - A_{char} \qquad (55)$$

The Energy Balance

The energy balance in a bed cell is performed as if it was a thin reaction zone on the surface of the bed. The reasons for this approach and the development of the energy balance are discussed in this section. A case in FLUENT requires that the boundary conditions between the wall and fluid phase be specified. Zero fluid velocity at the wall is the usual boundary condition for fluid flow, but there are more options for the thermal boundary condition.

A temperature must be specified for each type of wall cell, but the specified temperature can be further acted on by other options. FLUENT has four options for the thermal boundary condition, three of which may be relevant to the bed: an isothermal wall, an adiabatic wall, and a specified heat flux at the wall. These boundary conditions will be shown to be inadequate for use in the bed model energy balance if they are not modified. After discussing the merits of these three boundary conditions in FLUENT, a modified boundary condition will be discussed.

An isothermal wall specifies the temperature at which heat is exchanged with the surroundings. The isothermal wall boundary condition uses the wall temperature originally specified in the case. A bed temperature of 1300 K, for example, means that the bed radiates heat into the furnace at 1300 K and receives heat back from the furnace at the gas temperature. The difference between these two quantities is the net heat flux to or from the bed.

If the calculated bed temperature is 1300 K, the furnace energy balance is satisfied; if the calculated bed temperature is not 1300 K, there will be some inconsistency in the furnace energy balance because 1300 K was used in the radiation calculation.

An adiabatic wall is a second type of boundary condition. The heat flux from the surface into the bed is small relative to the heat flux between the surface and the gas phase, but the surface can not be considered adiabatic since chemical reactions are occurring there. The subsurface of the bed acts as an insulator and the bed surface can be considered as an adiabatic or reradiating wall. This boundary condition is obtained in FLUENT by "cutting the link" between the wall cell and the first gas cell so that the net heat flux at the interface is zero. Cutting the link causes a zero gradient condition at the boundary. A temperature gradient of zero results in no heat flux to the wall. In essence, the bed temperature in this case would consist of the temperatures of the gas cells adjacent to the bed cells which comprise the char bed.

Alternatively, the heat flux at the boundary can be specified. This boundary condition would be similar to the adiabatic wall if a heat flux of zero is specified. An important difference is that a zero heat flux would still use the specified boundary temperature in the heat balance, causing some inaccuracy in the overall energy balance.

The adiabatic wall is inadequate because it uses the temperature of the gas cell adjacent to the bed surface in the energy balance rather than the surface temperature. Furthermore, the adiabatic wall does not allow for energy exchange due to chemical reaction. The isothermal wall and zero heat flux boundary conditions are also inadequate. Thus, a new boundary condition was established whereby a surface energy balance was used to calculate a surface

temperature, and that temperature is used to calculate the radiative heat transfer between the bed surface and the furnace cavity. The bed surface will be considered adiabatic to the extent that heat transfer into the subsurface of the bed is negligible compared to heat exchange between the surface and the furnace cavity.

This last point is demonstrated by treating the subsurface bed as a slab in which heat flows only from the bed surface to the furnace floor. For a char bed, the conductivity as a function of temperature has been estimated as follows:[18]

$$k = (1-f)\{0.05 + 4\phi D_p \sigma T^3\} + 0.26f \qquad (56)$$

where

σ = $0.1712 * 10^{-8}$ BTU/hr-ft^2-°R^4
D_p = 0.00328 ft = assumed pore radius
ϕ = 0.7 = assumed void fraction
f = 0.2 = assumed fraction of bed occupied by liquid smelt.

Thus,

$$k = 0.092 + 1.57*10^{-11} T^3 \qquad (57)$$

The flux , q, into the bed is k(T)dT/dx. If the bed temperature is 1800 °F, the floor temperature is 600 °F, and the bed height is five feet, the flux into the bed is roughly -42 BTU/hr-ft^2. This flux is small compared to the fluxes into the furnace which are on the order of 1000 - 10,000 BTU/hr-ft^2. Thus, the subsurface of the bed acts like an insulator in the furnace.

The approach taken in the bed model is to calculate a surface temperature rather than a gas cell temperature. The calculated temperature in each cell replaces the boundary condition temperature that was initially specified when the base case simulation was set up. A few cells have extreme temperatures, so the surface temperature is not allowed to go above 1700 K or

below 900 K when extreme temperatures are calculated. The high surface temperatures are a result of artificially high temperatures in the gas phase which cause radiation back to the surface to be overestimated. The low temperatures can be caused by cooling of the surface by the primary air. In this case, the bed cell may not have enough thermal capacity to keep the calculated temperature near the melting point of smelt. Setting the lower bound to 900 K is rationalized by assuming that the cell can draw on the thermal capacity of the subsurface to keep the temperature at 900 K. There are few cells where it is necessary to cut off temperatures outside the range of 900 - 1700 K. The calculated temperature updates the previous value each time BED is called.

The energy balance on the thin surface layer is comprised of the following terms:

	1)	convection in via gases
	2)	convection in via mass of particles
IN	3)	convection of mass in from subsurface (when accumulation < 0)
	4)	radiation in from gas phase
	5)	exothermic reaction
	6)	convection out of combustion gases
	7)	flow of smelt out
	8)	endothermic reaction
	9)	heat of fusion
OUT	10)	radiation out
	11)	convection out of excess char (when accumulation > 0)
	12)	convective heat exchange
	13)	conduction to subsurface (assumed negligible)
	14)	latent heat of water

The sensible heat terms were based on average heat capacities at 1100 K -- the assumed reference temperature for the energy balance. Table 14 shows the values used and the literature reference.

Table 14. Heat capacities used in bed cell energy balance.

	Value, J/Kg-°C	Source
Fuel	1194	--
H_2O	2326	34
O_2	1015	34
CO	1194	34
CO_2	1115	34
Smelt	1788	35
Char carbon	1788	--

The heat of fusion was assumed to be $3.16 * 10^5$ J/Kg -- the value for sodium carbonate from the JANAF tables[35]. Table 15 lists the assumed heats of reaction:

Table 15. Heats of reaction.

Reaction	J/Kg carbon * 10^6
$C/Na_2SO_4 \rightarrow CO_2$	7.11
$C/Na_2SO_4 \rightarrow CO$	10.57
Na_2S/O_2	-12.30
$C/O_2 \rightarrow CO_2$	-32.86
$C/O_2 \rightarrow CO$	-9.42
C/CO_2	14.04
C/H_2O	11.36

A convective heat transfer coefficient of 10 BTU/hr-ft^2-°F was assumed based on a typical value for convective heat transfer coefficients found in Bird[25]. A simple convective heat transfer model is sufficient since radiative heat transfer will dominate the energy balance in the lower part of the furnace. The heat transfer coefficient can be updated to take the same form as the mass

transfer coefficient when a final mass transfer correlation is developed. Heat transfer coefficients calculated using the laminar flat-plate correlation range between 2 and 20 BTU/hr-ft^2-°F. The value 10 BTU/hr-ft^2-°F is a good average.

The radiative exchange between the bed surface and gas phase is calculated using the formula that was used in the original version of FLUENT. The same methodology was used for consistency. FLUENT uses a six-flux radiation model for calculating the radiative heat fluxes in the furnace. The net heat flux between the bed cell and the gas phase is calculated using Equation (58)[36]:

$$Q_{rad} = \frac{2 * \varepsilon_w}{2 - \varepsilon_w} * \text{Area} * (\sigma T^4 - \text{RAY}) \qquad (58)$$

where

ε_w = emissivity of the wall
σ = Stefan-Boltzman constant = 5.67 * 10^{-8} W/m^2-K^4
RAY = radiant flux in the vertical direction (from the six-flux model)
T = bed surface temperature, K

The energy balance for each bed cell is calculated based on the heat flows into and out of the cell and the heats of reaction in the cell. The Newton-Raphson method is used to solve the energy balance for temperature since there are first- and fourth-order terms.

THE BASE CASE

Jones constructed a simulation of the entire recovery boiler to test FLUENT/RFM. The base case was shown to converge, and several modifications have since been made with respect to BED and the method of releasing pyrolysis gases from the bed. These modifications are examined in the DISCUSSION section. A diagram of the base case is shown in Fig. 16.

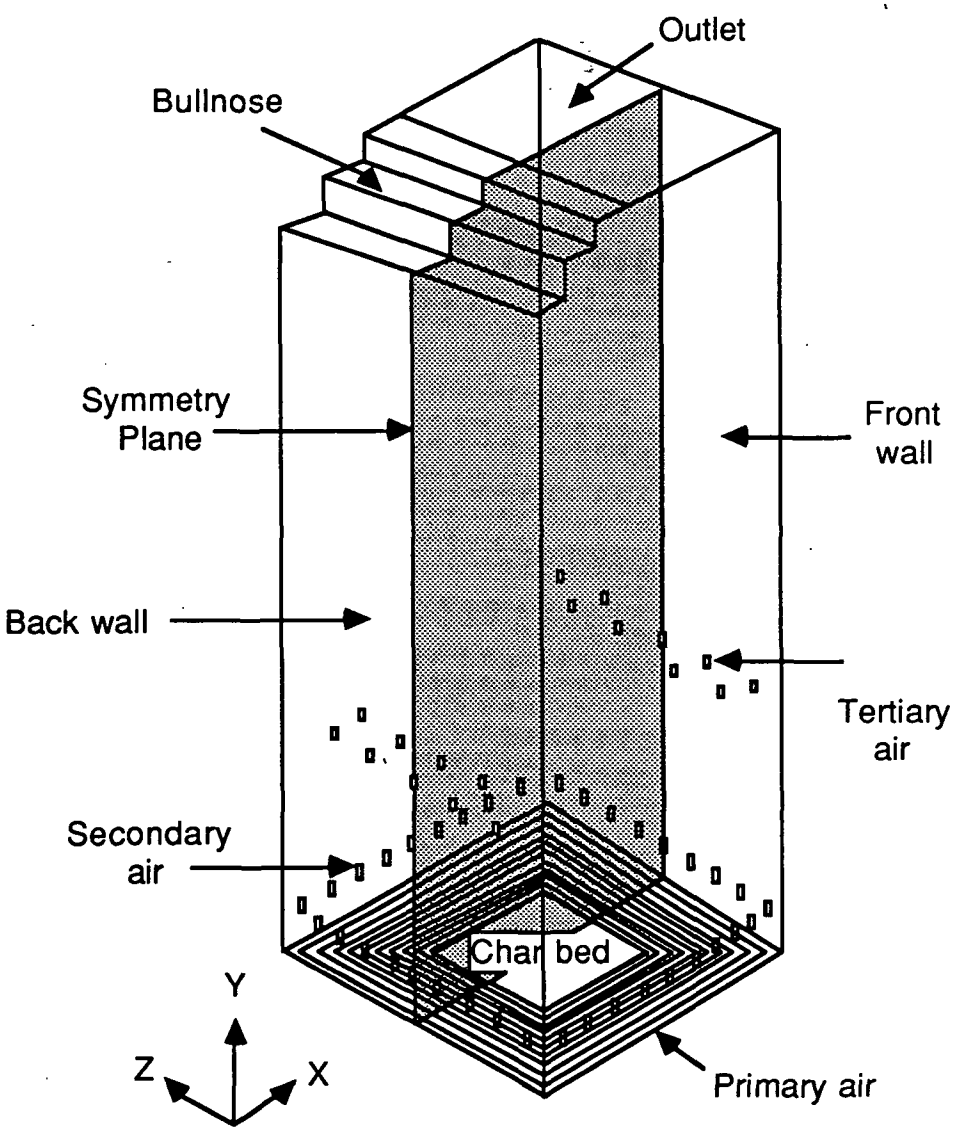

Figure 16. Outline of the base case.

The furnace cavity is modeled by packing 50,000 cells into half the furnace and assuming a vertical plane of symmetry. This treatment allows a finer grid to be used. The furnace is ten meters wide, five meters deep (ten meters when the symmetry plane is taken into account), and thirty meters high. If the cells were perfect cubes, the average dimension of a cube would be 31 centimeters on a side; however, the node requirements around the air ports and the bed are such that unusual cell shapes occur. The bullnose is sloped downward towards the back of the furnace, and occupies approximately half the cross-sectional area of the furnace. The 50,000 cells are distributed as follows: 40 in the Y direction, 25 in the Z direction, and 50 in the X direction.

The char bed has the shape of a truncated pyramid. The sloped faces of the bed are represented by a stair-step structure which is fine enough so that there are no observable artifacts caused by the grid structure.

In the base case, the primary air port is a slot jet, the secondary air ports are on all four walls, and high-velocity tertiary air ports are located on the front and back wall. Table 16 lists relevant parameters for the air ports. The air flow rate was ten percent in excess of the stoichiometric requirement of the black liquor.

Table 16. Air port parameters.

	velocity	% of supply	#/wall	shape	location
Primary	43 m/s	45	1	slot, 0.026 m	floor
Secondary	39 m/s	34	9	0.114 x 0.214 m	2 m above primary
Tertiary	93 m/s	21	9	0.114 x 0.111 m	front and back wall 8.5 and 9.75 m above floor

The black liquor was sprayed at a rate of 2.25 pounds of black liquor solids per square foot hearth per minute. One black liquor nozzle is located six meters above the hearth in the center of each wall. The droplet sizes were

assumed to follow a lognormal distribution. A breakdown of the black liquor is shown in Fig. 17. The liquor is 65% solids; the solids are 50% inorganic salts, 30% pyrolysis gases, and 20% char carbon; the in-flight char combustion products are 90% CO and 10% CO_2 ; the products of pyrolysis gas combustion are split evenly between CO and H_2O although provision is made to specify a fraction of CO_2 .

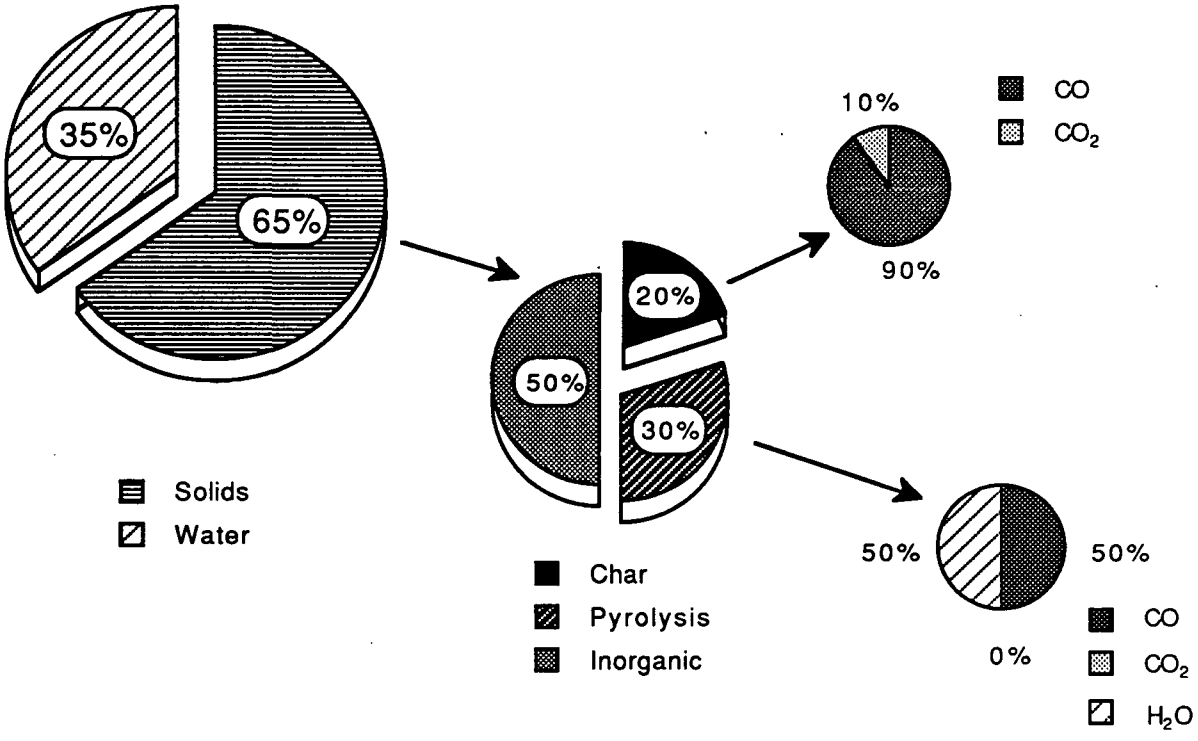

Figure 17. Assumed black liquor pathways.

The C/CO_2 and C/H_2O reactions were excluded in the base case bed model. Their effect on the bed model will be discussed the GASIFICATION REACTIONS section.

RESULTS

After the base case was converged, changes were made to the bed model to study their effect on bed and furnace behavior. The results of the base case show many aspects of bed behavior which are common to all of the cases. These general results found in the base case will be presented first. The effects of the changes to the bed model will then be presented in the discussion section.

The results of bed calculations that are presented in the form of contour or color raster plots are displayed using the plan view (looking down from above). The three-dimensional bed is mapped onto a two-dimensional plane. The spacing between lines on the contour plots indicates the size of the gradient, while the color scale is used on the color raster plots to show the variation across the surface of the bed. The general color scheme uses violet for a low value and red for a high value. The colors between the high and low proceed through the color spectrum as follows: red, orange, yellow, green, blue, indigo, and violet.

Figure 18 is a contour plot of the mass reaching the bed which includes the char carbon and inorganic material but excludes water or volatiles. The water and volatiles are put instantaneously into the gas cell immediately above the bed cell. The material reaching the bed includes particles which hit the bed during flight, "chunks" of partially pyrolyzed solids from the wall, smelt drops which have first hit the wall, and smelt drops which hit the bed during flight. The particle tracking algorithm assumes that any particles which hit the bed are trapped at the location where they hit. The contour plot shows that most of the residual black liquor solids fall on the periphery of the bed. The closeness of spacing between the contour lines indicates the magnitude of mass

reaching the bed. Very little material is reaching the middle of the bed (few contour lines) , while most of the mass flux to the bed lands on the periphery of the bed (many contour lines).

There is a discrepancy between the mass reaching the bed and the assumed bed shape. The material reaching the bed suggests a build up of the bed around its periphery. The bed shape is rationalized by assuming that the excessive material landing on the periphery is redistributed by the force of the primary jets to arrive at the assumed bed shape. The issue of bed shape is discussed more fully in the section titled EFFECT OF BED SHAPE ON FURNACE BEHAVIOR.

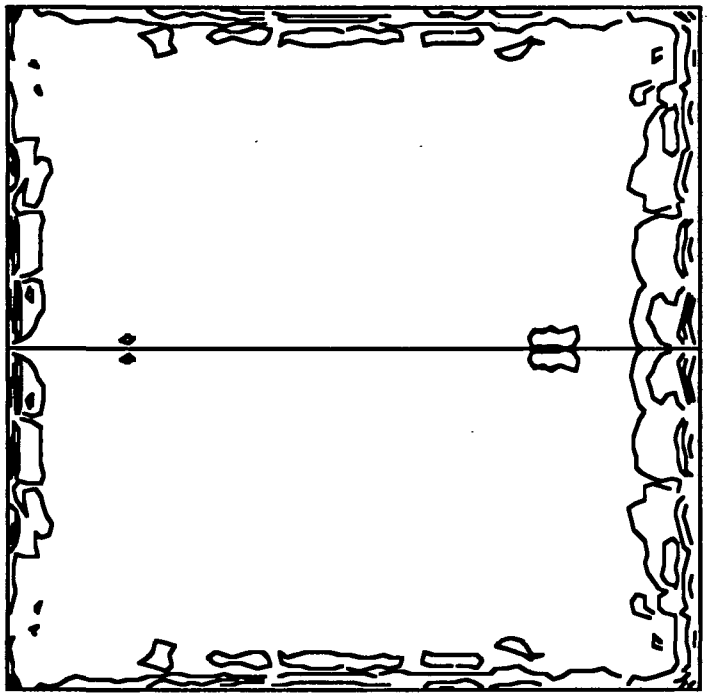

Figure 18. Mass of black liquor solids reaching the char bed.

Figure 19 shows a color raster plot of the fuel concentration in the gas-phase cells immediately above the bed. The grid structure of the bed is superimposed on the color raster plot to show the bed shape. There are three

vertical lines on the left side of the picture which span the width of the furnace; these three lines indicate the location of the bullnose at the top of the furnace cavity. The fuel comes from the volatile component of the particles which reach the bed. The fuel is concentrated on the periphery of the bed since most of the particles land there. The front- and back-wall locations receive more fuel than the side-wall part of the bed due to differences in the behavior of sprays on each wall. The front- and back-wall nozzles tend to spray more liquor directly on the bed on the opposite wall to the nozzle while the material reaching the bed near the side wall is more completely pyrolyzed.

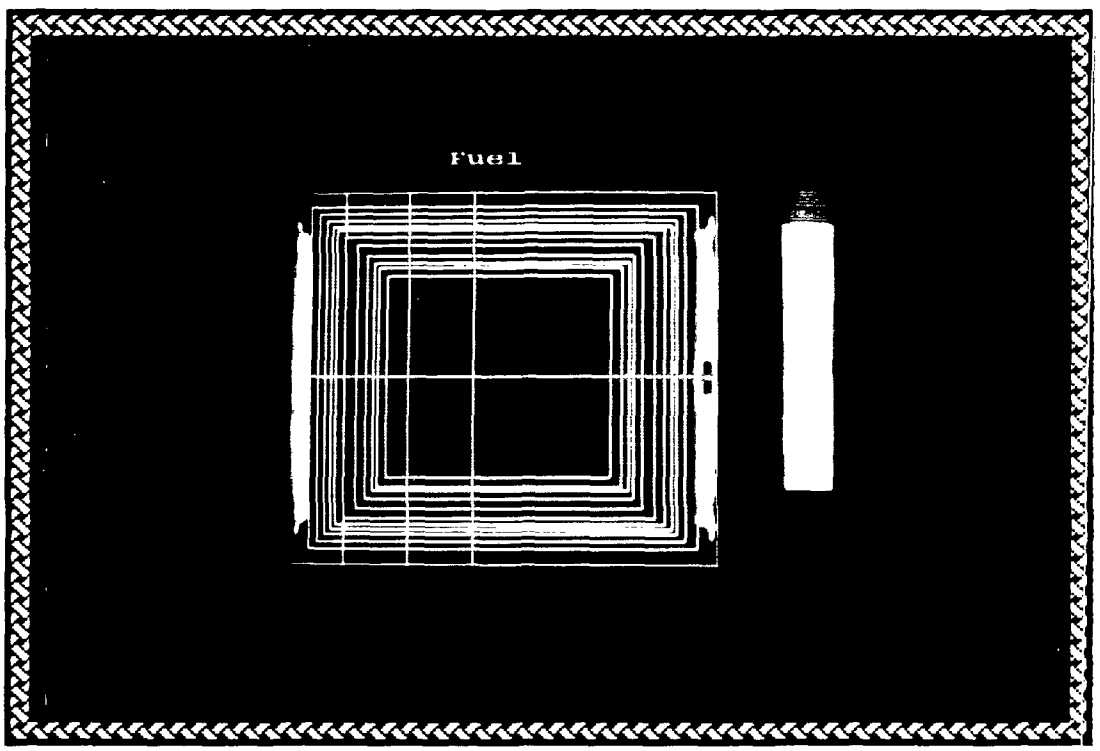

Figure 19. Fuel concentration immediately above the char bed.

Figure 20 shows the surface temperature profile. The hot spots are located on the periphery of the bed and in the center of the bed. Radiative exchange is a dominant term in the bed cell energy balance, so the surface

temperature profile is affected by the gas-phase temperatures above the surface. The hot temperatures on the periphery are caused by high combustion rates on the surface and by radiation back to the surface from hot gas cells above the bed. The hot gas cell temperatures are due to combustion of the volatiles coming off the bed. The volatiles at the periphery of the bed are carried by the primary air jets and mix and burn as the gases flow over the bed. Some of the heat generated in these gas-phase reactions is radiated back to the bed. The center hot spot is also caused primarily by radiation from the gas phase back to the surface. The gas above the center of the bed is oxygen deficient, so little exothermic combustion can take place on the surface of the bed. The gases which come off the bed are burned in the gas phase, and the hot gases formed at the periphery converge in the center of the furnace. Thus, a hot "core" of gases form in the center of the furnace, and the core radiates heat back to the surface of the bed.

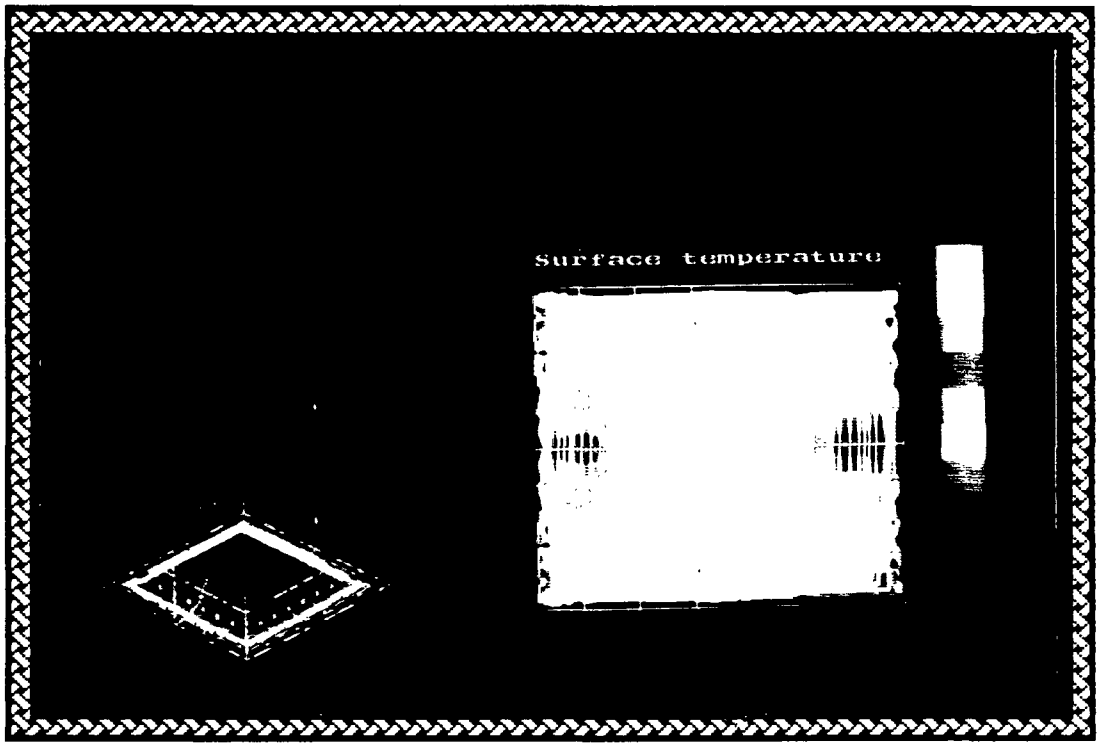

Figure 20. Temperature profile of the char bed surface.

The reduction efficiency profile is shown in Fig. 21. The reduction efficiency, r, is defined as the molar ratio of sodium sulfide to total sulfur in the smelt. The value of r is close to one over most of the bed, but the mass-average value of r is 0.74 in the base case. The peripheral areas of the bed where r is near zero have greater flow rates of smelt than areas where r is near one (see Fig. 18), bringing the global mass-average reduction efficiency down. The zero reduction efficiency is caused by low bed temperatures. If temperatures were hot enough, a high reduction efficiency could be maintained in spite of high oxygen mass transfer rates, but temperatures on the periphery are on the order of 900 K, decreasing the sulfate reduction rate.

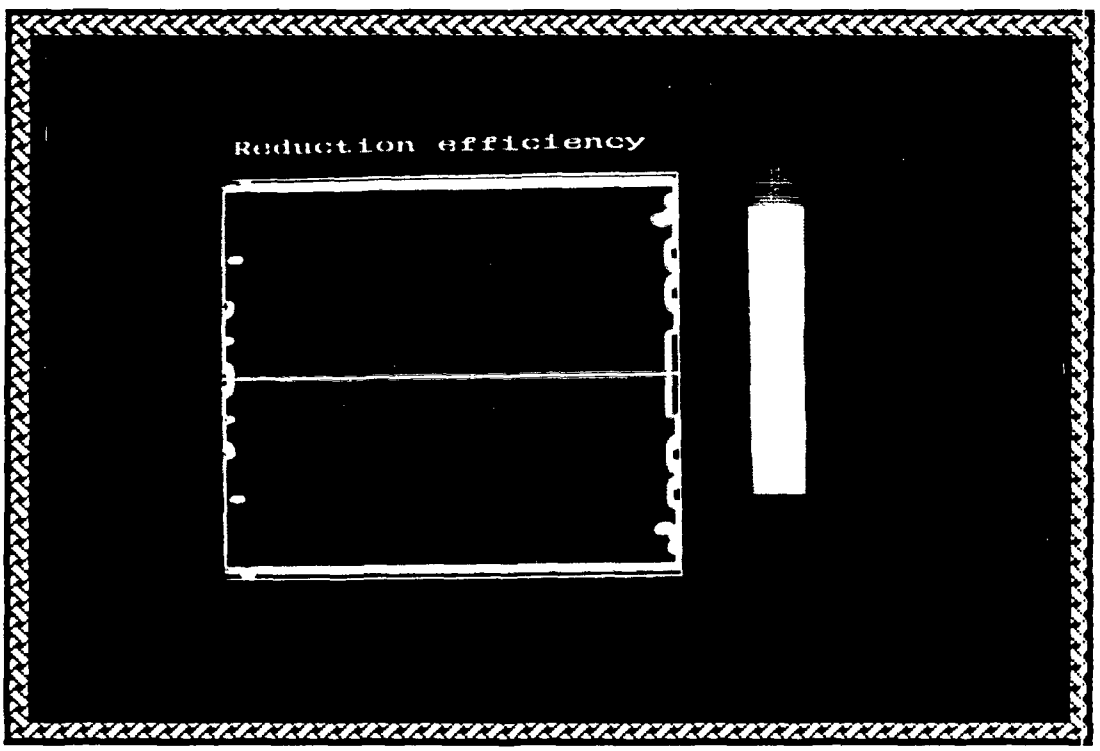

Figure 21. Reduction efficiency distribution.

The low temperatures on the periphery are not realistic, as they are not seen in actual recovery boilers. The cause for the low temperatures is the

assumption that char particles and smelt drops instantly equilibrate with the gas temperature of the cell that the particle is in. This assumption causes particles falling near the periphery of the bed to acquire a temperature near that of the primary jets. The cool particles then land on the edge of the bed. Because most of the mass lands on the edge of the bed in the base case, large quantities of cool mass "black out" the edge of the bed. This result is unrealistic and is caused by assuming that char particles or smelt drops have the temperature of the cell they are in.

Walsh[32] made this assumption for the purpose of calculating the sensible heat contribution of the particle to the gas-cell energy balance. The particle temperature would normally not be critical in the char combustion and smelt oxidation stages for Walsh's model because the only process occurring is oxygen mass transfer. If a hot particle enters a hot cell, the particle temperature remains hot; however, when a hot particle enters a cold cell such as one near the primary air port, it becomes cold instantly and then falls on the bed cold. Assuming that the particle temperature equals the gas temperature causes error in this case. The fact that the primary air enters as a slot jet means that all particles landing directly on the edge of the bed are forced to pass through a cold region immediately before hitting the bed. The sensible heat of these particles is released to the primary jet rather than supplied to the bed. The unrealistically low reduction efficiency (0.74) is therefore caused by a breakdown of an assumption in the in-flight particle model.

When the gasification reactions are included in the bed model, the average reduction efficiency is 0.9. The same phenomenon -- cold temperatures on the edge of the bed -- is still occurring, but the larger gasification rate away from the edge of the bed results in a larger flowrate of reduced smelt, raising the global reduction efficiency from 0.74 to 0.9.

Figure 22 shows the rate of carbon combustion on the surface of the bed.

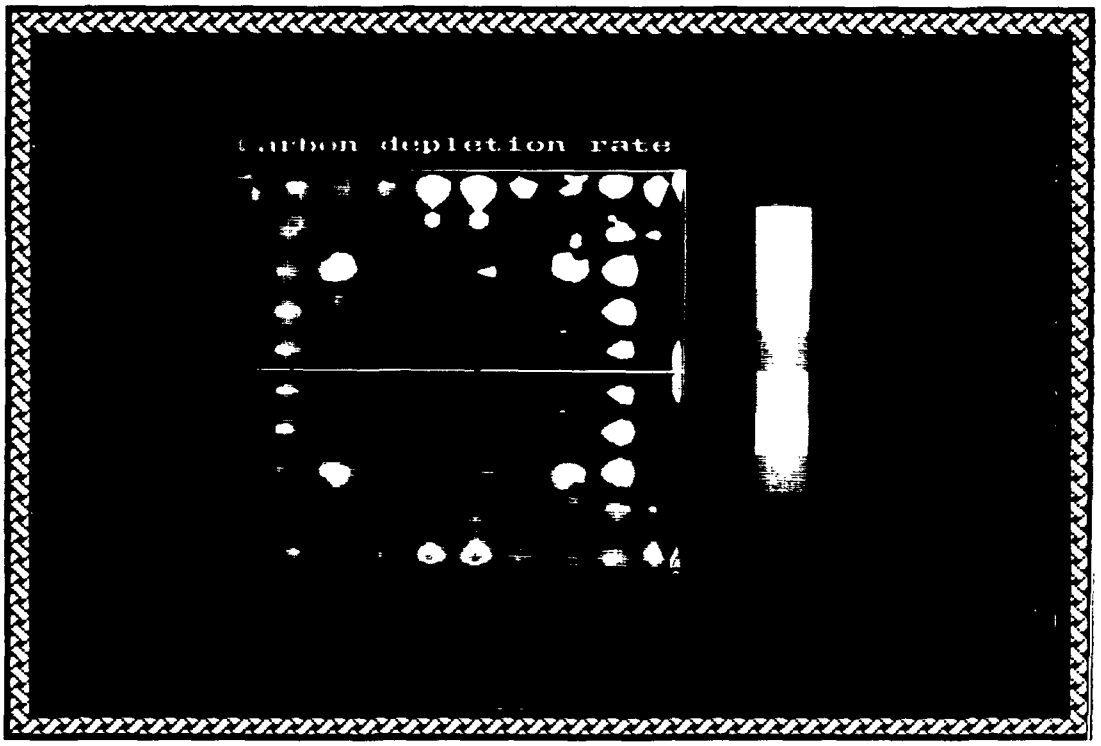

Figure 22. Carbon combustion rate on the char bed surface.

The combustion rate is highest away from the center of the bed where oxygen concentrations and velocities are highest. The blotchy appearance is an effect caused partly by the secondary air jets. There are nine secondary air ports which cause the nine blotches in each horizontal direction on the plot. The gas recirculation zones above the bed bring oxygen from the secondary jets to the bed surface. The plotting algorithm in FLUENT also contributes to the blotchy appearance.

The base case has been modified in different ways to examine the effect of changes on the char bed and furnace behavior. Extensive parametric studies are not feasible due to long times required for convergence of the simulation. Jones found that five months were required to converge a base case[31]. Changes made to the base case do not require an additional five months to reconverge, but times on the order of one to two months are necessary for reconvergence. Thus, the study of char bed behavior was limited to the following:

1) The gasification reactions were added to the bed model, resulting in the doubling of the bed burning rate. The bed mass balance is changed from a growing bed in the base case to a bed which is shrinking at a small rate.

2) The way pyrolysis gases were emitted from the bed was changed. The particles hitting the bed previously released all remaining pyrolysis gases in the gas cell immediately above the bed. This made it possible for artificially high amounts of fuel to be released in certain cells. The large amount of fuel would mix with the turbulent primary air and burn immediately, resulting in temperatures as high as 2500 K. A partial fix to the problem was made by spreading the pyrolysis gases over more cells. The high temperatures were moderated as a result.

3) The effect of the mass transfer coefficient was studied. The base case used the Ranz correlation while the modified BED used Brown's experimental mass transfer correlation[30]. The bed burning rate using Brown's correlation was roughly double that in the case with the gasification reactions.

4) The bed shape was varied to investigate its influence on furnace and bed behavior. The truncated pyramid shape

was transformed into a crater shape by hollowing out the center of the bed. A lower bed was also made by cutting down the size of the truncated pyramid from two meters to one meter.

The results of these studies will now be discussed in more detail.

DISCUSSION

GASIFICATION REACTIONS

The base case represents the results when char is allowed to react only with oxygen. BED was modified to allow the gasification of char carbon with CO_2 and H_2O. Figure 23 shows that gasification reactions are a very significant contributor to char combustion. Recall that the black liquor is sprayed at a rate of 2.25 lb BLS/ft^2-min and the solids are 20% char carbon. The first bar on Fig. 23 shows that 40% of the char burning occurs during flight, 32% occurs on the bed, and 28% of the char remains unburned. Only 72% of the char entering the furnace is being burned. The bed is therefore growing and the liquor firing rate would have to be reduced to get the char supply and depletion to match. The bed in the base case has a high surface area, the primary air is 45% of the incoming air, and the combustion product is assumed to be carbon monoxide. Despite these factors in favor of high bed burning rates, the bed is growing in the case without the gasification reactions. These results suggest that the char/oxygen reactions are not the only significant consumers of char carbon.

The second bar on Fig. 23 shows that the inclusion of the gasification reactions causes 105% of the incoming char to be consumed. The bed is shrinking slightly since more carbon is consumed than enters the furnace. The in-flight char combustion is 42%, and 63% of the incoming char carbon is burned on the bed. In the case where gasification reactions are included, the contributions to char burning are split evenly between the three reaction paths for char carbon: 19% reacts via char/O_2, 23% via C/CO_2, and 21% via C/H_2O. The char/O_2 reactions play a larger role in the base case (32 versus 19% of incoming char carbon) because the average oxygen concentration is higher (7

versus 5%). The gasification reactions cause more oxygen consumers to be released from the bed, reducing the amount of oxygen that reacts directly with the char surface.

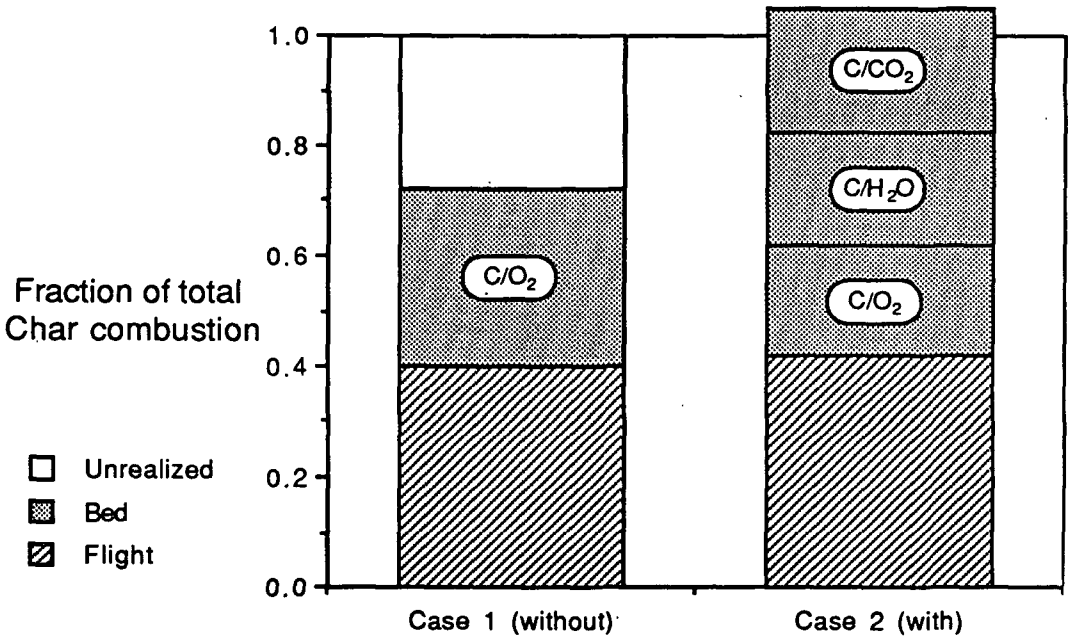

Figure 23. Comparison of char burning without and with gasification reactions.

The oxygen supply to the char can be divided into oxygen from the combustion gas and oxygen as sodium sulfate in the smelt droplets. Oxygen from smelt is about 12% of the oxygen supplied. This is a small but significant fraction of the oxygen supply to the bed. In another case with different spray parameters, it is conceivable that smelt droplets could be a more significant source of oxygen to the bed. The estimate of the oxygen contribution from the smelt may be conservative. The particle calculations assume no overlap between char combustion and smelt oxidation. If there is some overlap between the char combustion and sulfide oxidation steps, more oxygen in the form of sulfate would reach the bed. Furthermore, the importance of the gasification reactions means that in-flight char combustion is underestimated, so more particles would be expected to burn out during flight with subsequent reoxidation of sulfide. (The char combustion model for particles assumes that

char burning is mass transfer limited in oxygen and does not include the gasification reactions.)

The global average of CO relative to total carbon gases above the bed was higher in the case with gasification: 44% vs. 21% in the base case. The higher value is due to the gasification reactions which release more CO and consume CO_2 ; the lower average oxygen concentration means less gas phase CO oxidation. The combustion product of the char/O_2 reactions was assumed to be all CO. Whether 80% or 100% is assumed may not greatly affect the overall combustion rate for several reasons. Firstly, the char/O_2 reactions play a reduced role in the overall rate when the gasification reactions are included. Secondly, CO is rapidly oxidized in the gas phase if any oxygen is present, so the net result is the same: carbon is oxidized to carbon dioxide. The fact that carbon forms carbon dioxide in two steps or one makes a slight difference in where the heat of reaction is released, but the global result is not affected if the two steps occur in close proximity to each other.

The average surface temperatures are quite similar -- 1433 K in the base case vs. 1415 K in the gasification case -- but the way the energy balance arrived at the two temperatures is quite different. The average temperature in the first gas cell above the bed is 1506 K in the base case while it is 1729 K in the gasification case. The bed is a net emitter of radiation in the base case, but it is a net receiver in the other ones. The gas emissivity is 0.4 and the emissivity of the bed surface is 0.8, so the bed can be a net emitter of radiation even though its average temperature is slightly less than the gas immediately above it. The bed in the gasification case has endothermic as well as exothermic reactions occurring, and the CO and fuel combustion occurring right above the bed radiate enough heat back to the bed to keep a high bed temperature.

THE METHOD OF PYROLYSIS NEAR THE BED

Some of the temperatures around the bed are unreasonably high in the base case. Temperatures as high as 2500 K have been calculated in some cells. The radiation back to the bed would therefore be overpredicted, and the bed combustion could be overestimated as a result. The high-temperature problem is caused by the arbitrary injection of volatiles from particles landing near the primary air port. Large amounts of "fuel" are released near cells with turbulent, oxygen-rich conditions. Unreasonably high temperatures are calculated which then tend to be propagated in the cells above the bed due to the strong convection of the primary air jets. The origin of the problem is discussed here in more detail.

A coordinate is considered two-way if the conditions at a location are influenced by conditions on either side of that location[37]. Alternatively, a coordinate is one-way if it is influenced by conditions on only one side of a location. Time is an example of a one-way coordinate since present events affect the future, but future events do not affect the present. Space is normally a two-way coordinate; but it can become a one-way coordinate under certain circumstances. Space becomes a one-way coordinate when the fluid flow is strongly unidirectional. A dominant flow in one direction often means that significant influences travel only from upstream to downstream.

Figure 24 depicts a two-dimensional system in which there is a high flow rate in the x direction. The system is essentially one-way since the condition at P is predominantly influenced by W and very little by E.

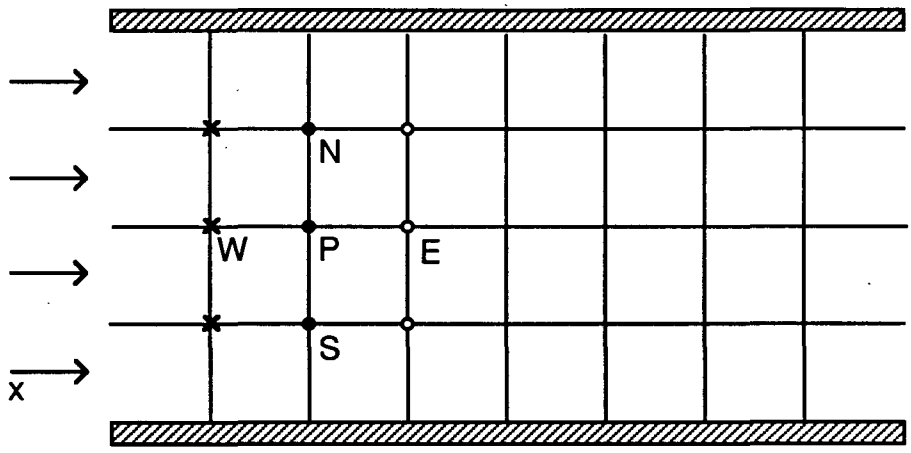

Figure 24. One-way space coordinates.

Recall the algebraic form of the general differential equation:

$$\phi_p \sum_i (A_i - S_p) = \sum_i A_i \phi_i - S_c \qquad (48)$$

When this is expanded to a three-dimensional case, Equation (49) is obtained in which the subscripts E, W, N, S, T, B, and P denote east, west, north, south, top, bottom, and point, respectively:

$$a_P\phi_P = a_E\phi_E + a_W\phi_W + a_N\phi_N + a_S\phi_S + a_T\phi_T + a_B\phi_B + S \qquad (49)$$

When the flow is strongly unidirectional as in Fig. 24, the coefficient a_E becomes zero. Thus, E has no influence on P while W will have a strong influence.

It can be shown that certain locations in the base case contain unidirectional flow. Furthermore, excesses which occur in upstream cells can be carried downstream. The flow near the primary airports provides an example of unidirectional flow in which excessive temperatures may have a tendency to be propagated downstream. The excessive temperatures are

caused by a combination of high mixing, large amounts of fuel and oxygen, irregular cell shapes, and an insufficient number of cells.

A particular section near the primary air ports will be used as a basis for discussion of the generation and propagation of excessive temperatures. Figure 25 shows the cells in the third vertical plane of the base case near the primary air ports.

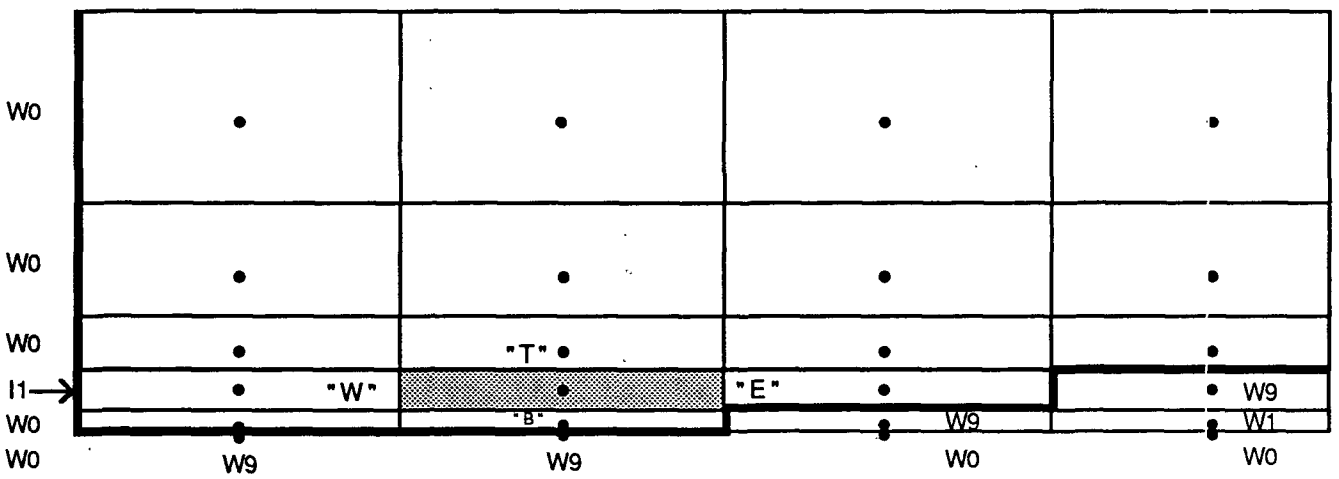

Figure 25. The cell structure near the primary air ports.

The shaded cell is located at the I, J, K coordinate 3, 3, 3. The cell types, grid points, and shapes are accurately represented by Fig. 25.

The shaded cell is an example of a location where unidirectional flow occurs. This is represented numerically by setting a_E equal to zero. The cell also happens to have much oxygen, excessive fuel, and a great deal of turbulence, leading to enormous reaction rates which cause temperatures as high as 2500 Kto be predicted. The high temperatures approach the adiabatic flame temperature with hot reactants. The oxygen and the turbulence come from the primary air ports while the fuel comes from pyrolysis gases released from the bed. Once an excessive temperature is calculated, there is a tendency

for it to be propagated downstream for as long as the flow is unidirectional. Thus, high temperatures generated near the primary air ports tend to spread across the char bed and may cause an overprediction of radiative heat transfer from the gas phase to the bed surface.

The high-temperature problem is caused by a coincidence of spray variables, cell structure, and pyrolysis methodology. The particular base case chosen has a gas flow pattern and liquor spray pattern which cause most of the black liquor particles to hit the furnace walls. In the model, if a particle is still wet when it hits the wall, it dries and emits 50% of its pyrolysis gases afterwhich it is dropped into the second cell in from the wall on the char bed surface. If the particle is dry when it hits the wall, it is placed back in the gas stream and allowed to continue on its trajectory. Because of the downflow near the walls, these latter particles tend to land on the bed in the first cell in from the wall. The particles on the bed then released their residual pyrolysis gases directly to the gas cells above. Thus, because of the particular characteristics of the base case, a great deal of pyrolysis gas is being released in the first and second cells in from the wall.

The cell structure of the base case exacerbates the problem in several ways. The primary air ports are represented by a slot, the cells are irregularly shaped, and there is an insufficient number of cells in an area where so many events are occurring. The representation of the primary air ports by a slot forces the fuel from the peripheral bed cells to pass through a plane of high oxygen content. There is no place for the fuel to go but upward into the turbulent, oxygen-rich cell. Furthermore, the number and location of cells is such that the first gas cell above the bed has almost all fuel and no oxygen while the second cell up has high oxygen content and turbulence. Extreme gradients exist between these two cells, and the fuel in the first cell is forced into the

oxygen-rich cell. (More cells in this area would allow a more accurate representation of the ports and decrease the severe gradients between the cells.) The turbulence near air ports is so great that reaction between the fuel and air proceeds as far as stoichiometry allows. Since the release of pyrolysis gas is handled somewhat arbitrarily, it is possible to inject an artificially high amount of fuel in certain cells. If excessive fuel is injected into oxygen-rich, turbulent areas, unreasonably high temperatures may be predicted (ca. 2500 K). The same process also occurs on the wall, but the high-temperature problem does not appear because there is less oxygen and turbulence, so the fuel has a chance to diffuse before reacting. A greater number of cells near the primary air ports would allow the fuel to diffuse and spread the combustion out over more cells. Thus, the high-temperature problem is caused mostly by the case morphology and to a lesser extent the methodology of releasing the pyrolysis gases.

A change in the way the pyrolysis gases are distributed has been made which reduces the high-temperature problem. Rather than releasing all the pyrolysis gas in the first and second surface cells in from the wall, the gas is spread over the first four gas cells in the horizontal and vertical directions. Thus the gas is released in sixteen cells rather than two cells. Table 17 shows that spreading the pyrolysis gases in this manner reduces the severity of the high temperatures. The temperatures are taken on the third vertical slice of the base case, the same slice shown in Fig. 25. The bold value at location 3, 3 in the table is the temperature of the shaded cell in Fig. 25. The lines in the table mark the boundary between the bed surface and the gas phase. The old temperature at 3, 3 was 2500 K. The temperature predicted by spreading the pyrolysis gases is 1800 K. The downstream temperatures are moderated as well.

Table 17. Temperatures before and after spreading pyrolysis gases.

Before

J	I = 1	2	3	4	5	6	7	8
10	900	1400	1500	1500	1600	1700	1700	1800
9	900	1300	1500	1600	1700	1700	1800	1900
8	900	1200	1600	1700	1800	1800	1900	2100
7	900	1400	1700	1700	1800	2000	2100	2100
6	900	1300	1500	1700	1900	2100	2200	1600
5	900	1200	1600	2000	2200	2300	1500	1300
4	900	1100	1900	2400	2400	1500	1300	1300
3	400	1000	**2500**	2400	1400	1300	1300	1300
2	900	880	1400	1400	1300	1300	1300	1300
1	900	900	1400	900	900	900	900	900

After

J	I = 1	2	3	4	5	6	7	8
10	900	1500	1500	1500	1500	1600	1600	1700
9	900	1400	1500	1500	1500	1600	1700	1800
8	900	1400	1500	1500	1600	1700	1800	1900
7	900	1400	1500	1500	1600	1700	1900	2000
6	900	1400	1500	1600	1700	1900	2000	1500
5	900	1000	1300	1600	1800	2000	1500	1300
4	900	860	1300	1800	2200	1500	1300	1300
3	400	800	**1800**	2200	1400	1300	1300	1300
2	900	1400	1600	1400	1300	1300	1300	1300
1	900	1200	1400	900	900	900	900	900

The coefficients for enthalpy balance of cell 3, 3 are displayed in Table 18 to show the unidirectional effect and to demonstrate the dominance of the source term in the energy balance. The two main things to notice in Table 18 are the zero coefficients and the relative magnitude of the source terms. The zero coefficients indicate that the numerical scheme considers the flow to be influenced predominantly from west to east and from bottom to top. The source term in the base case is 40% greater than that calculated in the scheme where the pyrolysis gas is spread out. A reconstruction of the entire enthalpy balance shows that it is completely dominated by the source term in

both cases; thus, the temperature of 2500 K is 40% greater than 1800 K because the source term is 40% greater.

Table 18. Coefficients from enthalpy balance on cell 3, 3.

	Old pyrolysis	New pyrolysis
a_P	-0.3606	-0.4532
a_E	0	0
a_W	0.0591	0.0821
a_N	5.39E-5	3.26E-5
a_S	1.25E-4	6.84E-6
a_T	0	0
a_B	8.71E-3	6.17E-3
S	-1.41E6	-1.00E6
T K	2500	1800

Thus, spreading the pyrolysis gases moderates the problem, but a less arbitrary method of releasing pyrolysis gas would be desirable. This will be discussed in the future work section. Modification of the base case is also expected to relieve the problem.

Figure 26 demonstrates the moderation of the temperatures. The gas temperatures at this plane are still high. The spreading of the pyrolysis gases helps but does not eliminate the problem. Another aspect of the problem is the parameters used for the k- ε turbulence model. Any combustibles which contact oxygen are predicted by the k- ε model to mix and burn instantaneously. All the heat of reaction is released in one cell rather than mixing occurring over several cells. Thus, the spreading of pyrolysis gases is a partial but incomplete solution to the artificially high temperatures. The parameters for the k- ε model should be modified to reduce the amount of mixing.

Figure 26. Gas temperatures before and after spreading pyrolysis gases.

An experiment was done to determine the extent to which excessive temperatures affect the bed calculations. A uniform temperature field was patched in the gas phase. All other variables such as the velocities and gas concentrations remained the same as in the converged case. BED was then called to determine the effect of the gas temperature on the surface reactions. In general, the mass-transfer limited reactions were not changed with temperature while reactions controlled by the kinetic rate were increased by increasing temperature.

Mass-transfer controlled reactions are not heavily influenced by

temperature because of factors which cancel each other. The form of the mass-transfer coefficient is such that it is proportional to temperature. Since the gas concentration is inversely proportional to temperature, the flux -- the product of the mass transfer coefficient and concentration -- is essentially independent of temperature. On the other hand, rates limited more by the kinetic rate are strongly influenced by temperature due to the exponential term in the rate expression.

Four temperatures were patched into the gas phase: 1300, 1400, 1500, and 1700 K. The average surface temperature, radiant flux to the bed, and overall burning rate increased with increasing gas-phase temperature. Figure 27 is a plot of overall burning rate versus the average surface temperature of the bed. The rate is plotted relative to the maximum rate calculated. The four points correspond to the four gas-phase temperatures cited above.

The bed burning rate does not change when the average surface temperature is above the upper 1300's K; all reaction rates become mass-transfer limited. The kinetic rate becomes increasingly important as the average surface temperature decreases. Thus, the error in the burning rate caused by excessive temperatures will be less than 2% when the average surface temperature exceeds 1350 K. The error in the burning rate calculation will be on the order of 10-20% if unreasonably high gas temperatures radiate enough heat back to the bed to artificially push bed burning into the mass-transfer controlled regime.

The effect of excessive temperatures on the calculated reduction efficiency is minor since the sulfate/sulfide cycle is essentially mass-transfer limited even at lower temperatures. The gasification reactions and direct oxidation of char carbon are the reactions which are dominated by the kinetic

rate until the higher temperatures, causing the shape of the curve in Fig. 27.

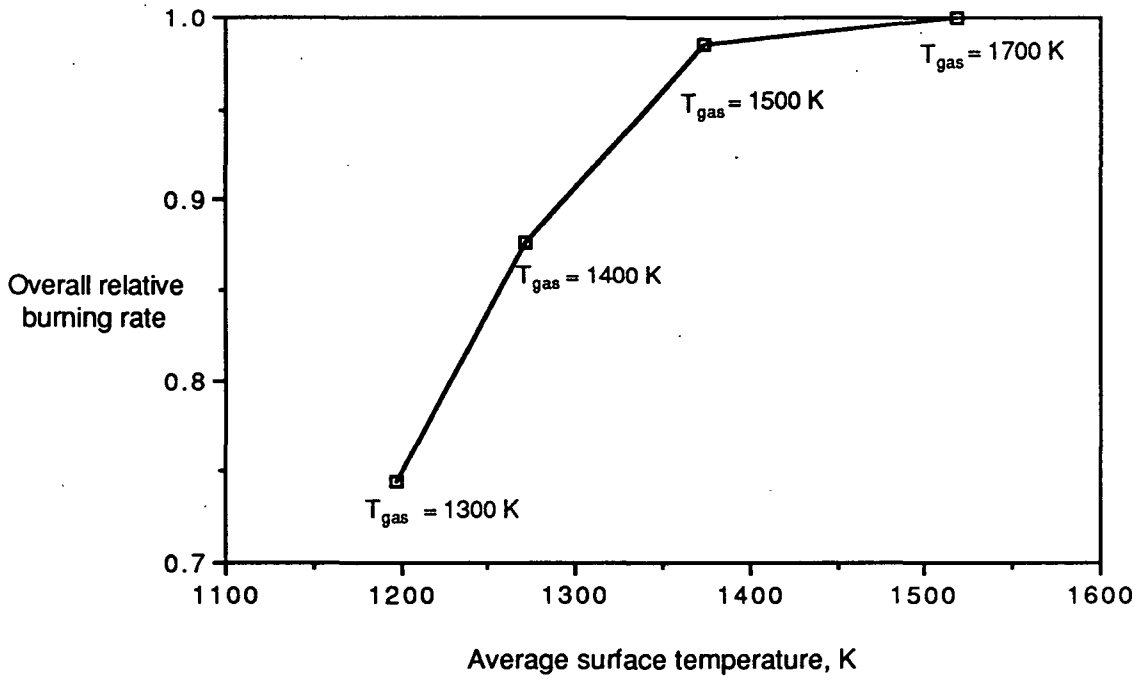

Figure 27. Effect of gas-phase temperatures on burning rate.

EFFECT OF THE MASS TRANSFER COEFFICIENT

The modifications to the base case discussed so far have used the Ranz correlation to calculate the mass transfer coefficient. This section compares two cases whose only difference is the mass transfer coefficient. One case uses the Ranz correlation and the other case uses the empirical Brown correlation with a linear dependence on velocity. The Ranz case uses the most conservative estimate of the mass transfer coefficient while the Brown case uses the most optimistic estimate of the mass transfer coefficient. The bed burning rates reported should bracket actual bed behavior for similar conditions.

Brown's mass transfer correlation results in large bed burning rates as shown in Fig. 28. The first two bars of Fig. 28 are taken directly from Fig. 23 which was discussed earlier. The third bar shows that Brown's correlation results in a bed burning rate which is 83% greater than the rate

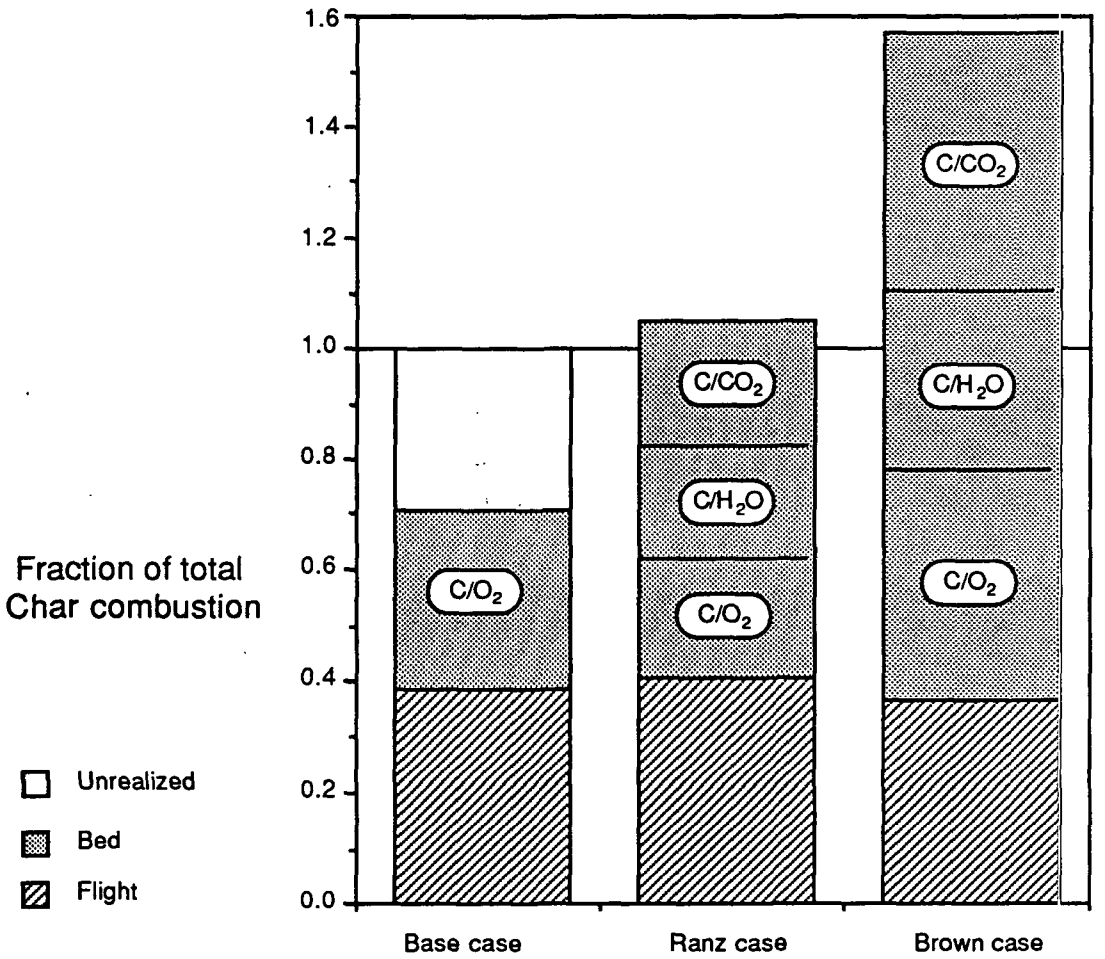

Figure 28. Relative contribution to char burning with different mass transfer coefficients.

obtained using the Ranz correlation, and the total char burning rate in the furnace is 50% greater when the Brown correlation is used. The larger rate is caused by the larger Brown mass transfer coefficient. The Brown coefficient is 3.3 times greater at 50 m/s than the Ranz coefficient due to the dependence on velocity. The Brown correlation has a linear dependence on velocity while

the Ranz correlation has a square root dependence, causing a large departure in calculated values at velocities higher than ca. 6 m/s (see Fig. 9). The average velocity in the cells immediately above the bed is approximately ten meters per second, but velocities can be much larger than average near the primary air ports.

The actual dependence on velocity will be between 0.5 and 1.0 as discussed in an earlier section. The calculated bed burning rates therefore bracket the bed burning rates that would be expected in practice for similar conditions. For a similar furnace fired under similar conditions, most of the char combustion can take place on the bed. Thus, firing strategies can be devised to maximize bed burning which would in turn reduce carryover by allowing the use of coarser sprays.

The rate of carbon combustion for each reaction is compared in Table 19. All of the rates increase in the Brown case except for direct carbon oxidation.

Table 19. Comparison of carbon combustion rates.

[=] kg/s	Ranz case	Brown case
C/O_2	0.19	0.04
C/SO_4	0.21	0.70
C/CO_2	0.41	0.86
C/H_2O	0.38	0.58

The average bed temperature in the Ranz case was 1380 K while it was 1253 K in the Brown case. The char oxidants are oxygen, water, and carbon dioxide. The last two oxidants engage in endothermic reactions. High mass transfer rates increase the rate of endothermic surface reaction if enough heat is radiated back to the bed from gas phase combustion of fuel. The Brown case

has high bed burning rates because the combustion above the bed is able to supply heat back to the bed, preventing the kinetics from slowing the rate too much. The surface temperature, however, is lower in the Brown case due to large endothermic reaction rates.

The lower surface temperatures result in some of the reactions being kinetically limited. When the terms "mass transfer limited" and "kinetically limited" are used, they do not necessarily indicate that the condition applies to every part of the bed, but that as a whole, a surface reaction appears to have a certain character. The kinetic rate expression selected for direct carbon oxidation results in a kinetically limited rate in the Brown case. The C/O_2 rate in the Brown case is 20% of that in the Ranz case; this is caused in part by the average oxygen concentration above the bed being reduced by 50% and in part by the cooler surface temperatures. The reduction efficiency is similarly affected but to a lesser extent. The average reduction efficiency in the Brown case is 67% compared to 90% in the Ranz case. Figure 21 showed that the areas of low reduction efficiency occur near the primary air ports. The oxygen supply to the bed near the primary air ports is even greater in the case using Brown's correlation. A higher mass transfer coefficient combined with generally cooler temperatures decrease the average reduction efficiency. An increase in the assumed reaction depth from 2 cm would increase the reduction efficiency by making the reactor volume larger.

The gas concentrations immediately above the bed affect the rates in Table 19 to an extent. The oxygen and water concentrations immediately above the bed are twice as high in the Ranz case as the Brown case, and the carbon dioxide concentration is 1.8 times as high. The higher Brown coefficient causes greater consumption of oxidants. The carbon monoxide concentration immediately above the bed is more than double in the Brown case due to the

larger surface combustion rates.

The bed burning rate in the Brown case tends to be an upper limit for several reasons. The experimental values used in the correlation have since been revised downward to about 75% of their original values due to different assumptions in developing the experimental mass transfer correlation. The assumed combustion products were changed from 100% CO_2 to 50% CO and 50% CO_2. Secondly, extrapolating beyond the experimental maximum of 6 m/s using a linear dependence on velocity gives the highest mass transfer coefficient. Thirdly, the bed shape assumed is as high as a bed would get in normal practice, so the surface area is at a maximum. Fourthly, assuming CO as the combustion product from the bed gives the most optimistic value for bed burning. On the other hand, it is wrong to draw generalized conclusions from a couple cases.

EFFECT OF THE BED SHAPE ON FURNACE BEHAVIOR

The bed shape has been found to affect furnace behavior in several ways. The increasing surface area with increasing bed size is the most obvious effect of the bed shape. A larger surface area allows a higher combustion rate, all other things being equal. The bed shape also affects gas flow patterns which in turn influence carryover.

The three bed shapes in Fig. 29 were used to show their effect on overall furnace behavior. The cross section of each bed is outlined. The bed shape assumed in the base case is outlined in red. The bed is shaped like a truncated pyramid with the top level with the secondary air ports. The top of the bed and the secondary ports are two meters above the floor of the furnace. The second assumed bed shape was obtained by forming a crater in the first bed shape. The green outline indicates the shape of the crater. The third bed

shape is a low bed which is one meter high instead of two meters high as in the base case. The top of the low bed is indicated by the yellow line in Fig. 29.

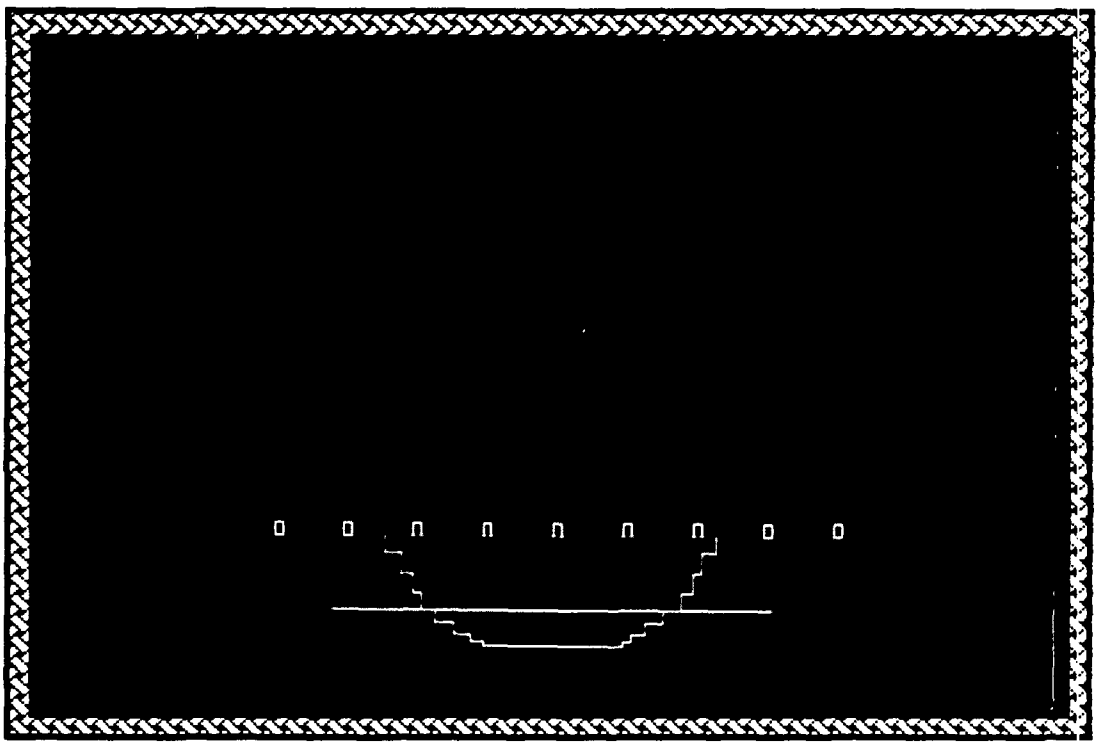

Figure 29. Assumed bed shapes.

The gas flow patterns around each bed shape are shown in Figures 30, 31, and 32.

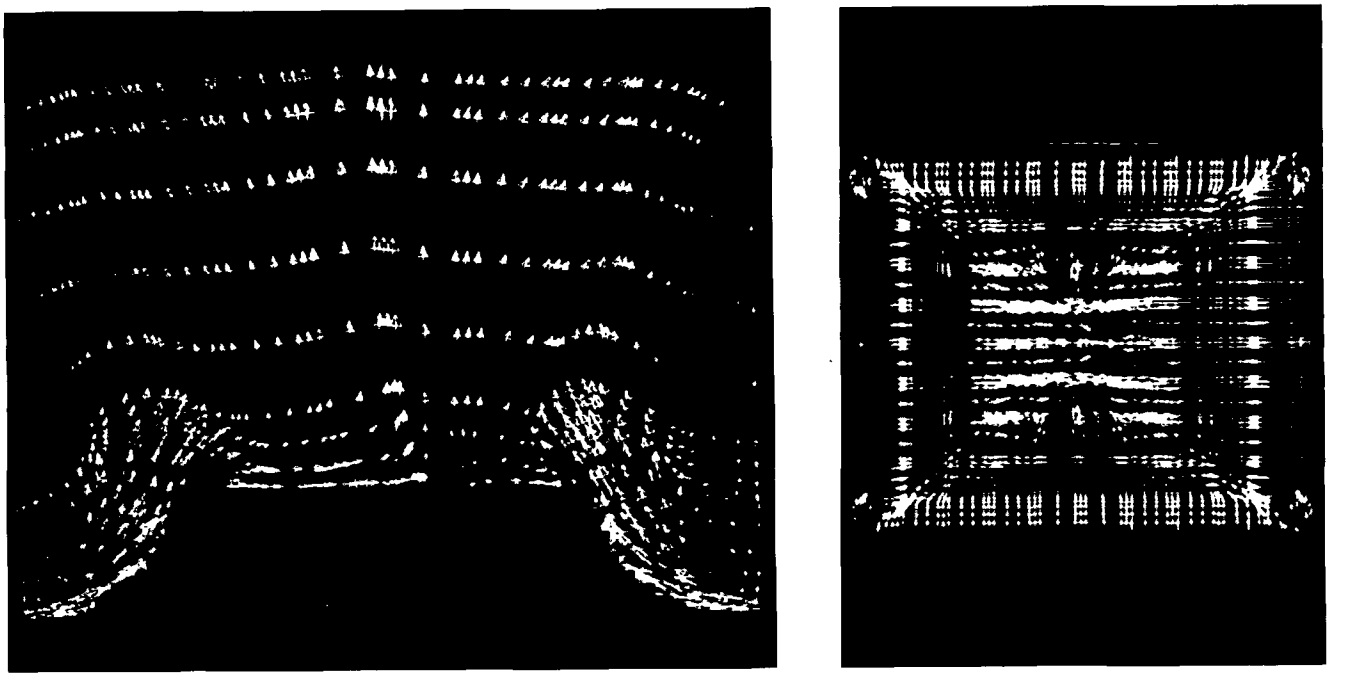

a. Side view

b. Plan view

Figure 30. Gas flow patterns around a pyramid bed.

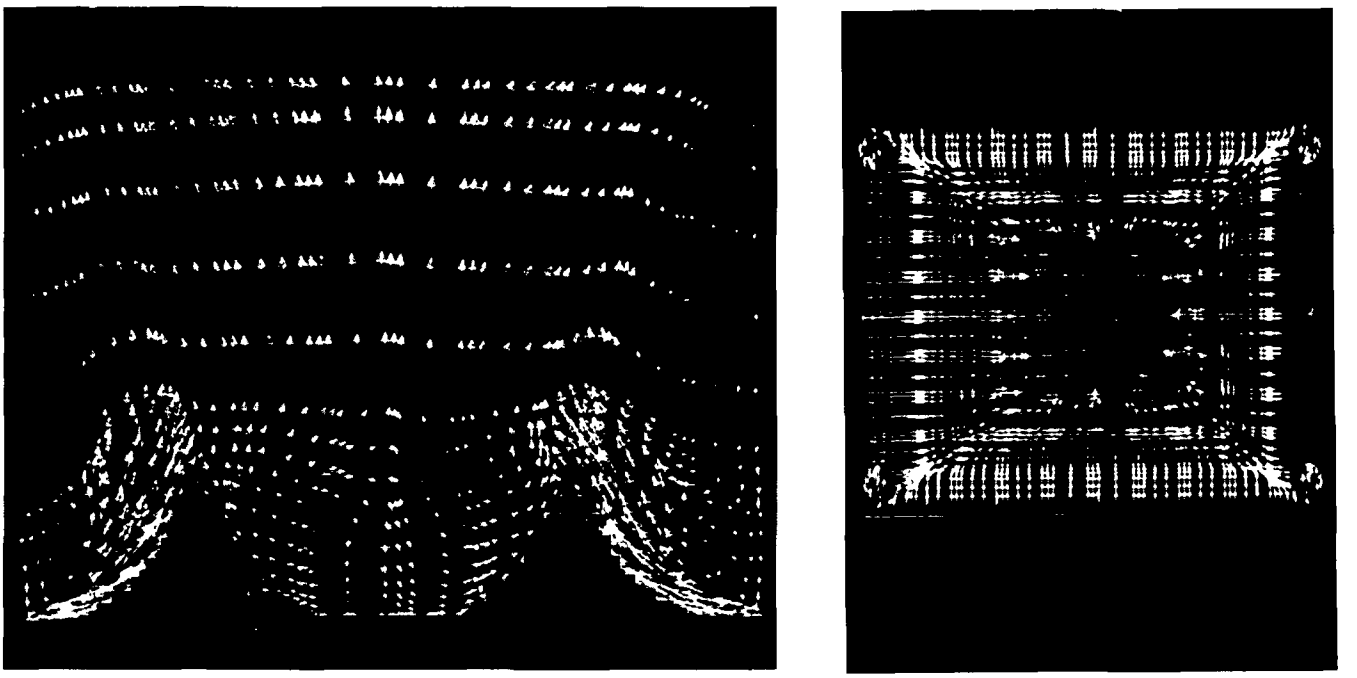

a. Side view

b. Plan view

Figure 31. Gas flow patterns around a crater bed.

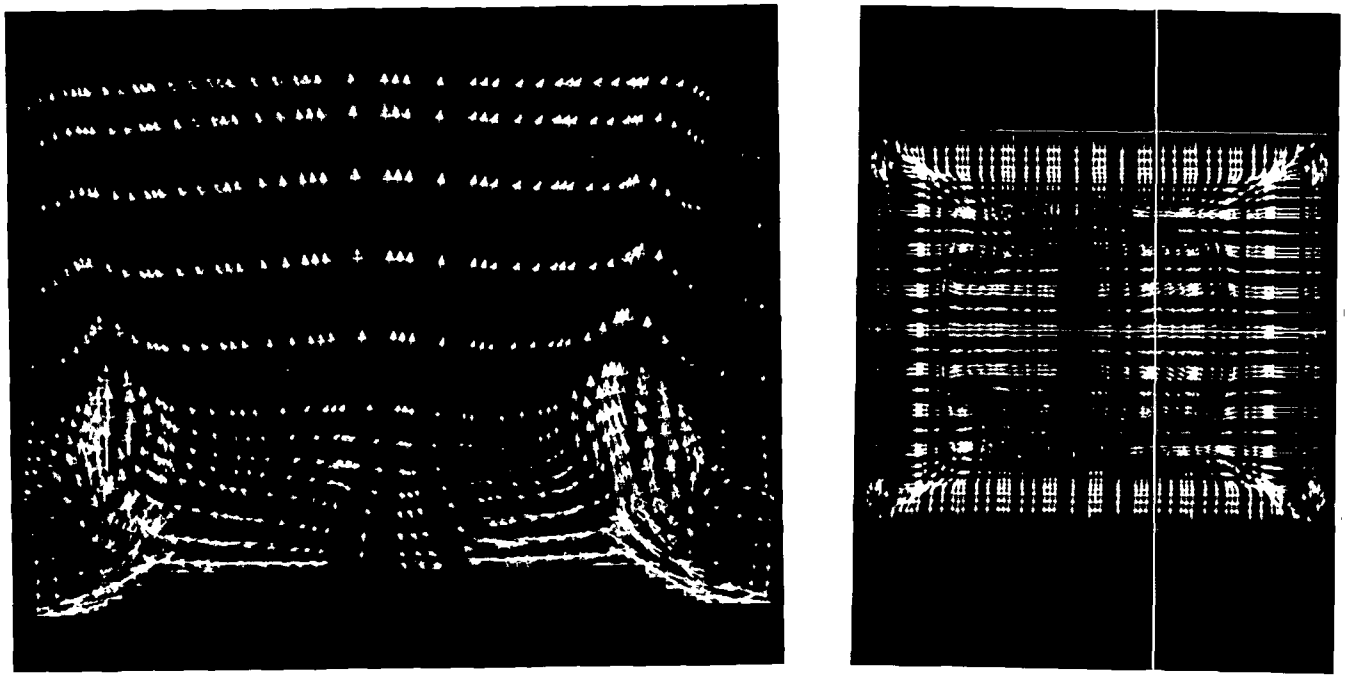

a. Side view

b. Plan view

Figure 32. Gas flow patterns around a low bed.

The front view shows a vertical plane near the center of the furnace. The plan view shows the velocity vectors looking down from above. The plan velocity vectors are those in the gas cell immediately above the bed, so it represents a three-dimensional velocity field on a two-dimensional image.

The vectors in Figures 30a and 30b show how the primary and secondary jets flow over the bed and converge in the center of the furnace. The gas is deflected upward in the center of the furnace since the bed prevents downward deflection. It will be shown that the flow patterns around the high bed appear to detrimentally affect carryover.

In contrast to the high bed, a crater-shaped bed results in a recirculation zone above the center of the bed (Fig. 31a). Outside the crater, the flow is from the periphery of the bed towards the center; but inside the

crater, the gas flow is from the center of the bed towards the periphery (Fig. 31b). One result of the recirculation pattern appears to be the reduction of carryover. The crater bed is not necessarily desirable, however, since the flow inside the crater is fairly stagnant and very oxygen deficient relative to the flow outside the crater. The combustion rate on the crater bed is 5% less than that on the pyramid bed even though the crater bed has 17% more surface area. The center area of the bed is not effectively used for char burning.

If it is assumed that the gas redistributes char on the bed, the flow patterns around the pyramid and crater beds are consistent with the bed shapes. The gas flow above the pyramid bed is from outside towards the center of the bed, so char which lands on the periphery of the bed could potentially be carried to and deposited on the center of the bed. The combustion rate is less in the center of the bed, so the redistributed char would burn more slowly and the bed would tend to get bigger in the center. The crater bed shape is also consistent with the flow patterns. The gas flows toward the rim of the crater, so redistributed char would tend to be deposited there (see Fig. 31).

The low bed (Fig. 32) causes flow patterns similar to those of the crater bed. The secondary jets meet in the center of the furnace and partially recirculate. The primary jets are not deflected upward as much as in the case of the crater bed.

Figure 33 shows the inorganic carryover in the three cases as a function of iteration number. Carryover is intimately coupled with the flow patterns. Since small changes in the flow patterns affect carryover, the carryover takes a long time to converge (on the order of months). The carryover reaches a point where its value approaches convergence by damped oscillations around a steady state value. The converged value of the carryover can therefore be estimated by

determining the center point of the oscillations. Figure 33 shows that the carryover is worst in the pyramid case. The carryover in the crater case and the low bed case is 23% and 46% lower than the carryover in the pyramid case. These numbers were obtained by estimating the converged value of the carryover. The pyramid case shows an even, damped oscillation, and the converged value for the carryover is estimated to be 0.52 kg/sec. The crater case carryover is estimated to be 0.40 kg/sec. The low bed is still decreasing although it is getting closer to convergence. The converged value is estimated to be 0.28 kg/sec. Thus, the bed shape affects carryover by influencing the gas flow patterns around the bed; however, since carryover is the last variable to converge, this conclusion is tentative.

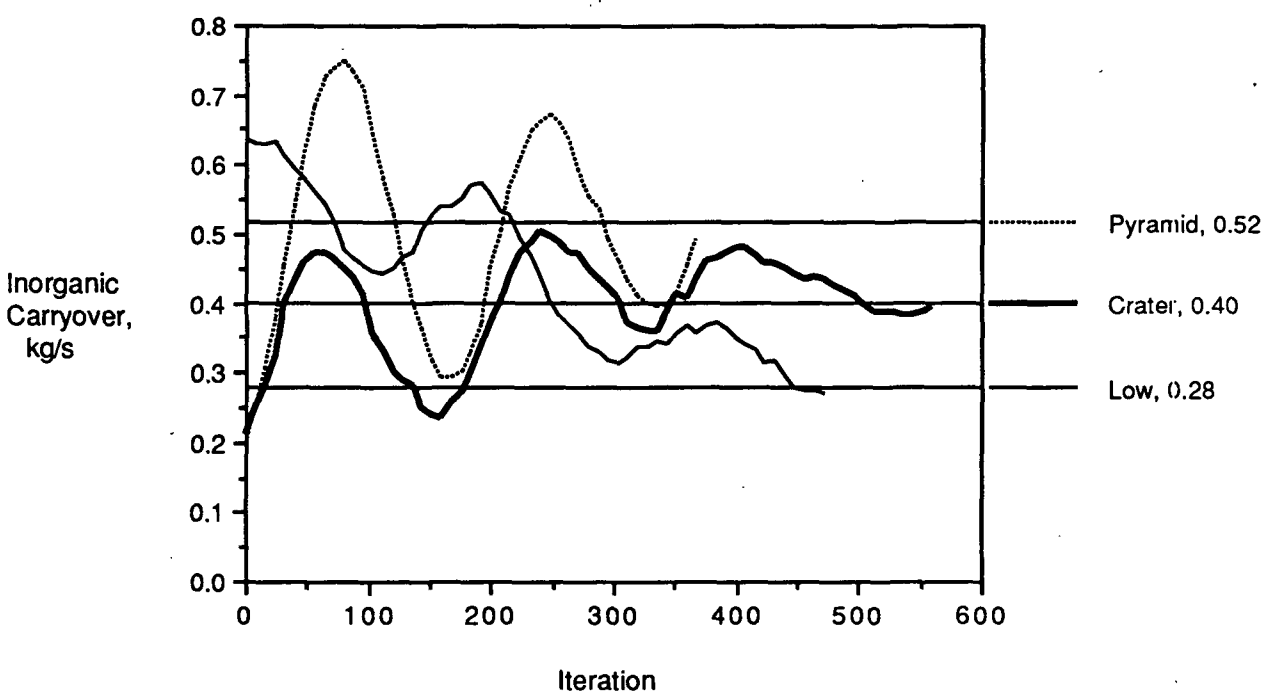

Figure 33. The effect of bed shape on carryover.

Figure 34 shows the vector field in one slice and the profiles of upward velocity. The vector plots show similar flow patterns for the three cases except

in the lower furnace. The profile plots on the right of the figures show the upward velocity by the shape and color of the profile. Peaks on the profile indicate higher upward velocity. Yellow is higher upward velocity, and deep blue indicates downflow in some parts. The overall features of the gas flow patterns above the secondary air ports appear similar as shown in the profile plots. There is a slightly more intense "core" of upward velocity in the pyramid case, but the profile plots do not show any gross differences in the flow patterns. On the other hand, the vector fields show substantial differences between the cases in the lower furnace. The apparent difference in carryover between the cases may be influenced by the flow patterns around the bed.

Figure 34. Flow patterns in the furnace.

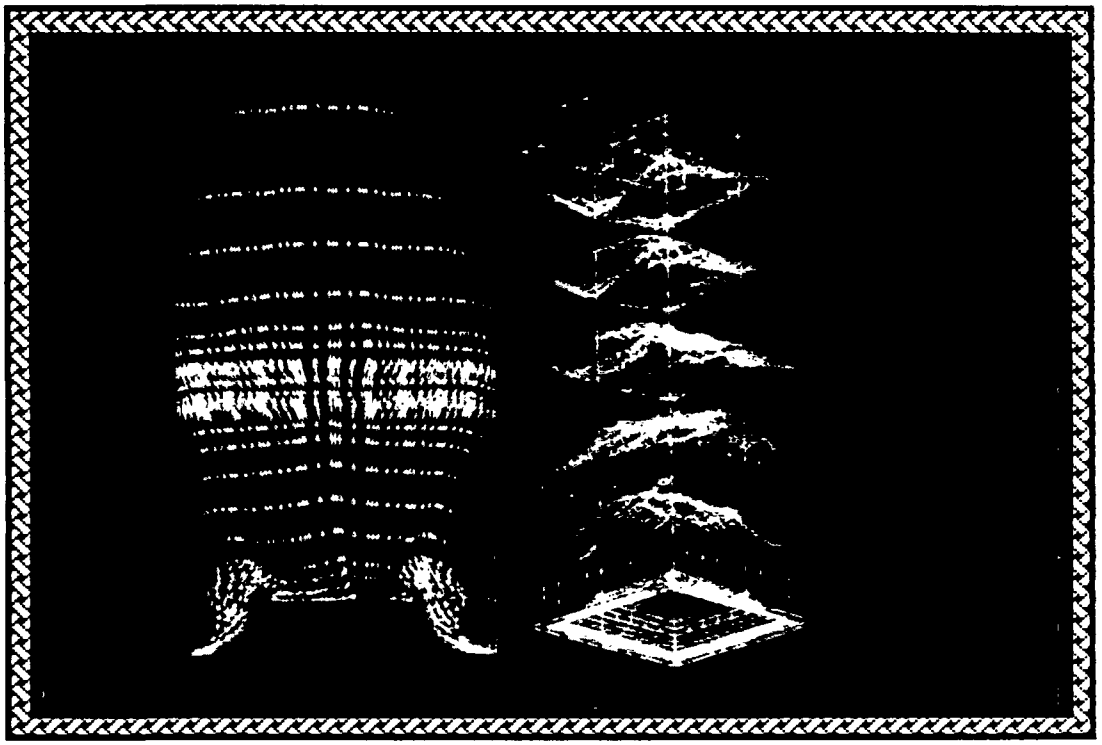

a. Pyramid

Figure 34 (continued).

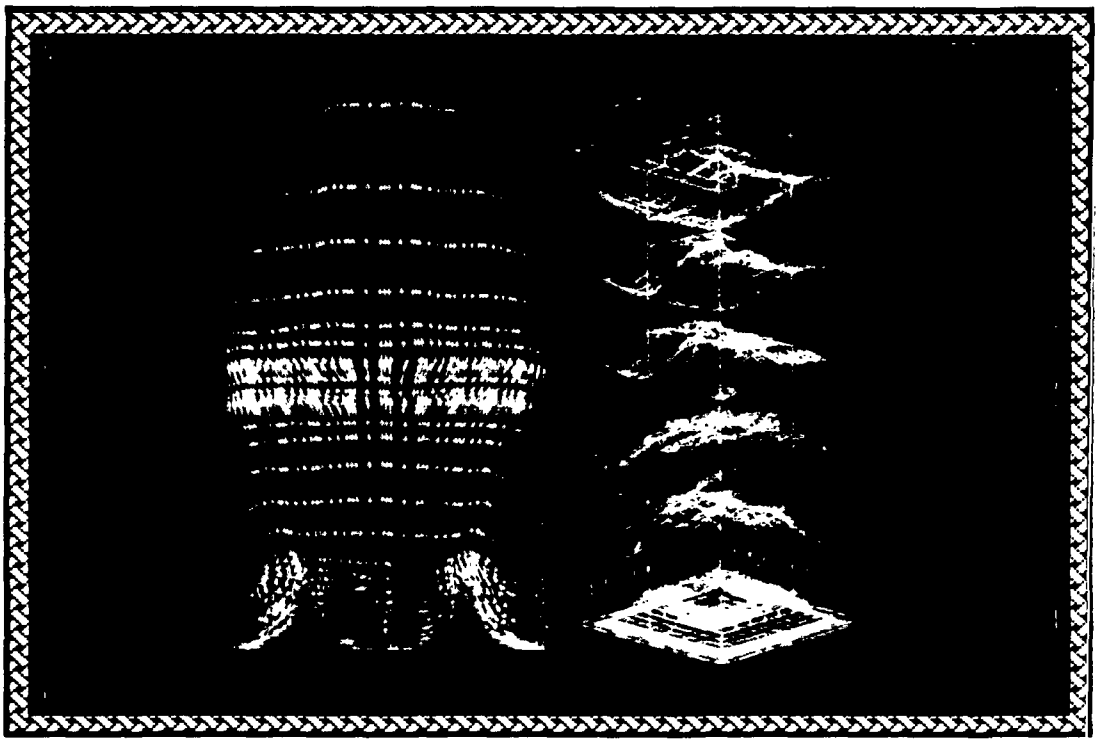

b. Crater

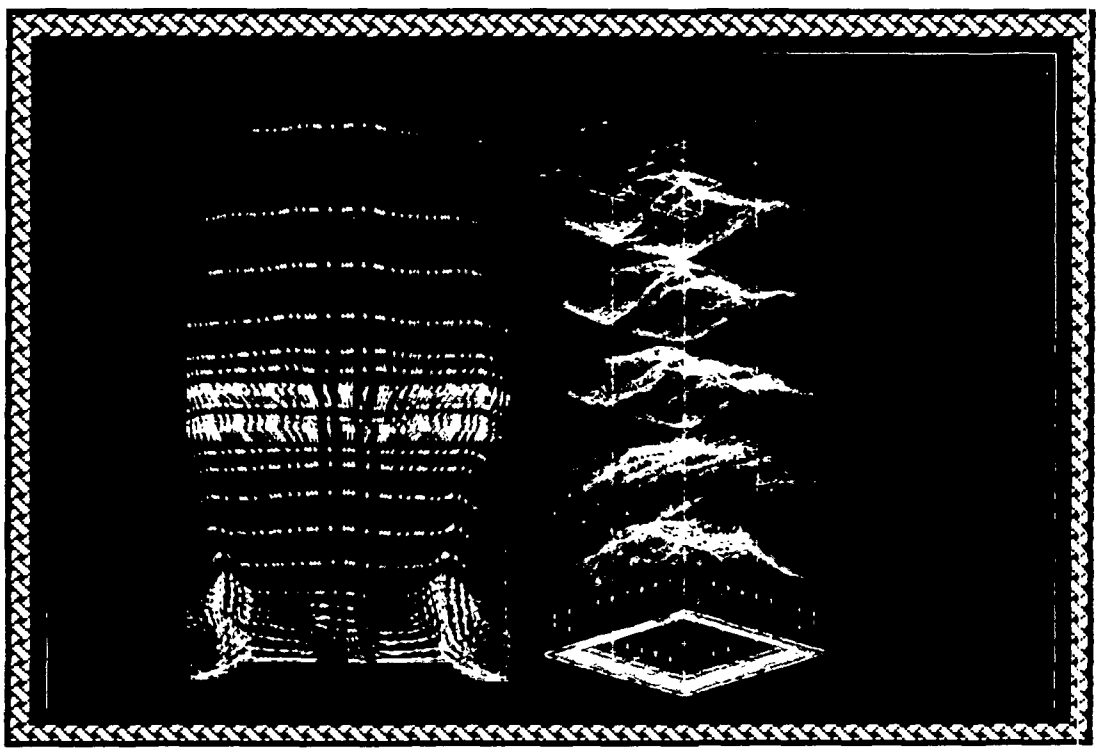

c. Low bed

DETERMINING A STEADY STATE BED SHAPE

Bed height control in operating boilers is sometimes a difficult task. The processes inside a recovery boiler are never at steady state. The bed shape is constantly changing as black liquor quality, gas flow patterns, etc., change. Many of the furnace processes are deterministic, but there are also many stochastic processes. The breaking of chunks of char off the wall and the redistribution of char on the bed are two processes which are difficult to predict. On a steady state basis, of course, there cannot be buildup of black liquor solids on the wall. Similarly, bed growth or decay must be zero for a strictly steady state solution. In fact, each bed cell should have a closed mass balance for a steady state solution. It would be possible to have zero bed growth on a global scale while individual cells are growing and shrinking.

The simulations discussed so far have individual cells which may be growing or shrinking, and the global bed growth or decay is not zero. Residual black liquor solids reach the bed at a location and state which depend on in-flight processes. The bed burning rates are completely independent of the supply rate from the in-flight calculations; thus, there is no inherent reason why a bed cell should have a closed mass balance.

Figures 35 and 36 show the mass reaching the bed and the net growth in the low bed case. The gas flow and liquor spray patterns cause most of the liquor to hit the walls before reaching the bed. Most of the residual black liquor solids therefore land on the periphery of the bed. The bed burning is greatest toward the outside of the bed, but Fig. 36 shows that the bed would be growing at the outside edge of the bed.

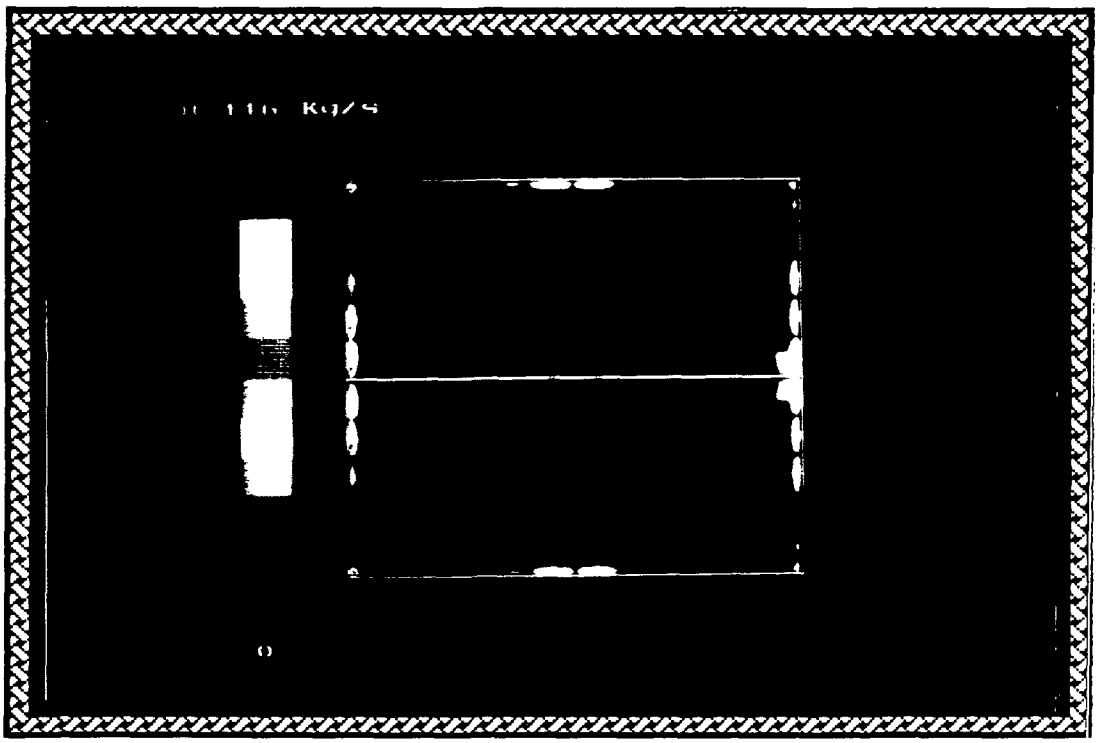

Figure 35. Mass reaching bed (low bed case).

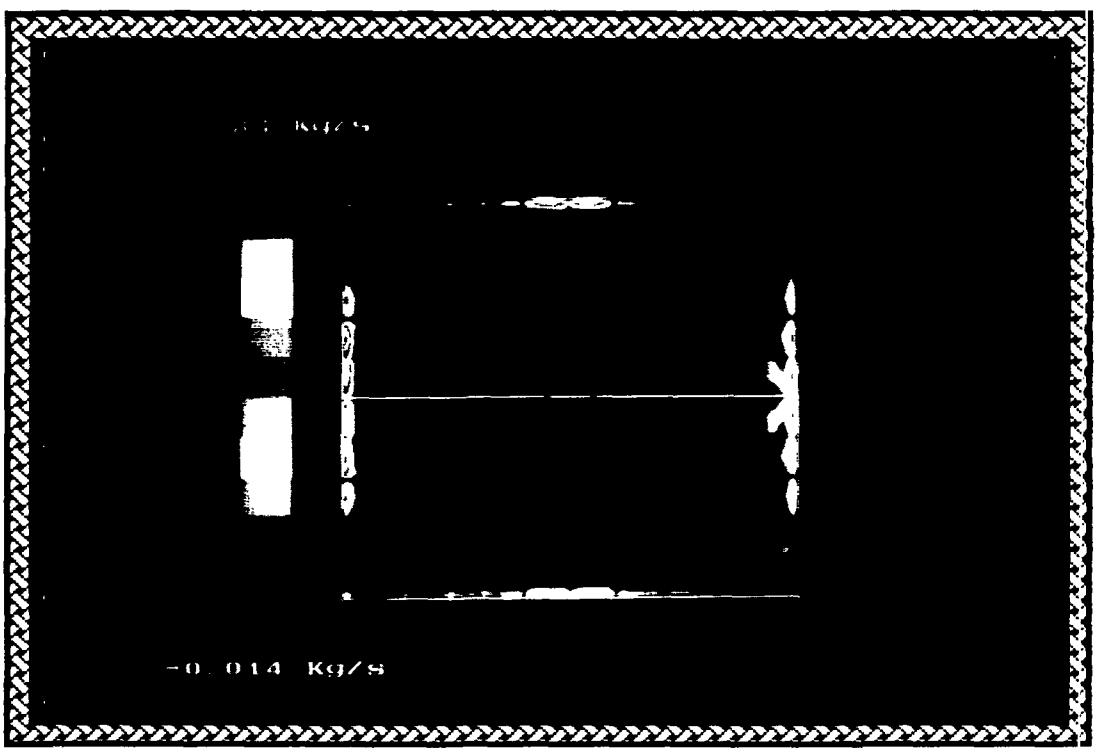

Figure 36. Bed growth and decay (low bed case).

Since there is a discrepancy between the bed shape and the calculations, the results must be rationalized. The simulation predicts growth near the primary air ports. In actual practice, the boiler operator would manually keep the ports clear. In the simulation, this process would have to be done by arbitrarily moving char to different cells. This redistribution is not done in the simulation, but is assumed to occur to match the assumed bed shape.

What is ultimately desired is an algorithm to determine a steady state bed shape. There are several ways to do this, but any algorithm to determine the bed shape will have some degree of arbitrariness. There are two extremes which bracket the range of possibilities for determining a bed shape. One extreme is to specify a shape and redistribute material reaching the bed to achieve a closed mass balance in each cell. The other extreme is to change the bed shape to match the simulation calculations. The discussion that follows considers the merits of the various approaches to determining a steady state bed shape.

Consider the extreme where the bed shape is changed to match the bed burning rate in individual cells. This would be done either by changing the FORTRAN source code to add or subtract bed cells or by interactively changing the case to add or subtract bed cells to growing or shrinking areas of the bed. Growing areas would require more bed height (more bed cells) while shrinking areas would require less height (fewer bed cells). A converged case with an assumed bed shape would be reconverged after bed cells were added or deleted where necessary. This approach would require enormous amounts of computer time and would not work due to random processes which are not taken into account. For example, a shrinking area of the bed would not necessarily reach steady state just by taking bed cells away. The actual bed may be undercut until it partially collapses, filling in the area that was shrinking.

The "steady state" shape in such a case would perhaps lay between a high bed at that site and a low bed, but an algorithm which adds or subtracts cells would keep shrinking until the bed reached the hearth: even then it would not necessarily be at steady state. The situation for a growing area of the bed is analogous. A growing area of an actual bed may topple after reaching a certain height; this is a random, non-steady state effect which can be put on a steady state basis only by specifying a steady state shape. Consider the "growing" cells on the edge of the bed shown in Fig. 36. If the growing areas have cells added, the primary ports will be blocked or the jets will be deflected upward. This can happen in actual practice, but on a steady state basis the ports are kept clear by the boiler operator. An algorithm to match the bed shape to the model calculations without assuming some redistribution will not work.

The other extreme in determining the bed shape is to assume a shape and redistribute the material so that all the bed cells have a closed mass balance. The global carbon balance in the furnace would first have to be closed by increasing or decreasing the liquor firing rate to achieve a zero global bed growth. The material reaching the bed could then be redistributed using some physical reasoning. An example of how physical reasoning could be used is to assume that "nonsticky" particles hitting the bed are carried by the force of the primary jets rather than being trapped where they land. The final adjustments on some cells, however, will be arbitrary. Thus, the bed shape determined by an algorithm which uses only redistribution of char is ultimately arbitrary.

An algorithm for determining bed shape can be constructed by borrowing ideas from the extremes discussed above. The adding or deleting of cells could be used where it would cause an increase or decrease in the bed burning rate. For example, adding a cell or two may raise a growing area into a

region of higher oxygen content where the combustion rate would be higher; or, taking away bed cells may move a shrinking area out of a high combustion rate zone.

Redistribution of char can be accomplished by allowing certain particles hitting the bed to remain in the gas phase. The current model traps the particles at the site where the particles strike the bed. The particles then give up their remaining water and volatiles, sometimes releasing artificially high amounts of fuel in certain cells. Allowing certain particles to remain in the gas phase would spread the particles over the bed in a physically realistic way as well as spreading out the pyrolysis gases in a less arbitrary way than the model now does.

The particle tracking algorithm was modified to determine the effect of allowing certain particles to remain in the gas phase. The particles in the pyrolysis stage when they hit the bed are placed back into the gas cell immediately above the bed. The particles are then acted on by the force of the flowing gases. A comparison of Fig. 37 with Fig. 18 shows that the particles are redistributed from the periphery towards the center of the bed when some particles are allowed to remain in the gas phase. The mass reaching the bed in Fig. 18 is trapped on the periphery while the primary air sweeps the low density particles towards the center of the bed in Fig. 37. Allowing particles in the pyrolysis stage to remain in the gas phase is a physically realistic way of spreading the mass over the bed and also results in the spreading out of pyrolysis gases in a more realistic way.

The modified algorithm results in more in-flight pyrolysis and more carryover. The bed pyrolysis decreased from 0.776 kg/s to 0.371 kg/s. The carryover increased from 4.7% to 5.7% of char entering the furnace. It should

not be concluded that this is an accurate estimate of the increase in carryover due to the change although it is reasonable to expect an increase in the amount of carryover. The particle tracking algorithm could be further modified to keep bed particles from being carried beyond the first gas cell above the bed. The particles could be swept along the bed surface until they left the pyrolysis stage, fell to the bed due to densification, or perhaps until they encountered a shrinking cell. This last criterion is the most arbitrary of the three cited, but would be one way to close the mass balances in shrinking cells.

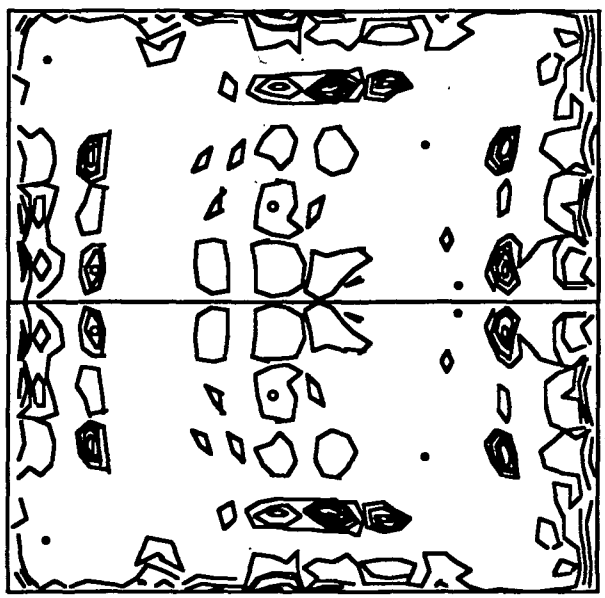

Figure 37. Mass in when pyrolyzed particles reaching the bed are put back in gas phase.

It is not possible to determine a steady state bed shape without making some arbitrary assumptions. The arbitrariness of the assumptions determines the extent to which the bed shape is arbitrarily defined. Different assumptions could lead to different bed shapes. As shown earlier, the bed shape affects furnace behavior, but a deterministic way of determining a bed shape is elusive.

Developing a bed shape algorithm may cause more problems than it solves; a preferable approach is to take bed shape into account in the furnace simulations. Bed shapes which have been observed in practice can be assumed,

and their effect on furnace behavior can be examined. Some bed shapes may be preferable to others; the "desirable" bed shapes can then be incorporated into operating objectives for real furnaces.

The fact that a bed is growing or shrinking in a steady state case does not invalidate the model. The time constant for changing the bed shape is expected to be much longer than the time constant for changing the flow patterns. A pseudo-steady-state bed is valid in the steady-state model.

CONCLUSIONS

A three-dimensional computer model of a kraft char bed has been developed in this thesis which satisfies the objectives stated earlier. The model handles important combustion reactions using the best information available for the individual chemical reactions. It is flexible enough to incorporate new data as it becomes available and to allow an arbitrary bed shape to be specified. It handles variations in temperature, velocity, and gas concentrations across the bed. The model predicts the char combustion rate and reduction efficiency on the bed.

The conclusions can be grouped into modeling issues and operating implications for the furnace. The conclusions associated with modeling issues are as follows:

1) It is possible to develop a char bed model in the context of a computation fluid dynamics program.

2) The C/CO_2 and C/H_2O reactions are responsible for approximately two thirds of the bed burning rate.

3) The fact that the gasification reactions are important on the char bed makes the in-flight char particle combustion model deficient. The gasification reactions are included in the bed model, but they are not included in the in-flight char combustion model. Walsh concluded that particles which are swept into a hot, oxygen-deficient core of upward-flowing gases are carried out of the furnace because they remain in a low density form[32]. This conclusion may be modified if the gasification reactions are included in the in-flight char particle

combustion model. CO_2 and H_2O in the oxygen deficient core could burn out some particles in an oxygen deficient core.

4) There is a problem with unreasonably high temperatures in some gas cells close to the char bed. The problem is caused by excessive fuel released near cells with high oxygen contents and a high degree of turbulence. The k- ε turbulence model apparently overpredicts mixing in regions of high shear rate near the primary ports. Fuel from the bed entering these cells reacts as far as stoichiometry allows. Unrealistic reaction rates lead to temperatures as high as 2500 K which tend to be propagated over the bed region. The resulting high temperatures above the bed cause a high radiant heat flux back to the bed. The bed energy balance is heavily influenced by radiation. The predicted surface temperatures are higher than expected, but the combustion rate is not overestimated if burning is mass transfer controlled (see Fig. 27). The problem of artificially high temperatures is moderated by spreading pyrolysis gases over more cells to reduce the heat release in individual cells.

5) The accuracy of the reduction efficiency prediction is affected by an assumption which is invalid in the particle tracking model near the primary air ports. The assumption that particles have the same temperature as the cell they are in causes particles landing on the periphery of the bed to become cold (ca. 500 K) immediately before landing on the bed. The cold particles "black out" the edge of the bed by supplying cold mass with little sensible heat. The cold temperatures on the edge of the bed resulting from this phenomenon cause low sulfate reduction rates. A low reduction

efficiency on the edge of the bed brings down the average reduction efficiency as much as 26%.

6) There is no way currently to construct a model in FLUENT/RFM which solves for the bed shape without introducing a high degree of arbitrariness. The bed shape must be arbitrarily specified in the current version of FLUENT/RFM, and there is no mechanism for closing the mass balance in individual cells. Individual cells can grow or shrink, and the global bed mass balance can likewise be out of closure. The bed shape suggested by the bed cell mass balances is not likely to be the same as the specified bed shape, but an algorithm to determine the bed shape must be physically realistic or the end result will be no better (and perhaps worse) than specifying an arbitrary bed shape. A preferable approach to trying to solve for a steady-state bed shape is to investigate the influence of bed shape in a given furnace simulation to determine the extent to which bed shape influences overall furnace behavior. FLUENT/RFM is not structured to facilitate solving for bed shape; other programs which have an adaptive grid structure are better suited for developing an algorithm for determining the bed shape.

7) A pseudo-steady-state bed is valid in FLUENT/RFM since the time constant for changes in bed shape are much longer than the time constant for changes in the flow patterns.

8) Allowing certain particles hitting the bed to remain in the gas phase is more physically realistic than arbitrarily trapping particles where they strike the bed. Some particles may be in a low-density state when they reach the bed, and the force of the primary jets would

sweep these particles across the surface of the bed if the model allows it. The high-temperature problem would be reduced since the volatiles would be more evenly distributed. Spreading the volatiles this way is more physically realistic than arbitrarily specifying a certain fraction of bed pyrolysis in the cells above the bed.

The conclusions related to recovery furnace operation are as follows:

1) Most of the char combustion can take place on the bed. The case using Brown's experimental correlation had bed burning rates which were 119% of the char entering the furnace. A firing strategy which seeks to maximize bed burning would permit coarser sprays to be used, and larger drops are less likely to be carried out of the furnace. Pluggage problems would decrease as a result, and energy efficiency would be improved due to less sootblowing steam usage and cleaner heat transfer surfaces.

2) Heat release in the lower furnace is desirable from the standpoint of keeping a high bed surface temperature which in turn promotes rapid burning rates and a high reduction efficiency. The C/CO_2, C/H_2O, and C/Na_2SO_4 reactions are endothermic reactions which will tend to cool the bed surface, but gas phase oxidation of CO and volatiles above the bed is a means of providing heat to the surface to keep the endothermic reaction rates high.

3) The bed shape influences the flow patterns in the lower furnace. There appears to be a difference in carryover caused by different bed

shapes, but this conclusion is very tentative since cases used to draw this conclusion were not completely converged.

4) A large oxygen supply should not jeopardize the reduction efficiency provided there is sufficient carbon and high temperatures. The model predicts that the sulfate/sulfide cycle is mass transfer limited in oxygen except around the perimeter of the bed. The reduction efficiency is in general not threatened by a large oxygen supply, but smelt leaving the furnace should be isolated from cool, oxygen-rich air. Oxygen from the primary ports is rapidly consumed by combustibles above the bed. Oxygen in the combustion air is a significant oxidant on the char bed surface, but gas-phase oxygen consumers such as pyrolysis gases and CO reduce the amount of oxygen that can make it to the surface. On the other hand, oxygen gets to the surface indirectly via oxidation of gases to CO_2 and H_2O which in turn react with the char bed surface. A sufficient oxygen supply in the lower furnace is therefore essential to fast bed burning rates.

FUTURE WORK

The future work needed to upgrade FLUENT/RFM as a whole was discussed in Jones' thesis[31]. This section will focus on issues pertaining to char burning in general and bed burning in particular.

A more comprehensive mass transfer correlation is desirable. Brown's correlation is the best available for char burning on the bed at present, but its range of applicability is limited to no more than 6 m/s. Extrapolation to higher velocities gives substantially different mass transfer coefficients depending on the assumed power dependence of velocity. A larger velocity range is necessary to determine the power dependence of velocity with statistical significance if possible.

Data on the C/CO_2 reaction rate is required to clear up the ambiguities involved in Li's rate expression. Data on the C/H_2O rate is also required since the form of Li's expression was used in the model rather than actual data for the C/H_2O reaction.

Some of the methods of redistributing the mass discussed above could be investigated and expanded. Any redistribution done to determine a bed shape should at least be physically realistic or nothing more will be gained than by arbitrarily specifying a bed shape.

A fuming model and a sulfur release model would be useful for investigating their effects on recovery boiler operation. A bed fuming model and particle fuming model could be incorporated into FLUENT/RFM as soon as more computer memory and rate data for fume generation and deposition become available. At present, the furnace simulation requires all 16 Mbytes in the MicroVax II station used in this thesis. Fume modeling would require one

more chemical species, and a sulfur model would require a reduced-sulfur species and an oxidized-sulfur species in FLUENT/RFM.

Little useful information could be gained from a subsurface model. Current modeling techniques are insufficient to accurately handle all the processes occurring beneath the surface of the char bed. A subsurface model would need to handle simultaneous endothermic chemical reaction, heat transfer, and three-phase flow through porous media with possible phase change. The main output of the model would be the final reduction efficiency of the smelt leaving the furnace. It has been shown earlier, however, that most of the reduction can occur near the surface. Thus, the additional information gained from a detailed subsurface model would not be that useful.

The in-flight particle combustion model should be modified to include the gasification reactions. This modification could have a substantial impact on predicted in-flight combustion and carryover. The method of determining the particle temperature in the char combustion and smelt oxidation stages should also be changed. One possible solution is to assume that particles hitting the bed have a temperature which is representative of a burning particle rather than assuming that the particle equilibrates instantaneously with the gas temperature.

The parameters used to determine k and ε in the turbulence model should be investigated to see to what extent they contribute to unrealistic combustion rates in the gas phase.

LITERATURE CITED

1. Hupa, M.; Solin, P. Combustion behavior of black liquor droplets. TAPPI Proceedings, 1985 International Chemical Recovery Conference, Book 3, p. 335.

2. Richardson, D. L.; Merriam, R. L. Study of cooling and smelt solidification in black liquor recovery boilers. Phase I report, prepared for The American Paper Institute, New York, February, 1977.

3. Richardson, D. L.; Merriam, R. L. Study of cooling and smelt solidification in black liquor recovery boilers. Phase II report, prepared for The American Paper Institute, New York, December, 1978.

4. Cameron, J. H,; Grace, T. M. Sulfate reduction with carbon is strongly influenced by bed surface temperature. TAPPI 65(7):84(1982).

5. Brown, C.; Grace, T.; Lien, S.; Clay, D. Char bed burning rates -- experimental results. TAPPI proceedings, 1989 International Chemical Recovery Conference, p. 65.

6. Aiken, G. The use of a char pile reactor to study char bed processes. Doctoral Dissertation. Appleton, WI, The Institute of Paper Chemistry, January 1988.

7. Li, J.; van Heiningen, A. R. P. Mass transfer limitations in the gasification of black liquor char by CO_2. JPPS 12(5):146(1986).

8. Grace, T. M.; Cameron, J. H.; Clay, D. T. Char burning, Project 3473-6, The Institute of Paper Chemistry, Appleton, WI, February, 1985.

9 Gehri, R.; Oldenkamp, R. Status and economics of the Atomics International aqueous carbonate flue gas desulfurization process. FGD Symp. Proc. Rept. EPA-600/2-76-136A, May, 1976.

10. Grace, T. M.; Cameron, J. H.; Clay, D. T. Role of sulfate/sulfide cycle in char burning -- experimental results and implications. TAPPI 69(10):108(1986).

11. Thorman, R. P.; Macur, T. S. Kinetics of sodium sulfate reduction by carbon in molten sodium carbonate. TAPPI Proceedings, 1985 International Chemical Recovery Conference, Book 3, p. 451.

12. Smoot, L. D.; Smith, P. J. Coal Combustion and Gasification, Plenum Press, New York, 1985.

13. Li, J. M. Eng. Thesis, Chapter 3, McGill University, Montreal, Feb. 1986.

14. Goerg, K., and Cameron, J. Kinetic study of kraft char gasification with carbon dioxide. AIChE Mtg.(Boston) Preprint no. 67g, 6p. (Aug 24-27) 1986.

15. Clay, D. T.; Grace, T. M.; Kapheim, R. J.; Semerjian, H. G.; Macek, A.; Charagundla, S. R. Fundamental studies of black liquor combustion. Report No. 1, Phase 1. US DOE Contract No. ACO2-83CE40637, cooperative program between The Institute of Paper Chemisrty, Appleton, WI and the National Bureau of Standards, Gaithersburg, MD.

16. IPC Lab notebook No. 3547, 1983.

17. Galtung, F. L.; Williams, T. J. A mathematical model and digital computer based advanced control system for a kraft mill recovery unit. Report number 43. Purdue University, October, 1971.

18. Merriam, R. L. Kraft, Version 2.0 computer model of a kraft recovery furnace, Vol. II: Engineering Manual, prepared for The American Paper Institute, New York, December, 1980.

19. Zhitkov, V. V.; Yukov, Y. Rate of Na_2SO_4 reduction in the presence of Na_2CO_3, Sb. Tr. VN11 Tsellyul- Bumazh, Prom. 61:96-99(1972).

20. Shiang, N. T.; Edwards, L. L. Kraft recovery furnace modeling and simulation: heat transfer and gas flow. AIChE Symposium Series No. 246, 81:85(1985).

21 Shiang, N. T. Doctoral Dissertation, University of Idaho, 1986.

22. Shiang, N. T. Personal communication, February, 1989.

23. Cussler, E. L. Diffusion: Mass transfer in fluid systems. Cambridge University Press, 1984.

24. Schlichting, H. Boundary Layer Theory, McGraw-Hill Book Company, New York, 1960.

25. Bird, R. B.; Stewart, W. E.; Lightfoot, E. N. Transport Phenomena, John Wiley & Sons, New York, 1960.

26. MacCallum, C.; Blackwell, B. R. Critical review of kraft recovery boiler air systems, Pulp and Paper Canada, 88(10):103(1987).

27. Sherwood, T. K.; Pigford; R. L.; Wilke, C. R. Mass Transfer, McGraw-Hill Book Company, New York, 1975.

28. Treybal, R. L. Mass-transfer Operations, McGraw-Hill Book Company, New York, 1980.

29. Ranz, W. E., and Marshall, W. R., Chem. Eng. Prog., 48: 173(1952).

30. Brown, C.; Grace, T.; Lien, S.; Clay, D. Experimental char bed burning rates -- first data under realistic controlled conditions, Unpublished report, The Institute of Paper Chemistry, January, 1989.

31. Jones, A. K. A model of the kraft recovery furnace. Doctoral Dissertation. The Institute of Paper Chemistry, Appleton, WI, December, 1988.

32. Walsh, A. R. Development of a computer model for in-flight black liquor combustion in a kraft recovery furnace. Doctoral Dissertation, The Institute of Paper Chemistry, Appleton, WI, October, 1988.

33. FLUENT Reference Manual. Creare, Inc. Hanover, NH.

34. Smith, J. M.; VanNess, H. C. Introduction to Chemical Engineering Thermodynamics, 3rd edition, McGraw-Hill Book Company, New York, 1975.

35. Stull, D. R.; Prophet, H. JANAF Thermochemical Tables, 2nd edition, NSRDS-NBS37, National Bureau of Standards, Washington, DC, June, 1971.

36. Gosman, A. D.; Lockwood, F. C. Incorporation of a flux model for radiation into a finite-difference procedure for furnace calculations. 14th Symposium on Combustion, 1972.

37. Patankar, S. V. Numerical Heat Transfer and Fluid Flow. New York, McGraw-Hill Book Co., 1980.

ACKNOWLEDGMENTS

I am grateful for all the support and direction I have received while at The Institute of Paper Chemistry. I thank the Institute and its member companies for providing me with a stimulating environment and an excellent learning experience. I appreciate the clear insight and wisdom of my advisor, Dr. Thomas Grace. I also value the contributions of the other members of my committee, Dr. Theodore Farrington and Dr. David Clay.

Critical components of the modeling effort were supplied by Creare, Inc. and Weyerhaeuser Paper Company. The FLUENT source code was made available through the efforts of Dr. Farrington, and a VAXstation II was loaned to the Institute thanks to Craig Brown.

I appreciated working as a group with Andy Jones and Al Walsh on FLUENT/RFM.

I am very thankful to my wife, Marie, and my children, Stephan and Julia, for their patience and endurance during difficult stretches of this work.

APPENDIX I

AN IMPROVED THEORY OF CHAR BURNING

D. W. Sumnicht, K. A. Kulas, and T. M. Grace
The Institute of Paper Chemistry
Appleton, WI 54912

INTRODUCTION

Kraft black liquor combustion proceeds through four distinct stages: drying, volatilization, char combustion, and smelt oxidation (1). Drying removes the water and volatilization produces gaseous organic compounds, leaving fixed carbon, a small amount of fixed hydrogen, and inorganic alkali salts. This residual mixture is referred to as char, and the organic carbon in the char is referred to as char carbon. Char combustion is the slowest stage of black liquor combustion and may not be completed during the flight of the particle in the recovery furnace. In such a case, the particle can fall onto the char bed at the bottom of the furnace where combustion of char carbon is completed. During char combustion, sodium sulfate (Na_2SO_4) is reduced to the active pulping chemical sodium sulfide (Na_2S).

The simultaneous oxidation of char carbon and reduction of sodium sulfate is described by the sulfate/sulfide cycle theory of char burning. The sulfate/sulfide cycle was first identified in molten sodium carbonate melts by Gehri and Oldenkamp (2) and later applied to kraft char burning by Grace et al. (3). The cycle is depicted in Figure 1. Oxygen reacts with sodium sulfide (Na_2S) to produce sodium sulfate (Na_2SO_4) which in turn reacts with char carbon to produce a mixture of carbon monoxide (CO) and carbon dioxide

(CO_2); sodium sulfide is regenerated in the reaction between char carbon and sodium sulfate. In the sulfate/sulfide cycle, the only pathway for carbon consumption is the C/Na_2SO_4 reaction, and the only source of oxygen for the Na_2S/O_2 reaction is oxygen from the combustion air. The relative amounts of sulfide and sulfate depend on the relative rates of the Na_2S/O_2 and C/Na_2SO_4 reactions. Sulfide predominates over sulfate while carbon is burned if the rate-limiting step is the Na_2S/O_2 reaction or oxygen mass transfer; it is therefore possible to have sulfide be the dominant sulfur species as char carbon is burned in air.

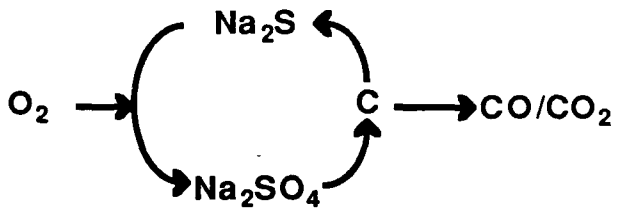

Figure 1. Sulfate - sulfide cycle.

Grace et al. (3) developed a quantitative treatment of the sulfate/sulfide cycle to predict the rate of carbon loss and the sulfur oxidation state for a burning char particle. Their theory used kinetic information on the C/Na_2SO_4 reaction and the Na_2S/O_2 reaction which was experimentally determined in smelt pool reactors. The application of their theory to the burning of single macroscopic char particles was successful at predicting mass versus time data including:

1. a constant weight loss period, indicative of external mass transfer control;

2. weight gains near the end of combustion due to sulfide reoxidation in the residual smelt drop;

3. an apparent high reduction efficiency during burning as manifested by the evidence for sulfide reoxidation at the end of the burn.

The simple sulfate/sulfide cycle theory has two weaknesses:

1. use of the smelt-pool C/Na_2SO_4 rate equation requires postulating temperatures as high as 1600 K in order to match experimental burning rates;

2. the model is incapable of predicting the burning rate for a soda liquor in which no sulfur is present.

The char burning model can be improved by including the following carbon reactions in addition to the C/Na_2SO_4 reaction:

$$C + \tfrac{1}{2} O_2 \rightarrow CO \quad (1)$$

$$C + O_2 \rightarrow CO_2 \quad (2)$$

$$C + CO_2 \rightarrow 2CO \quad (3)$$

$$C + H_2O \rightarrow CO + H_2 \quad (4)$$

The simple sulfate/sulfide cycle is most applicable to regions where smelt wets and covers the char carbon. In these cases, oxygen reacts with sulfide in the smelt, and the sulfate product reacts with carbon. However, not all of the char carbon is necessarily covered by smelt, and char carbon can react directly with the gases flowing over the char. Thus, reactions (1) - (4) can operate simultaneously with the sulfate/sulfide cycle.

One problem with the simple sulfate/sulfide cycle is the need to hypothesize high reaction temperatures. Char bed temperatures are in the range of 1200 - 1400 K, and char particle temperatures have been measured as high as 1473 K (1). The original sulfate/sulfide cycle theory of char burning, however, requires reaction temperatures as high as 1600 K in order to predict a fast enough C/Na_2SO_4 rate to match experimental particle burning rates and to maintain a high reduction efficiency until near the end of the particle burn.

At lower temperatures, Grace et al.'s equations predict net oxidation of the sulfide early in the particle burn instead of the experimentally observed oxidation of sulfide near the end of the burn.

The sulfate/sulfide cycle operates when the oxygen gas reacts with char carbon via liquid smelt, but direct gas/char-carbon contact is also possible. As a char particle burns, one can see small regions of molten inorganic salts ("smelt") and other regions that appear carbonaceous and which coexist with the molten regions. A more general theory of char burning would take direct gas/carbon reactions into account.

IMPROVED THEORY OF CHAR BURNING

This paper describes a revised theory of char burning that takes the carbon/oxygen and carbon/CO_2 reactions into account in addition to the sulfate/sulfide cycle. Carbon/H_2O reactions are not included because kinetic data for kraft char are not available. Equation (5) describes the carbon depletion rate:

$$-\frac{d[C]}{dt} = \frac{4}{2 - f_{cs}} R_{CS} + \frac{2}{2 - f_{cox}} R_{COX} + R_{CO_2} \qquad (5)$$

where

[C] = carbon concentration, mole C/mole Na_2
R_{CS} = C/Na_2SO_4 reaction rate, mole Na_2SO_4/mole Na_2-sec
R_{COX} = C/O_2 reaction rate, mole O_2/mole Na_2-sec
R_{CO_2} = C/CO_2 reaction rate, mole C/mole Na_2 -sec
f_{cs} = molar CO/(CO + CO_2) ratio for the carbon/sulfate reaction
f_{cox} = molar CO/(CO + CO_2) ratio for the carbon/oxygen reaction

Equation (6) is a sulfide balance:

$$\frac{d[Na_2S]}{dt} = s\frac{dr}{dt} = R_{CS} - R_{SO} \qquad (6)$$

where

$[Na_2S]$ = sulfide concentration, mole Na_2S/mole Na_2
R_{CS} = C/Na_2SO_4 reaction rate, mole Na_2SO_4/mole Na_2-sec
R_{SO} = sulfide oxidation rate, mole Na_2S/mole Na_2-sec
r = "reduction efficiency" = molar $Na_2S/(Na_2S + Na_2SO_4)$ ratio
s = moles sulfur/mole Na_2

Equations (5) and (6) describe the rate of char carbon consumption and the net oxidation state of the sulfur species. They provide a quantitative treatment of the combustion of a discrete quantity of char, provided that appropriate rate equations for the individual reactions are available. The next step in the development of the model is to choose representative rate equations for R_{CS}, R_{COX}, R_{SO}, and R_{CO2}.

Rate equation for the C/Na_2SO_4 reaction

Rate expressions have been developed for the C/Na_2SO_4 reaction in a molten carbonate melt for different types of carbon. A smelt pool reactor was used by Grace et al. (3) The reactor consists of a crucible which is heated to a set temperature by an induction furnace. Small quantities of char are placed in a smelt and the sulfate/sulfide cycle is active when an oxygen-containing gas is bubbled through the smelt. The system relies on the bubbling action for mixing the char/smelt mixture. The sulfide oxidation was found to be a very fast, mass-transfer-controlled reaction in this system. The rate expression for the C/Na_2SO_4 reaction takes the following form:

$$R_{CS} = -k_1 \left\{ \frac{[SO_4]}{k_2 + [SO_4]} \right\} [C] e^{\frac{-E_{CS}}{RT}} = -k_1 \left\{ \frac{(1-r)s}{k_2 + (1-r)s} \right\} [C] e^{\frac{-E_{CS}}{RT}} \quad (7)$$

where

$[SO_4]$ = sulfate concentration, mole sulfate/mole Na_2
[C] = carbon concentration, mole C/mole Na_2
k_1, k_2 = rate constants
E_{CS} = activation energy
R = gas constant
T = absolute temperature

Table 1 contains the rate constants for different types of carbon in batch experiments with great excess of molten salt.

Table 1. Rate parameters for carbon-sulfate reaction (3).

Carbon type	k_1, sec^{-1}	k_2, $\frac{\text{mole } SO_4}{\text{mole} Na_2}$	E, $\frac{cal}{mole}$
Kraft char	$1.31 \pm 0.41 \times 10^3$	0.0011 ± 0.0004	$29{,}200 \pm 1{,}000$
Pulverized graphite	$4.94 \pm 0.82 \times 10^4$	0.0013 ± 0.0003	$44{,}000 \pm 1{,}200$
Soda char	$3.04 \pm 0.73 \times 10^5$	0.0020 ± 0.0006	$39{,}850 \pm 1{,}500$

The C/Na_2SO_4 reaction was also studied by Thorman and Macur using activated carbon (4). Their rates were generally lower than those found by Grace et al. for kraft char. In this paper, the parameters shown in Table 1 were used.

Rate equation for the C/O_2 reaction

An appropriate rate equation for the carbon/oxygen reaction must be chosen. Limited weight loss data for combustion of soda char particles are available, but a rate equation has not been developed (3). It is possible to borrow the mathematical form of a rate equation from the coal literature, and

fit it to the soda char data.

A first-order rate constant expression for a bituminous coal char taken from Smoot and Smith (5) provides a reasonable fit:

$$k_r = 236\, T_g\, e^{\left(\frac{-11022}{T_p}\right)} \tag{8}$$

where

k_r = rate constant, cm/s
T_g = gas temperature, K
T_p = particle temperature, K

For an irreversible heterogeneous reaction which is first order in oxygen concentration, the rate of oxygen consumption is K^*C_{BO} where the reaction constant K is comprised of the mass-transfer resistance and chemical reaction resistance in series (6). The mass-transfer coefficient, k_m, and chemical reaction constant, k_r, make up K as follows:

$$K = \frac{1}{\frac{1}{k_m} + \frac{1}{k_r}} \tag{9}$$

Equation (10) shows the kinetic rate constant, and the mass-transfer coefficient is calculated using the Ranz correlation for flow past spheres (7).

$$Sh = \frac{k_m d}{D} = 2.0 + 0.6\, Re^{\frac{1}{2}}\, Sc^{\frac{1}{3}} \tag{10}$$

where

d = particle diameter
D = diffusivity
ν = kinematic viscosity
Re = Reynolds number = $\langle v \rangle d/\nu$
Sc = Schmidt number = ν/D

Figure 2 shows that Equations (8) through (10) do an adequate job of predicting soda char burning rates. The circles represent the actual data for a soda char burn while the lines are the predicted curves for 1300, 1400, and 1500 K. The effect of a range of temperatures is shown since the actual particle temperature was not measured. The indicated temperatures were assumed to be both the particle and gas temperatures. Note that soda char was used rather than kraft char so that the sulfate/sulfide cycle would not be occurring in parallel with the carbon/oxygen reaction. There is always

Figure 2. Predicted soda char rates using coal data.

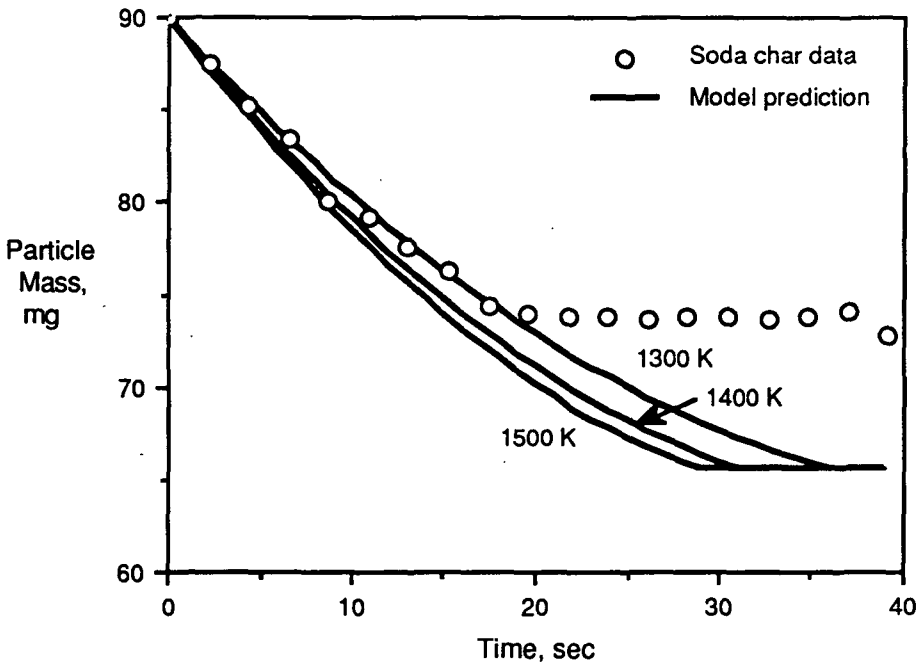

residual carbon at the end of a soda char burn, so the ultimate weight loss is not as great as if burnout was complete. The model assumes a constant temperature throughout the burn, but the heat of reaction near the end of a soda char burn is not great enough to maintain high temperature, so the reaction stops before the carbon is completely burned. The data where weight loss occurs is fit well by the predicted curve, so the expression chosen for the kinetic rate constant is adequate for use in the model.

Rate equation for the C/CO_2 reaction

The C/CO_2 reaction was studied by Goerg (8) at very low carbon concentration and by Li (9) at high carbon concentration. Li's data span the range of 1.2 - 5.8 mole C/mole Na_2 while Goerg's data span the range of 0.015 - 0.062 mole C/mole Na_2 . Li's data were taken in the temperature range of 973 - 1048 K to avoid mass-transfer interferences while Goerg's data were taken in the range of 1200 - 1283 K. Thus, Li's equation must be extrapolated to higher temperature while Goerg's equation must be extrapolated to higher carbon content to match the conditions found during char burning in the recovery furnace. When their rate expressions are put in the same units, they take the following form:

$$R_{CO_2} = \frac{-k_1 P_{CO_2}[C]}{1 + k_2 P_{CO_2} + k_3 P_{CO}} e^{\frac{-E_{CO2}}{RT}} \qquad (11)$$

The values of the constants are found in Table 3.

Table 3. Values for C/CO_2 rate equation.

Parameter	Goerg	Li
k_1	1.043×10^8 $(atm\text{-}sec)^{-1}$	9.53×10^7 $(atm\text{-}sec)^{-1}$
k_2	28.99 atm^{-1}	10.8 atm^{-1}
k_3	45.6 atm^{-1}	6.3 atm^{-1}
E	227,300 J/mole	187,000 J/mole

The inhibitory effect of CO and CO_2 is stronger in Goerg's data than Li's. The different activation energies have the biggest effect on the calculated rate. Goerg's activation energy is 21% greater than Li's. The overall result is that Li's predicted rate is two orders of magnitude greater than Goerg's predicted rate at 1300 K. This difference may be due to the different modes of C/CO_2 contact. The CO_2 in Goerg's system must interact with smelt before reacting with the

carbon whereas the CO_2 in Li's system can react directly with carbon. Li's system is more representative of a burning char particle than Goerg's, so Li's constants are used in this paper.

Rate equation for the Na_2S/O_2 reaction

The Na_2S/O_2 reaction rate, R_{SO}, can be equated to both the mass-transfer rate and the chemical reaction rate to determine the interfacial oxygen concentration:

$$R_{SO} = k_m (C_{BO} - C_{S_{(1-P)}}) A (1-P) = k_{R_{SO}} C_{S_{(1-P)}} A (1-P) \qquad (12)$$

where

R_{SO} = sulfide oxidation rate
A = external area of the particle
C_{BO} = bulk oxygen concentration
$C_{S_{(1-P)}}$ = oxygen concentration at the liquid surface
k_m = mass transfer coefficient
k_{Rso} = kinetic rate coefficient
P = fraction of the external surface that is solid carbon

The parameter "P" determines the fraction of the oxygen in the air which reacts with the solid carbon. The value of (1-P) is therefore the fraction which reacts with the liquid smelt.

Solving Equation (12) for $C_{S_{(1-P)}}$ and substituting back in, R_{SO} is found to be:

$$R_{SO} = K_{SO} C_{BO} A (1-P) \qquad (13)$$

where K_{SO} is defined by Equation (9). A similar analysis for the C/O_2 reaction

rate, R_{COX}, gives the same form with (1-P) replaced with P:

$$R_{COX} = K_{COX} C_{BO} A P \tag{14}$$

Grace et al. found the oxidation of sulfide to be controlled by oxygen mass-transfer under all practical conditions (3). Thus, K_{SO} is assumed to be equal to the oxygen mass-transfer coefficient, k_m. A factor of two is introduced into the R_{SO} term of the sulfide balance (Equation (6)) since it takes two moles of oxygen per mole of sulfide to get one mole of sulfate.

Given the appropriate equations for the C/Na_2SO_4, C/O_2, C/CO_2, and Na_2S/O_2 rates, the quantitative treatment of kraft char combustion becomes:

$$-\frac{d[C]}{dt} = \frac{4(1310)}{2 - f_{CS}} \left\{ \frac{(1-r)\,s}{0.0011 + (1-r)\,s} \right\} [C]\, e^{\frac{-E_{CS}}{RT}} + \frac{2}{2 - f_{COX}} K_{COX} C_{BO} A P + \frac{9.53 \times 10^7 P_{CO_2} [C]}{1 + 10.8 P_{CO_2} + 6.3 P_{CO}} e^{\frac{-E_{CO2}}{RT}} \tag{15}$$

$$\frac{dr}{dt} = \frac{1310}{s} \left\{ \frac{(1-r)\,s}{0.0011 + (1-r)\,s} \right\} [C]\, e^{\frac{-E_{CS}}{RT}} - \frac{k_m}{2\,s} C_{BO} A (1-P) \tag{16}$$

Equations (15) and (16) can be used to simulate single particle combustion in order to compare the predictions of the model with actual char combustion data. Equations (15) and (16) are two ordinary differential equations which can be solved simultaneously for the carbon concentration and reduction efficiency. If carbon loss and net oxygen gain/loss are assumed to be the only contributors to weight, the particle mass can be calculated as combustion proceeds.

Partition of oxygen between the solid and liquid surfaces

Part of the oxygen from air will react directly with carbon, and part will react with carbon via the sulfate/sulfide cycle. The partition of the oxygen between these two pathways will depend on the fraction of the particle surface which is solid carbon and that fraction which is liquid smelt. The solid fraction of the surface area is assumed to be carbon which reacts directly with oxygen, and the liquid fraction is a smelt/carbon mixture that reacts with oxygen via the sulfate/sulfide cycle. The partition will change as the combustion proceeds. Let "P" be defined as the fraction of the surface area which has gas/solid contact:

$$P = \frac{A_C}{A_C + A_I} \tag{17}$$

where

A_C = surface area of carbon
A_I = surface area of molten smelt

In spheres, the external surface area is proportional to the 2/3 power of volume. If the same relationship is assumed in the function of P, then

$$P = \frac{V_C^{\frac{2}{3}}}{V_C^{\frac{2}{3}} + V_I^{\frac{2}{3}}} \tag{18}$$

where

V_C = volume of carbon
V_I = volume of inorganic

Substituting in m/ρ for the volume and rearranging the terms gives

$$P = \frac{\left(\frac{m}{\rho}\right)_C^{\frac{2}{3}}}{\left(\frac{m}{\rho}\right)_C^{\frac{2}{3}} + \left(\frac{m}{\rho}\right)_I^{\frac{2}{3}}} = \frac{m_C^{\frac{2}{3}}}{m_C^{\frac{2}{3}} + \left(\frac{\rho_C m_I}{\rho_I}\right)^{\frac{2}{3}}} = \frac{\left(\frac{m_C}{m_{C0}}\right)^{\frac{2}{3}}}{\left(\frac{m_C}{m_{C0}}\right)^{\frac{2}{3}} + \left(\frac{\rho_C m_I}{\rho_I m_{C0}}\right)^{\frac{2}{3}}} = \frac{\left(\frac{[C]}{[C]_0}\right)^{\frac{2}{3}}}{\left(\frac{[C]}{[C]_0}\right)^{\frac{2}{3}} + \left(\frac{\rho_C m_I}{\rho_I m_{C0}}\right)^{\frac{2}{3}}} \tag{19}$$

where [C] is the carbon concentration and the subscripts "C", "I", and "0" denote char carbon, inorganic salts, and initial condition, respectively. Thus, P has a value less than one at the start of combustion and decreases nonlinearly to zero at the end of combustion.

The magnitude of P is determined by the char composition and the relative densities of smelt and char carbon. Grace et al. analyzed several chars and concluded that the char composition could be simplified to a few species (3). Based on their results, the kraft char used in the experimental particle burns can be assumed to have the composition shown in Table 4.

Table 4. Simplified char composition.

	mole/mole Na_2
Carbon	3.50
Na_2S	0.06
Na_2SO_4	0.06
Na_2CO_3	0.88

Smelt and amorphous carbon both have a density of about 2 g/cc; if these values are substituted into Equation (19), along with the ratio of m_I to m_C determined from Table 4, P becomes

$$P \cong \frac{\left(\frac{[C]}{[C]_0}\right)^{\frac{2}{3}}}{\left(\frac{[C]}{[C]_0}\right)^{\frac{2}{3}} + 1.86} \qquad (20)$$

However, char particles have considerable void space. If the void fraction is assumed to be located in a carbon matrix while the inorganic components are considered separate from the matrix, then ρ_C would be much lower than the

density of pure carbon. If a density of 0.2 g/cc is assumed for the "char carbon", P becomes

$$P = \frac{\left(\frac{[C]}{[C]_0}\right)^{\frac{2}{3}}}{\left(\frac{[C]}{[C]_0}\right)^{\frac{2}{3}} + 0.4} \qquad (21)$$

Figure 3 shows Equations (20) and (21) which describe how P varies as combustion proceeds.

Figure 3. Fraction of surface area that is carbon as combustion proceeds.

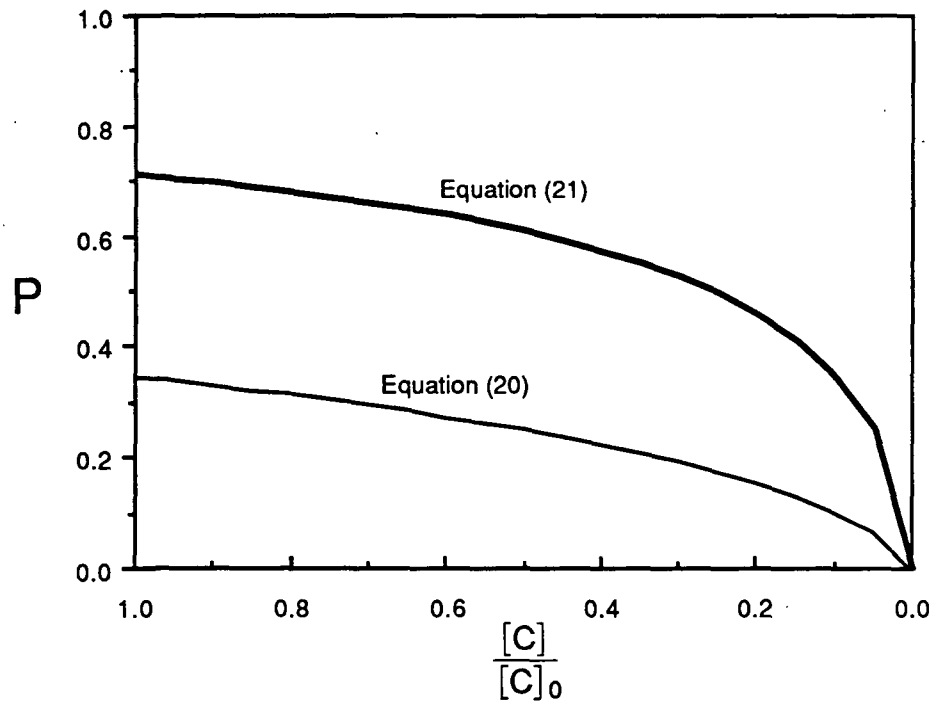

External surface area

The surface area of a sphere can be calculated from variables that are known as combustion proceeds. The volume of the particle, which is just the mass of the particle divided by the density, can be used to calculate the

external surface area. The change in particle mass is due to carbon loss and oxygen loss/gain from the sulfate (weight change from fuming and sulfur loss are assumed to be negligible). Thus, the mass as a function of time is known from Equations (15) and (16), and the volume can be calculated as a function of mass by dividing the mass by a calculated density.

The change in density with mass loss is determined by considering a char particle to be comprised of carbon, inorganic salts, and void volume. It is assumed that the char particle maintains its low density during combustion because of the strength of the carbon matrix. The particle densification during burning is then directly related to the shrinkage of the matrix due to carbon loss. The density of the particle is

$$\rho_p = \frac{m_C + m_I}{V_C + V_I + V_{VOID}} \tag{22}$$

where the subscripts C and I denote carbon and inorganic. The volumes are calculated as the mass divided by the density, and the void volume is related to the amount of carbon left in the particle:

$$V_{VOID} = V_{VOID_0} \frac{m_C}{m_{C_0}} \tag{23}$$

The particle density becomes

$$\rho_p = \frac{m_C + m_I}{\frac{m_C}{\rho_C} + \frac{m_I}{\rho_I} + V_{VOID0} \frac{m_C}{m_{C_0}}} = \frac{m_C + m_I}{m_C\left(\frac{1}{\rho_C} + \frac{V_{VOID0}}{m_{C_0}}\right) + \frac{m_I}{\rho_I}} = \frac{m_C + m_I}{\frac{m_C}{\rho_{C_A}} + \frac{m_I}{\rho_I}} \tag{24}$$

where ρ_{C_A}, the "apparent" carbon density, is the reciprocal of the term in the

parentheses. The volume of the particle is thus

$$V_p = \frac{m_C + m_I}{\rho_p} = \frac{m_C}{\rho_{C_A}} + \frac{m_I}{\rho_I} \tag{25}$$

At the end of the burn, the particle will still have a finite volume since char has a high ash content:

$$\frac{V_\infty}{V_0} = \frac{x_{inorganic}\,\rho_{char}}{\rho_{inorganic}} \tag{26}$$

where

$x_{inorganic}$ = mass fraction of inorganic in the char
$\rho_{inorganic}$ = density of the inorganic material (2 g/cc)
ρ_{char} = initial char density (assumed to be 0.2 g/cc).

Through substitution and rearrangement, Equation (25) becomes:

$$\frac{V_p}{V_0} = \left(1 - \frac{V_\infty}{V_0}\right)\frac{[C]}{[C]_0} + \frac{V_\infty}{V_0} \tag{27}$$

Assuming a spherical geometry, the particle diameter is

$$d_p = d_{p_0}\left(\left(1 - \frac{V_\infty}{V_0}\right)\frac{[C]}{[C]_0} + \frac{V_\infty}{V_0}\right)^{\frac{1}{3}} \tag{28}$$

The external surface area is then πd_p^2.

Boundary layer calculations

The CO and CO_2 concentrations in the gas phase around the particle must be estimated in order to calculate R_{CO_2} from Equation (11). The estimates are obtained by doing a mass balance on the boundary layer. The boundary layer thickness is given by:

$$\delta = 5\sqrt{\frac{\nu\, d_p}{U_\infty}} \tag{29}$$

where

δ = boundary layer thickness
ν = kinematic viscosity
d_p = particle diameter
U_∞ = velocity past particle

The approximate volume of the boundary layer is

$$V_{bl} = \frac{\pi\,(d_p + 2\delta)^3}{6} - \frac{\pi\, d_p^3}{6} \tag{30}$$

The partial pressure of CO_2 and CO in the boundary layer is assumed to follow ideal gas behavior:

$$P_{CO2} = \frac{RT\, m_{CO2}}{44\, V_{bl}} \qquad P_{CO} = \frac{RT\, m_{CO}}{28\, V_{bl}} \tag{31}$$

where

m_{CO2} = mass of CO_2 in the boundary layer, g
m_{CO} = mass of CO in the boundary layer, g
R = gas constant, 0.08206 l-atm/mol-K

A CO_2 balance on the boundary layer is shown in Equation (32). The CO

balance is given in Equation (33).

$$\frac{d\,m_{CO2}}{d\,t} = \left\{\frac{2 * (1 - f_{COX})}{2 - f_{COX}} * R_{COX} + \frac{4 * (1 - f_{CS})}{2 - f_{CS}} * R_{CS} - R_{CO2} - F_{CO2}\right\} * M_{CO2} * n_{Na_2} \qquad (32)$$

$$\frac{d\,m_{CO}}{d\,t} = \left\{\frac{2 * f_{COX}}{2 - f_{COX}} * R_{COX} + \frac{4 * f_{CS}}{2 - f_{CS}} * R_{CS} - 2 * R_{CO2} - F_{CO}\right\} * M_{CO} * n_{Na_2} \qquad (33)$$

where

F_{CO2} = mass transport of CO_2 away from the boundary layer, mole CO_2/mole Na_2-sec

F_{CO} = mass transport of CO away from the boundary layer, mole CO/mole Na_2-sec

M_{CO2} = molecular weight of CO_2
M_{CO} = molecular weight of CO
n_{Na2} = moles Na_2 in particle

F_{CO2} and F_{CO} can be calculated using Equation (10) for the mass transfer coefficient and assuming zero concentration of CO and CO_2 away from the particle.

Experimental

The single particle reactor shown in Figure 4 was used to obtain data on char particle burning which can be used to test the model. An O_2-N_2 mixture was heated in an electrical furnace, directed through an insulated pipe, and passed through a flow straightener before flowing past a suspended particle. Weight loss data are obtained with a microbalance, burn times are taken from

videocamera recordings, particle temperatures are measured with an optical two-color pyrometer, and gas composition is measured by diverting a sample to analyzers.

Figure 5 shows the weight loss curve during burning of a kraft char particle. The char was prepared by pyrolyzing a dried black liquor pellet in nitrogen. The residual char was then burned in air. Experimental temperatures were not measured for this experiment, so a temperature-time

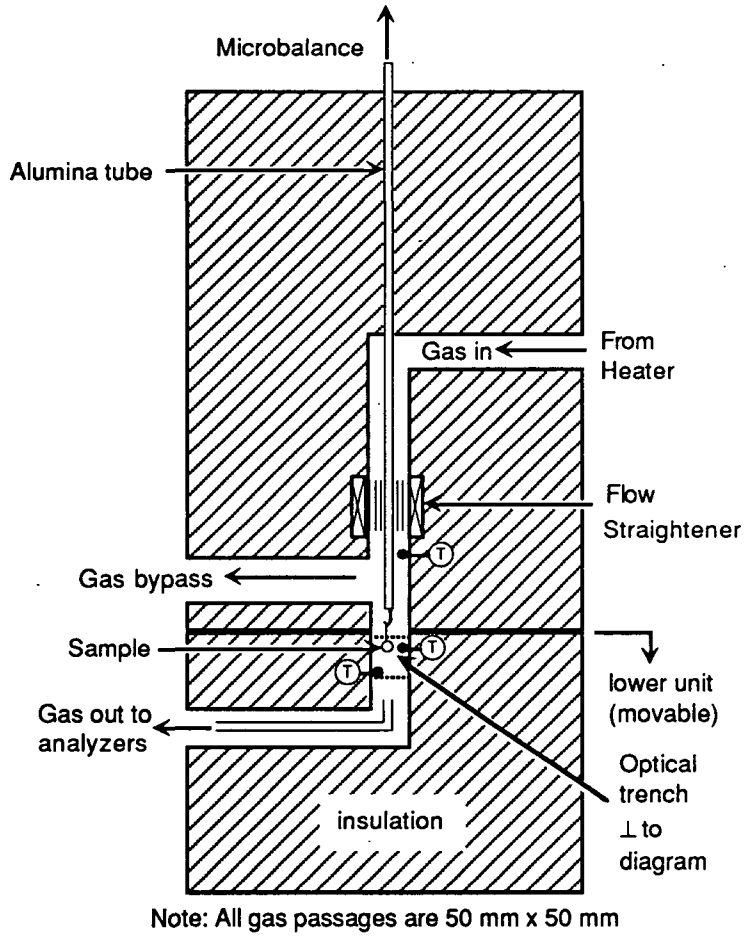

Figure 4. Single Particle Reactor.

profile must be assumed. For the weight loss curve shown in Figure 5, the particle temperature is assumed to begin at the gas temperature and ramp

linearly with time up to a maximum temperature. This pattern is consistent with that seen by Hupa in experimental char particle burns (1). Hupa found that the temperature of a particle burning in a muffle furnace increased with time in a linear manner until it reached a maximum temperature of 1473 K near the end of burning. The temperature for the char burn in Figure 5 was 1158 K, and the maximum particle temperature, T_{max}, was assumed to be 1473 K to match Hupa's result. The length of time to reach maximum temperature is a variable. Hupa found that T_{max} came near the end of char burning. In our case, T_{max} is assumed to occur at thirteen seconds.

A comparison between the model predictions, using Equation (21) to calculate P, and the experimental kraft particle burn is shown in Figure 5. The initial portion of the curve is influenced by the particle heatup. Because the particle is relatively cool in the initial period, i.e., a relatively slow C/Na_2SO_4 rate, reduction efficiency starts to decrease. The weight loss due to carbon gasification is partially offset by the weight gained by net oxidation of sulfide. As the particle continues to heat, however, the reduction efficiency is regained until it approaches a high level. Then, the combustion appears to be mass-transfer limited, and the weight-loss rate becomes fairly linear. The reduction efficiency begins to decrease at about thirteen seconds since there is not much carbon left to maintain a high C/Na_2SO_4 rate. A gain of weight is seen after fifteen seconds as sulfide is oxidized by the air.

The first curve follows the data well until about ten seconds, after which the data fall below the model prediction. The model assumes that the sodium remains constant during burning, but fuming occurs during char burning, so the actual weight loss would be greater than the prediction of the model. Another explanation for the discrepancy in final weights is that small bits of char or smelt break away from the particle as burning proceeds. If the data points after ten

seconds are moved up several mg, they are seen to follow the shape of the model prediction. Both fuming and loss of fragments will tend to make the actual weight loss greater than the predicted curve although fuming is the more likely explanation.

Figure 5. Model prediction vs. kraft char data.

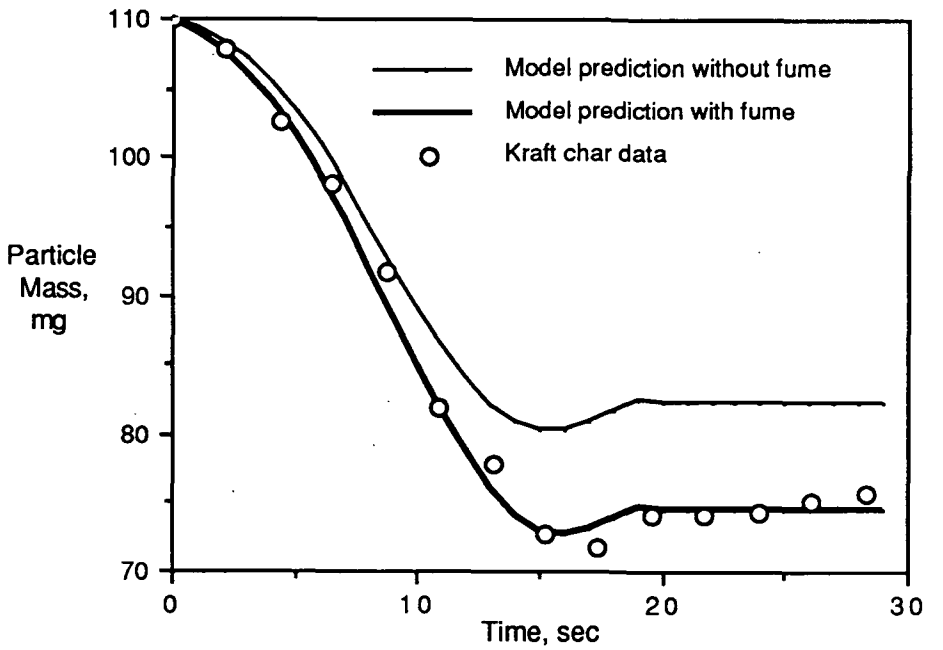

The discrepancy between the model prediction and the data can be eliminated if moderate fuming is assumed. If a total of 10% of the inorganic material is emitted at a constant rate over the first fifteen seconds of the burn, the model prediction fits the data very well as shown in Figure 5.

The parameters used to produce the most accurate prediction of the weight loss curve are consistent with experimental conditions and observations. The temperature profile (T_{max} at thirteen seconds) is consistent with Hupa's muffle furnace experiments in which the maximum temperature of 1473 K was reached near the end of the burn rather than near the beginning. In the case of the data simulated here, T_{max} at thirteen seconds represents a gradual heating

period which causes the initial portion of the weight loss prediction to be more gradual since the carbon loss is offset somewhat by sulfide oxidation.

The calculation of P by Equation (21) provided a more accurate simulation than the use of Equation (20). This suggests that the C/O_2 reaction plays an important role in protecting the reduction efficiency by providing an alternate path for the oxygen to react with the char. Equation (21) predicts that oxygen will go to the C/O_2 reaction to a greater extent of reaction than Equation (20). The reduction efficiency becomes increasingly vulnerable as combustion proceeds because more oxygen reacts with sulfide and because the carbon concentration decreases, causing a slower C/Na_2SO_4 rate.

The model can be further tested using times for the char burning stage in single drop burns. Three liquors -- kraft, soda, and soda spiked with sodium sulfate -- were burned. The kraft liquor was concentrated to 68% solids before burning. Combustion conditions in the single particle reactor were 2%, 5%, or 8% oxygen in the gas stream which was heated to 1073 K, 1143 K, or 1183 K. These conditions were constant throughout drying, volatilization, and char combustion. The initial mass of the black liquor drops ranged between 7 and 53 mg. The initial char particle diameter after drying and pyrolysis was calculated from the maximum swollen volume measurement. The mass of char at the start of char burning was assumed to be 65% of that of the initial black liquor solids. The char composition at the start of combustion was assumed to be 29.4% C, 2.1% S, and 26% Na, which is typical for char. A value of 0.9 was assumed for f_{COX} and f_{CS} .

Inputs to the model were initial char diameter, mass, composition, and gas stream conditions. The measured char burn time was used to construct a temperature-time profile. This set of experiments was completed prior to the

installation of a two-color pyrometer for measuring char surface temperature. The temperature profile is assumed to start at the gas temperature and ramp linearly to a maximum temperature at the end of char burning. The maximum temperature for char burning was later measured with the two-color pyrometer, and is approximately 1473 K for the kraft liquor used. The maximum temperature typically occurs near the end of the burn when smelt forms. This is assumed to occur at 1 wt. % carbon. Figure 6 shows good agreement between the observed and predicted burn times for a range of conditions. The model underpredicts the char burn times for 2% oxygen because of the experimental apparatus. The gas flow is automatically stopped after 29 seconds and had to be manually restarted to complete the longer burns.

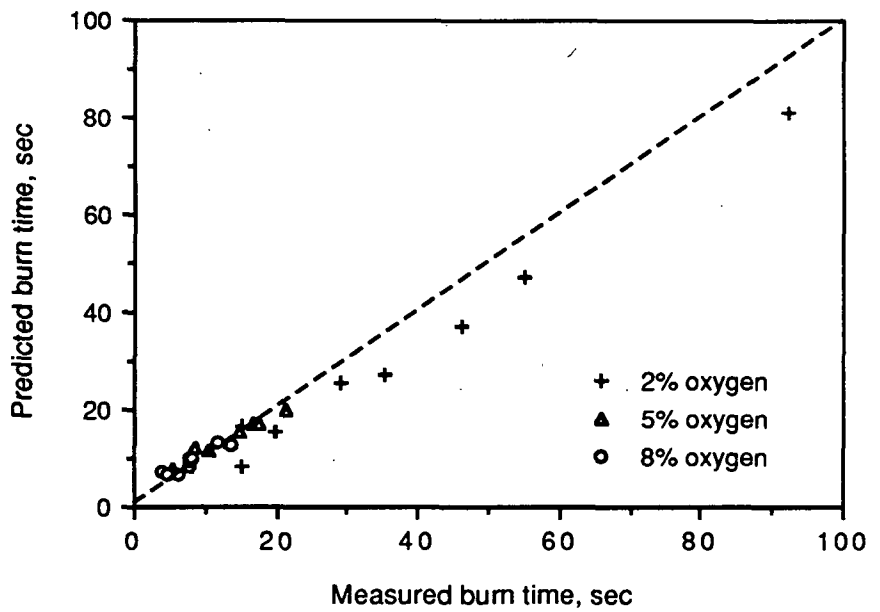

Figure 6. Comparison between model and experimental data for kraft liquor.

The soda liquor used was from a laboratory cook. The sulfur concentration in the spiked soda liquor was 6.2% on dried solids. The drops were dried and pyrolyzed in the reactor under nitrogen prior to the char burn. The surface temperature was measured with the two-color pyrometer and used

in place of the assumed temperature-time profile. Char burning started when the particle first started to glow. This always occurred at approximately the same time after air was added to the nitrogen stream. The measured char burn time extended from the first evidence of the glow to when the visible flame surrounding the particle went out. The comparison between the model and experimental data is shown in Figure 7. It is evident that the soda liquors spiked with sulfate burned faster than the pure soda liquor in agreement with the predictions of the sulfate/sulfide cycle. The measured burn times for the pure soda liquor are in agreement with the model predictions. However, the measured char burn times for the soda liquor spiked with sulfate tended to be greater than those predicted by the model. This is primarily a temperature effect. A large amount of sulfate was used in spiking the samples and the endothermic heat of the initial reduction tended to hold internal temperatures below the measured surface temperature.

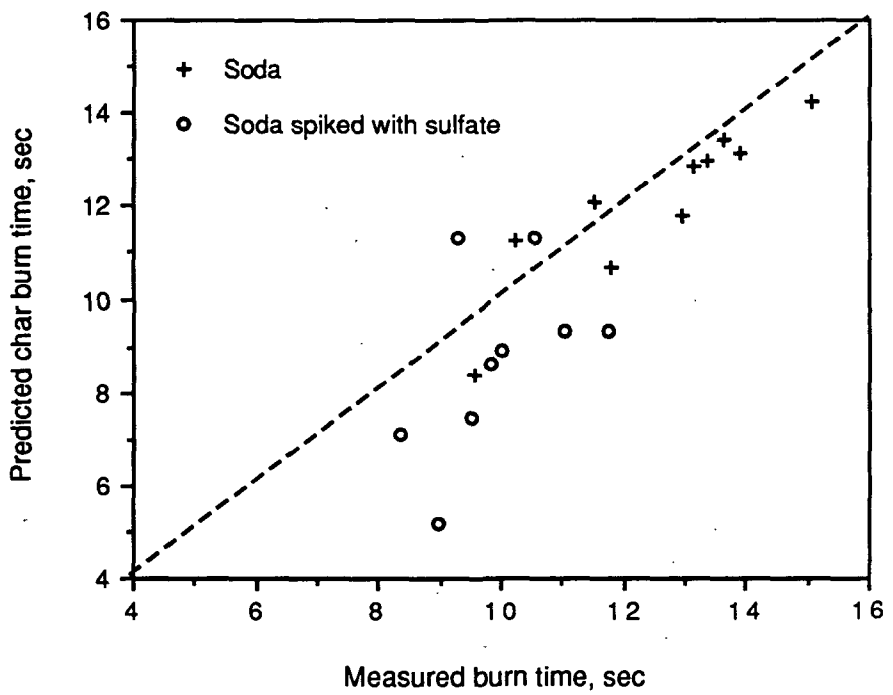

Figure 7. Comparison between model and experimental data for soda liquor.

CONCLUSIONS

The implications of the sulfate/sulfide cycle were discussed by Grace (3). The oxidation of char carbon and the reduction of sulfate are not mutually exclusive. It is possible to maintain a high reduction efficiency while carbon is burned if the reaction temperature is high enough. Oxygen need not be kept away from the bed; in fact, air should be supplied to the bed to meet the stoichiometric requirement of the material reaching the bed. The implications of the sulfate/sulfide cycle provide an impetus to maximize bed burning in order to improve furnace operation by achieving a high reduction efficiency and reducing carryover.

The accuracy of the model prediction suggests that the combustion of char in an oxygen-rich atmosphere is adequately described by the rate equations discussed in this paper. The model describes the rate of char carbon combustion as well as the reduction efficiency during combustion -- two important process variables. Fuming cannot be neglected if an accurate weight loss prediction is desired, but it can be neglected if the only variables being calculated are the carbon combustion rate and the reduction efficiency.

The char burning model presented in this paper is an improvement of the original sulfate/sulfide theory of char burning, and provides a framework for a general theory of char burning. Although applied to burning particles in this paper, the equations can also be applied to char bed geometries, and other reactions such as the C/H_2O reaction can be incorporated to model overall bed behavior.

ACKNOWLEDGMENTS

Portions of this work were used by D. W. S. and K. A. K. as partial fulfillment of the requirements for the Ph. D. degree at The Institute of Paper Chemistry.

LITERATURE CITED

1.) Hupa, M.; Solin, P. Combustion behavior of black liquor droplets. TAPPI Proceedings, 1985 International Chemical Recovery Conference, Book 3, p. 335.

2.) Gehri, R.; Oldenkamp, R. Status and economics of the Atomics International aqueous carbonate flue gas desulfurization process. FGD Symp. Proc. Rept. EPA-600/2-76-136A, May, 1976.

3.) Grace, T. M.; Cameron, J. H.; Clay, D. T. Role of sulfate/sulfide cycle in char burning -- experimental results and implications. TAPPI Proceedings, 1985 International Chemical Recovery Conference, Book 3, p. 435.

4.) Thorman, R. P.; Macur, T. S. Kinetics of sodium sulfate reduction by carbon in molten sodium carbonate. TAPPI Proceedings, 1985 International Chemical Recovery Conference, Book 3, p. 451.

5.) Smoot, L. D.; Smith, P. J. Coal Combustion and Gasification, Plenum Press, New York, 1985.

6.) Cussler, E. L. Diffusion: Mass transfer in fluid systems. Cambridge University Press, 1984.

7.) Ranz, W. E., and Marshall, W. R., Chem. Eng. Prog., 48: 173(1952).

8.) Goerg, K., and Cameron, J. Kinetic study of kraft char gasification with carbon dioxide. AIChE Mtg.(Boston) Preprint no. 67g, 6p. (Aug 24-27) 1986.

9.) Li, J. M. Eng. Thesis, Chapter 3, McGill University, Montreal, Feb. 1986.

APPENDIX II. CONVERSION OF LI'S EQUATION TO GOERG'S FORM.

Li's rate equation is reported in the following form:

$$-r_{w,i} = \frac{\frac{dw}{dt}(t=0)}{w_{t=0} - w_{t=\infty}} \qquad (1)$$

$$-r_{w,i} = \frac{K\, C_{CO_2}}{1 + K_{CO_2} C_{CO_2} + K_{CO} C_{CO}} \qquad (2)$$

The rate is taken as the initial slope of the weight loss curve, shortly after CO_2 is introduced into an initially inert gas stream, divided by the total weight loss. The values of the constants are shown in Table 1.

Table 1. Kinetic constants for Equation (2).

Constant	Value
K	2.26×10^{-3} m^3/mole-s
K_{CO_2}	0.91 m^3/mol
K_{CO}	0.53 m^3/mol

These constants were determined at 750 ° C. An activation energy of 187,000 J/mole was measured, so K can be put into the usual arrhenius form: $K = A\, e^{\frac{-187,000}{8.314(750+273)}}$. The pre-exponential factor is therefore 8.0×10^{6} m^3/mole-s. The constants in m^3/mole-s are converted to $(atm\text{-}s)^{-1}$ by dividing by RT at 750 ° C. The converted values are those shown in Table 1 in the main body.

Returning to Equation (1), the first order dependence on carbon concentration is in the denominator. All the weight loss is attributed to carbon loss, so $w_{t=0} - w_{t=\infty}$ is just the carbon loss. Carbon concentration in any units can be used since they cancel out of $-r_{w,i}$. Thus, multiplying $-r_{w,i}$ by [C] completes the conversion of Li's equation into the same form as Goerg's.

APPENDIX III. COMPARISON OF LI'S RATE EQUATION WITH IPC DATA.

One experiment has been performed on the single particle reactor to determine the significance of the C/CO_2 reaction. The data are found in Test 12 of IPC lab notebooks 3547 and 3649. A single kraft char particle was pyrolyzed in nitrogen at 895 °C before reacting the residual char with 7.4% CO_2 and 92.6% N_2. The char particle weighed 133 mg at the point in time when CO_2 was introduced. The gas flowrate was 98 slpm through a 2x2 inch cross-sectional area. The calculated velocity is therefore 248 cm/sec. Figure 1 shows the CO and CO_2 concentrations during the course of the experiment. The CO_2 concentration goes off scale since it was 7.4% while the CO concentration levels out at 200 ppm. A flowrate of 98 slpm converts to 1.95 g/s using the ideal gas law, so the reaction rate of the C/CO_2 reaction is:

$$\frac{200 \text{ mole CO}}{10^6 \text{ mole gas}} \times \frac{1.95 \text{ g gas}}{\text{s}} \times \frac{\text{mole gas}}{28 \text{ g gas}} = 1.4 \times 10^{-5} \ \frac{\text{mole}}{\text{s}} \qquad (1)$$

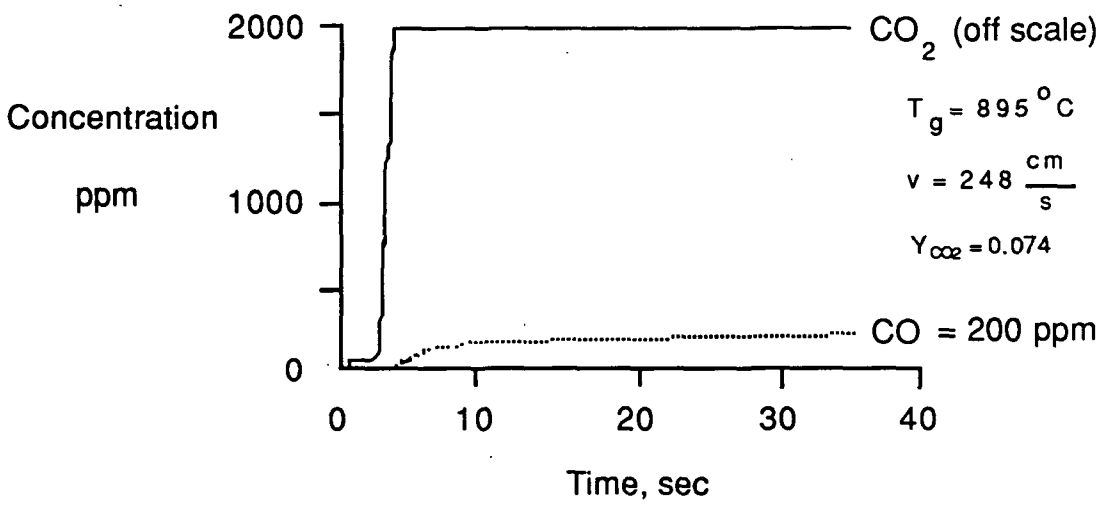

Figure 1. IPC data for carbon/carbon dioxide reaction.

The reaction rate on the single particle reactor can be compared to Li's rate equation to see if they are on the same order of magnitude. Assume that the external mass transfer is the only mass-transfer resistance. Then the mass transfer rate can be equated to the kinetic rate as follows:

$$R_{CO_2} = k_m A \left(C_{CO2_B} - C_{CO2_S}\right) = \frac{k_R C_{CO2_S} [C] m_{Na_2}}{1 + k_1 C_{CO2_S} + k_2 C_{CO_S}} \qquad (2)$$

In Equation (2), the subscripts B and S refer to bulk and surface concentrations, [C] is mole C/mole Na_2, and m_{Na_2} is the moles Na_2 in the particle.

The surface concentration of CO_2 can be obtained by solving Equation (2). Calculating C_{CO2_S} requires the solution of a quadratic equation:

$$C_{CO2_S} = \frac{-C_2 \pm \sqrt{C_2^2 - 4 C_1 C_3}}{2 C_3} \qquad (3)$$

where the constants are calculated as follows:

$$C_1 = k_m A C_{CO2_B} + k_m k_2 A C_{CO2_B} C_{CO_S}$$

$$C_2 = k_m k_1 A C_{CO2_B} - k_m A - k_m k_2 A C_{CO_S} - k_R [C] m_{Na_2}$$

$$C_3 = - k_m k_1 A$$

The surface concentration can then be plugged back into Equation (2) to obtain the rate.

The mass transfer coefficient is calulated using the Ranz correlation for spheres. The particle volume is calculated by taking the initial mass of 133 mg and dividing it by an assumed density of 0.2 g/cc. The diameter is calculated by

assuming a spherical geometry, resulting in a calculated diameter of 1.08 cm. The viscosity is assumed to be that of air, and the diffusivity is taken to be that calculated for CO_2 in nitrogen according to the Wilke and Lee modification of the equation by Hirschfelder, Bird, and Spotz as reported on p. 3-231 of Perry. The gas velocity of 248 cm/s completes the list of parameters needed to calculate k_m. The mass-transfer coefficient is therefore 15.6 cm/s.

The carbon and sodium content is assumed to be that found in the typical char reported in the char burning report. The carbon concentration is 3 mole C/mole Na_2 and the sodium content is:

$$0.133\ \text{g char} \times \frac{\text{mole } Na_2}{144\ \text{g char}} = 9.24 \times 10^{-4}\ \text{mole } Na_2.$$

k_R is calculated by assuming a reaction temperature of 850 ° C even though the gas temperature is 895 ° C. The lower assumed temperature is reasonable since the C/CO_2 reaction is endothermic. The reaction coefficient is thus $8 \times 10^{12} \frac{cm^3}{mole - s} \times \exp\left(\frac{-187{,}000}{8.314 \times (850+273)}\right) = 1.60 \times 10^4 \frac{cm^3}{mole - s}$.

The surface concentration can now be calculated from the constants C_1, C_2 and C_3. Then the overall reaction rate is calculated from Equation (2). The predicted reaction rate is 1.53×10^{-5} mole/s compared with a measured rate of 1.4×10^{-5} mole/s on the single particle reactor. The reaction rates are very comparable and are certainly within the range of possible error introduced in making the assumptions. The point of these calculations is to demonstrate that Li's rate equation is quite comparable to data obtained on a different system. The use of Li's rate expression in the char bed model is reasonable.

APPENDIX IV DETERMINATION OF CHARACTERISTIC LENGTH

The Ranz correlation for unidirectional flow past spheres was used to calculate the mass-transfer coefficient for one version of the bed model[1]. The correlation was tied to experimental data from the IPC char bed reactor. The mass-transfer coefficient was assumed to follow the same form as the Ranz correlation for all other conditions encountered in the furnace.

The greatest oxygen flux measured in the IPC char bed reactor was $100 * 10^{-6}$ gmole/cm^2-s [2]. The conditions or estimates of conditions are listed in Table 1:

Table 1. Experimental conditions for flux measurement.

velocity est., cm/s	400
oxygen fraction est.	0.17
T gas est., K	1023
T surface, K	1423
T film, K	1223

The measurment was based on the flat surface area, but the bed model uses a factor of 1.91 to account for the contours of the char surface (see Appendix V). The measured flux is accordingly reduced by a factor of 1.91 to give a value of $52.4 * 10^{-6}$ gmole/cm^2-s. The flux, N_{O_2}, is related to the mass-transfer coefficient and oxygen concentration as follows:

$$N_{O_2} = k * C_{B_{O2}} \qquad (1)$$

[1]Ranz, W. E., and Marshall, W. R., Chem. Eng. Prog., 48, 173(1952).

[2]Craig Brown, personal communication.

where k = mass-transfer coefficient, cm/s
C_{BO2} = bulk oxygen concentration, mole/cm^3

When the ideal gas law is used to calculate the gas concentration, and this value is divided into the flux, the mass-transfer coefficient is 25.8 cm/s.

The calculated mass-transfer coefficient can be substituted into the Ranz correlation, and the corresponding characteristic length determined. The Ranz correlation is:

$$Sh = \frac{k_m d}{D} = 2.0 + 0.6\, Re^{\frac{1}{2}}\, Sc^{\frac{1}{3}} \qquad (2)$$

where d = particle diameter
D = diffusivity
ν = kinematic viscosity
Re = Reynolds number = $\langle v \rangle d/\nu$
Sc = Schmidt number = ν/D.

The diffusivity and kinematic viscosity, using a film temperature of 1223 K, are calculated to be 2.488 and 1.640 cm^2/s, respectively. When the appropriate values are substituted into Equation (2), it becomes:

$$\frac{25.8\, d}{2.488} = 2.0 + 0.6\, (244\, d)^{\frac{1}{2}} (0.659)^{\frac{1}{3}} \qquad (3)$$

Equation (3) yields a particle diameter of 0.966 ≈ 1.0 cm. This was the characteristic length used in the Ranz correlation of the BED module.

APPENDIX V CALCULATION OF PHYSICAL PROPERTIES

The physical properties of the combustion gas must be known as a function of temperature in order to calculate good estimates of the mass-transfer coefficient. The kinematic viscosity, ν, defined as the ratio of viscosity to density, was assumed to be that of air. Values from Özisik[3] where fit to a quadratic polynomial with an $r^2 = 1.000$ over the temperature range of 400 - 2000 K. The polynomial is as follows:

$$\nu = -0.13327 + 7.2699\times10^{-4}T + 5.9149\times10^{-7}T^2 \text{ [=] } cm^2/s \qquad (1)$$

The diffusion coefficients for oxygen, water, and carbon dioxide were calculated using the Wilke and Lee modification of the equation of Hirschfelder, Bird, and Spotz[4]. In each case, the binary diffusion coefficient is calculated assuming nitrogen as the second gas in the pair. The diffusion coefficient, $\mathcal{D}$, is calculated from the following equation:

$$\mathcal{D} = \frac{BT^{\frac{3}{2}}\sqrt{1/M_1 + 1/M_2}}{Pr_{12}^2 I_D} \qquad (2)$$

where

$\mathcal{D}$ = gas diffusivity, cm^2/s

$B = (10.85 - 2.50\sqrt{1/M_1 + 1/M_2}) \times 10^{-4}$

T = absolute temperature, K

M_1, M_2 = molecular weights of components 1 and 2

P = absolute pressure, atm.

---

[3]Heat Transfer: A basic Approach. McGraw-Hill, Inc. 1985.

[4] Perry, R.H. and Chilton, C. H. Chemical Engineers Handbook, 5th Ed., p 3-230, McGraw-Hill, Inc. , 1973.

r_{12} = collision diameter, angstroms = $\frac{(r_0)_1 + (r_0)_2}{2}$

(r_0 from Table 3-308)

I_D = collision integral for diffusion, function of kT/ε_{12} (Table 3-309)

$\varepsilon_{12} = \sqrt{\left(\frac{\varepsilon_1}{k}\right)\left(\frac{\varepsilon_2}{k}\right)}$ (Table 3-308)

The following formulas were obtained for the gas diffusivity:

$$\mathcal{D}_{CO_2} = \frac{1.682 \times 10^{-5} T^{\frac{3}{2}}}{I_D} \quad (3)$$

$$\mathcal{D}_{O_2} = \frac{2.125 \times 10^{-5} T^{\frac{3}{2}}}{I_D} \quad (4)$$

$$\mathcal{D}_{H_2O} = \frac{3.039 \times 10^{-5} T^{\frac{3}{2}}}{I_D} \quad (5)$$

Values for I_D can be obtained from Table 3-309 to use in Equations (3), (4), and (5) to calculate the diffusivity. A quadratic curve fit of the diffusivities gives the following equations which are valid over the temperature range of 400 - 2000 K:

$$\mathcal{D}_{CO_2} = -0.20141 + 9.0103\times10^{-4}T + 6.7304\times10^{-7}T^2 \text{ [=] } cm^2/s \quad (6)$$

$$\mathcal{D}_{O_2} = -0.19389 + 1.0385\times10^{-3}T + 9.4380\times10^{-7}T^2 \text{ [=] } cm^2/s \quad (7)$$

$$\mathcal{D}_{H_2O} = -0.34941 + 1.4816\times10^{-3}T + 1.2056\times10^{-6}T^2 \text{ [=] } cm^2/s \quad (8)$$

The physical property values from Equations (1), (6), (7), and (8) are used to calculate the mass transfer coefficient in the BED module.

APPENDIX VI. CALCULATION OF SURFACE AREA ENHANCEMENT.

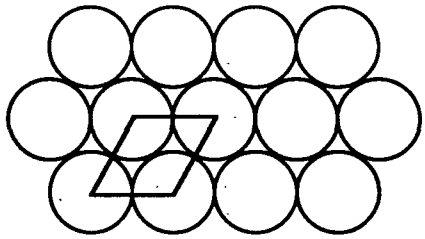

Top

Side

Area of hemisphere $= \frac{\pi d^2}{2}$

$A_{flat} = h * d = \frac{\sqrt{3}}{2} * d^2$

$A_{unshade} = \frac{\pi d^2}{4}$

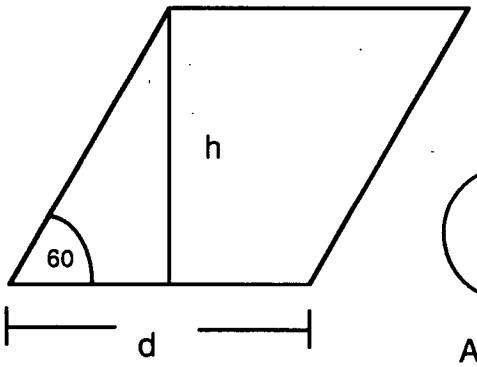

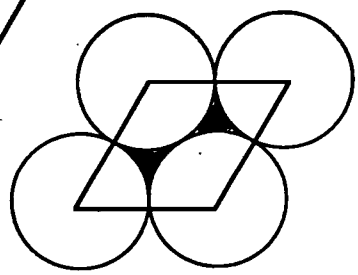

$A_{shade} = A_{flat} - A_{unshade}$

$$\text{Ratio of actual to flat surface area} = \frac{A_{hemisphere} + A_{shade}}{A_{flat}} = \frac{\frac{\pi d^2}{2} + \frac{\sqrt{3} d^2}{2} - \frac{\pi d^2}{4}}{\frac{\sqrt{3} d^2}{2}}$$

$$= 1.91 * \text{flat surface area}$$

APPENDIX VII. SOURCE CODE FOR BED SUBROUTINE.

```
      SUBROUTINE BED
C
CCCCCCCCCCCCCCCCCCCCCCCCCCCCCCCCCCCCCCCCCCCCCCCCCCCCCCCCCCCCCCCCCCCCCCCCC
C                                                                       C
C     BED CALCULATES THE EXCHANGE TERMS BETWEEN THE CHAR BED AND THE    C
C     FURNACE CAVITY.  THE SULFATE/SULFIDE CYCLE KINETICS ARE INCLUDED. C
C                                                                       C
CCCCCCCCCCCCCCCCCCCCCCCCCCCCCCCCCCCCCCCCCCCCCCCCCCCCCCCCCCCCCCCCCCCCCCCCC
C
      INCLUDE 'COMMON.FOR'
      CHARACTER*4 CHR1
      CHARACTER*8 CHR2
      REAL MINORG, NA2CO3, NA2S, KMO2, KMCO2, KR, KCOX
      SO4TOT=0.
      O2TOT=0.
      TMINORG=0.
      VELAVE=0.
      CRATE1=0.
      CRATE2=0.
      CRATE3=0.
      CRATET=0.
      TCARBN=0.
      SUMMER=0.
      TAVERG=0.
      TW9AVG=0.
      RAVG=0.
      TCOUNT=0.
      TAREA=0.
      COCO2=0.
      RDTION=0.
      O2AVE=0.
      H2OAVE=0.
      CO2AVE=0.
      FUELAV=0.
      T1AVE=0.
      T2AVE=0.
      T3AVE=0.
      T4AVE=0.
      T4AAVE=0.
      T4BAVE=0.
      T4CAVE=0.
      T4DAVE=0.
      T6AVE=0.
      WVAPAV=0.
      TO1AV=0.
      TO2AV=0.
      TO3AV=0.
      C3AV=0.
      C4AV=0.
      SMELTO=0.
C
C     SCROLL THROUGH THE CELLS AND PERFORM BED OPERATIONS ONLY IF A
C     W9 CELL IS ENCOUNTERED.  CALCULATE THE RATE OF OXYGEN SUPPLY AND
C     STORE IT IN BEDCEL(L+NI).  THE BEDCEL ARRAY
C     IS USED FOR MANY PURPOSES TO OPTIMALLY USE THE MEMORY:
C
```

```
C                L +12NI    LATENT HEAT OF WATER IN WET PARTICLES
C                L +11NI    TOTAL CARBON DEPLETED
C                L +10NI    CARBON DEPLETED FROM H2O/C REACTION
C                L + 9NI    CARBON DEPLETED FROM CO2/C REACTION
C                L + 8NI    RATIO OF CO TO TOTAL CARBON GASES ABOVE BED
C                L + 7NI    INORGANIC FROM BURNED OUT DROPS
C          CELL  L + 6NI    CARBON DEPLETED FROM O2 REACTIONS
C                L + 5NI    REDUCTION EFFICIENCY
C                L + 4NI    BED GROWTH
C                L + 3NI    INORGANIC INTO CELL WITH UNBURNED CHAR
C                L + 2NI    CARBON INTO CELL
C                L +  NI    OXYGEN SUPPLY FROM GAS PHASE
C                L          BED CELL
C
      WRITE(IO,*)'BEGIN BED CALCULATIONS'
      DO 20 K = 1, NK
         DO 20 J = 1, NJ
            DO 20 I = 1, NI
               L = LINDIX(I,J,K)
               IF(ICELL(L).NE.10) GO TO 20
C
C     CALL NEIGHB TO FIND NEIGHBORING CELL TYPES AND LOCATIONS.
C
                  CALL NEIGHB
C
C     CALCULATE THE SURFACE AREAS FOR THE N-S, E-W, AND HORIZONTAL FACE
C     A FACTOR OF 1.91 IS INTRODUCED TO ACCOUNT FOR THE CHAR SURFACE
C     BEING MODELED AS PERFECTLY PACKED SPHERES RATHER THAN A FLAT
C     SURFACE.
C
                  SARNSV = SX(I) * SY(J+1) * 1.91
                  SAREWV = SZ(K) * SY(J+1) * 1.91
                  SAREAH = SX(I) * SZ(K)   * 1.91
C
C     THERE ARE FIVE REACTIONS THAT ARE ASSUMED TO OCCUR ON THE BED:
C     THE NA2S/O2 REACTION, THE C.NA2SO4 REACTION, THE C/O2 REACTION,
C     THE CO2/C REACTION AND THE H2O/C REACTION.
C     NA2SO4 THAT IS CARRIED INTO THE BED BY BURNED OUT DROPS REACTS
C     WITH C IN AN ENDOTHERMIC REACTION.  THE MASS TRANSFER COEFFICIENT
C     FOR THE BED IS BASED ON THE RANZ CORRELATION FOR
C     FLOW PAST SPHERES.  THE CHARACTERISTIC LENGTH, 1.0 CM, IS CHOSEN
C     TO MATCH EXPERIMENTAL DATA ON CHAR COMBUSTION TO THE CORRELATION.
C
C     HSCO2    = HEAT OF REACTION FOR 2C + NA2SO4 = 2CO2 + NA2S
C                   7.11*10**6 J/KG CARBON
C     HSCO     = HEAT OF REACTION FOR 4C + NA2SO4 = 4CO  + NA2S
C                   10.57*10**6 J/KG CARBON
C     HNA2S    = HEAT OF REACTION FOR NA2S + 2O2 = NA2SO4
C                   -12.30*10**6 J/KG NA2S
C     HOXCO2   = HEAT OF REACTION FOR  C + O2 = CO2
C                   -32.86*10**6 J/KG CARBON
C     HOXCO    = HEAT OF REACTION FOR  C + 1/2 O2 = CO
C                    -9.42*10**6 J/KG CARBON
C     HCO2C    = HEAT OF REACTION FOR  CO2 + C = 2CO
C                   14.04*10**6 J/KG CARBON
C     HH2OC    = HEAT OF REACTION FOR  H2O + C = H2 + CO
C                  11.36*10**6 J/KG CARBON
                  HSCO2    =          7.11*10**6
                  HSCO     =         10.57*10**6
                  HNA2S    =       - 12.30*10**6
                  HOXCO2   =       - 32.86*10**6
```

```
                HOXCO    =        - 9.42*10**6
                HCO2C    =         14.04*10**6
                HH2OC    =         11.36*10**6
C
C       CALCULATE THE OXYGEN SUPPLIED FROM THE GAS PHASE.  BEDCEL(LYP) IS
C       THE KM*A*O2CONC.  ALSO CALCULATE THE CO2 AND WATER MASS TRANSFER.
C
C       DIFFUSIVITIES ARE BASED ON QUADRATIC REGRESSION OF VALUES CALULATED
C       FROM METHOD ON P 3-230 OF PERRY OVER THE TEMPERATURE RANGE OF
C       400 - 2000 K.  KINEMATIC VISCOSITY IS THAT OF
C       AIR AND ASSUMED TO BE APPLICABLE FOR CO2 AND H2O SC CALCULATION.
                TFILM  = (T(LYP)+T(L))/2.
                DIFCO2 = -0.20141+9.0103E-4*TFILM+6.7304E-7*TFILM**2.
                DIFH2O = -0.34941+1.4816E-3*TFILM+1.2056E-6*TFILM**2.
                DIFO2  = -0.19389+1.0385E-3*TFILM+9.4380E-7*TFILM**2.
                VISC   = -0.13327+7.2699E-4*TFILM+5.9149E-7*TFILM**2.
C       SCHMIDT NUMBER
                SCCO2 = VISC/DIFCO2
                SCH2O = VISC/DIFH2O
                SCO2 = VISC/DIFO2
C
                VELOC  =(((U(LYP)+U(LYP+1))/2)**2  +((V(LYP)+V(LYP+NI))/2)**2
     1                    + ((W(LYP)+W(LYP+NI*NJ))/2)**2)**0.5
                REYN = 1.0 * VELOC * 100/VISC
C       SHERWOOD NUMBER
                SHCO2 = 2.0 + 0.6 * REYN**0.5 * SCCO2**0.333
                SHH2O = 2.0 + 0.6 * REYN**0.5 * SCH2O**0.333
                SHO2  = 2.0 + 0.6 * REYN**0.5 * SCO2 **0.333
C       MASS TRANSFER COEFFICIENTS
                KMCO2 = DIFCO2 * SHCO2/1.0/100
                KMH2O = DIFH2O * SHH2O/1.0/100
                KMO2  = DIFO2  * SHO2 /1.0/100
C
                KR = 2.36 * T(LYP) * EXP(-11022./T(L))
                KCOX = 1./(1./KR + 1./KMO2)
                SFAREA = SAREAH
                TAREA = TAREA + SAREAH
C
C       CHECK FOR VERTICAL WALL FACES
C
                IF(ICELL(LYP+1).NE.10) GOTO 30
C               THERE IS A W9 CELL FACE TO THE EAST
                SFAREA = SFAREA + SAREWV
                TAREA = TAREA + SAREWV
30              IF(ICELL(LYP-1).NE.10) GOTO 40
C               THERE IS A W9 CELL FACE TO THE WEST
                SFAREA = SFAREA + SAREWV
                TAREA = TAREA + SAREWV
40              IF(ICELL(LYP+NI*NJ).NE.10) GOTO 50
C               THERE IS A W9 CELL FACE TO THE NORTH
                SFAREA = SFAREA + SARNSV
                TAREA = TAREA + SARNSV
50              IF(ICELL(LYP-NI*NJ).NE.10) GOTO 60
C               THERE IS A W9 CELL FACE TO THE SOUTH
                SFAREA = SFAREA + SARNSV
                TAREA = TAREA + SARNSV
60              CONTINUE
C
C       "P", THE FRACTION OF THE SURFACE THAT IS CARBON, IS 0.656
C       BASED ON EQN 23 OF PAPER AND [C]/[C0] = 0.67.
C
```

```
                O2NA2S  = KMO2*DEN(LYP)*O(LYP)*SFAREA*(1.-0.656)
                O2COX   = KMO2*DEN(LYP)*O(LYP)*SFAREA*0.656
                O2SO4   = OMASEX(LYP)
                BEDCEL(LYP) = O2NA2S + O2COX
C
C       CALCULATE THE NET GROWTH AND REDUCTION EFFICIENCY.
C
                VR  = SX(I)*SZ(K)*0.02
                RED = 0.
                FR = (1-RED)/(0.0033 + 1 - RED)
                TBED  = AMAX1(900.,T(L))
                TBED = AMIN1(TBED,1700.)
C       CALCULATE THE CARBON DEPLETION DUE TO OXYGEN.  RATE1 IS THE
C       C/NA2SO4 REACTION AND RATE2 IS THE C/O2 REACTION.
C       THE CARBON CONCENTRATION IS ASSUMED TO BE 2 MOLE C/MOLE NA2
C                                  ^
                RATE1 = 142900 * VR * FR * 2 * EXP(-14696/TBED)/(2-QBED)
                RATE2 = 2./(2.-QBED)*12./32.*O2COX
C
C       THE REACTION RATE CAN BE NO GREATER THAN THE SUM OF THE
C       OXYGEN SUPPLIED BY THE AIR AND THE BURNED OUT DROPLETS.
C       THE RATE IS MASS TRANSFER CONTROLLED IF THE KINETIC RATE
C       EXCEEDS THE OXYGEN SUPPLY.
C
                IF(RATE1*(2.-QBED)/2.*32./12..GE.(O2NA2S+O2SO4))THEN
                  RATE1 = (O2SO4+O2NA2S)*12./32.*2./(2.-QBED)
                  FR = RATE1/(142900 * VR * 2 * EXP(-14696/TBED)/(2-QBED))
                  RED = (1-(1+0.0033)*FR)/(1-FR)
                 IF(RED.GT.0.95)TMTCNT = TMTCNT + 1
                 IF(RED.LT.0) RED=0.
                ELSE
                 RED=0.
                  IF(RATE1*(2.-QBED)/2.*32./12..GE.O2SO4)THEN
                    O2NA2S = RATE1*(2.-QBED)/2.*32./12.-O2SO4
                    BEDCEL(LYP) = 02NA2S+O2COX
                 ELSE
                   O2NA2S = 0.
                   BEDCEL(LYP) = O2COX
                    RATE1 = O2SO4*12./32.*2./(2.-QBED)
                 ENDIF
                ENDIF
C
C       CALCULATE THE CARBON DEPLETION RATE DUE TO C/CO2 AND C/H2O
C
                CO2BLK  =  DEN(LYP)*C(LYP)/0.044
                COBLK   =  DEN(LYP)*Q(LYP)/0.028
                ACO2 = KMCO2 * SFAREA * 0.012 * 0.91
                BCO2 = 8*10**6*EXP(-22493/TBED)*2.*27.27*VR - 0.012 * KMCO2
     1                 *SFAREA * CO2BLK * 0.91 + 0.012 * KMCO2 * SFAREA
     1               +0.012 * KMCO2 * SFAREA * COBLK * 0.53
                CCO2 = -0.012 * KMCO2 * SFAREA * CO2BLK - 0.012 * KMCO2
     1                * SFAREA * CO2BLK * COBLK * 0.53
                CO2SF  = (-BCO2 + SQRT(BCO2**2.-4*ACO2*CCO2))/(2*ACO2)
                BEDCEL(L+9*NI) = 0.012 * KMCO2 * SFAREA * (CO2BLK - CO2SF)
C
                H20BLK  =  DEN(LYP)*B(LYP)/0.018
                AH20 = KMH20 * SFAREA * 0.012 * 0.91
                BH20 = 8*10**6*EXP(-22493/TBED)*2.*27.27*VR - 0.012 * KMH20
     1                 *SFAREA * H20BLK * 0.91 + 0.012 * KMH20 * SFAREA
     1                +0.012 * KMH20 * SFAREA * COBLK * 0.53
                CH20 = -0.012 * KMH20 * SFAREA * H20BLK - 0.012 * KMH20
```

```
     1          * SFAREA * H20BLK * COBLK * 0.53
                H20SF  =  (-BH20  +  SQRT(BH20**2.-4*AH20*CH20))/(2*AH20)
                BEDCEL(L+10*NI) = 0.012 * KMH20 * SFAREA * (H20BLK - H20SF)
C
                MINORG = BEDCEL(L+3*NI)
                CARBIN = BEDCEL(L+2*NI)
                O2CELL = BEDCEL(L+NI)
                TMINRG = TMINRG + MINORG + BEDCEL(L+7*NI)
                TCARBN = TCARBN + CARBIN
                SO4TOT = SO4TOT + OMASEX(L+NI)
                O2TOT = O2TOT + O2CELL
                DCDT = RATE1 + RATE2
                AC = CARBIN - DCDT - BEDCEL(L+9*NI) - BEDCEL(L+10*NI)
                IF(AC.GT.0.AND.CARBIN.GT.0) THEN
                  ACC = AC * (MINORG + CARBIN)/CARBIN
                ELSE
                  ACC = AC * (96.7+24.)/24.
                ENDIF
                FOUT = CARBIN + MINORG + BEDCEL(L+7*NI) - DCDT
     1               - BEDCEL(L+9*NI) - BEDCEL(L+10*NO) - ACC
                BEDCEL(L+4*NI) = ACC
                BEDCEL(L+5*NI) = RED
                BEDCEL(L+6*NI) = DCDT
                IF(Q(L+NI).GT.0.OR.C(L+NI).GT.0)THEN
                   BEDCEL(L+8*NI)  =  Q(L+NI)/28./(Q(L+NI)/28.+C(L+NI)/44.)
                ELSE
                  BEDCEL(L+8*NI) = 0.0
                ENDIF
                BEDCEL(L+11*NI)= DCDT + BEDCEL(L+9*NI) + BEDCEL(L+10*NI)
                OMASEX(L+NI) = 0.
                CRATE1 = CRATE1 + RATE1
                CRATE2 = CRATE2 + RATE2
                CRATE3 = CRATE3 + BEDCEL(L+9*NI)
                CRATE4 = CRATE4 + BEDCEL(L+10*NI)
                CRATET = CRATET + DCDT + BEDCEL(L+9*NI) + BEDCEL(L+10*NI)
C          TERM1 = NA2S/O2 REACTIONTERM2 = NA2SO4+C=CO REACTION
C          TERM3 = NA2SO4+C=CO2 REACTION                TERM4 = HEAT OF FUSION
C          TERM4A= C + O2 = CO2 REACTION                TERM4B= C+1/2O2=CO REACTION
C          TERM4C= C + CO2 = 2CO REACTION               TERM4D= C+H20=CO+H2 REACTION
C          TERM5 = RADIANT FLUX                         TERM6 = SENSIBLE HEAT IN
C          TOUT1 = SENSIBLE HEAT OUT GAS                TOUT2 = SENSIBLE HEAT OUT INRG
C          TOUT3 = SENSIBLE HEAT OUT ACC.               CON3 = CONVECTIVE HEAT EXCH
C          WVAP  = LATENT HEAT OF WATER
C
           TERM1 = HNA2S*O2NA2S*78./64.
           T1AVE = T1AVE + TERM1
           TERM2 = RATE1*QBED*HSCO
           T2AVE = T2AVE + TERM2
           TERM3 = RATE1*(1-QBED)*HSCO2
           T3AVE = T3AVE + TERM3
           TERM4 = 3.16E5*BEDCEL(L+11*NI)*70.7/24
           T4AVE = T4AVE + TERM4
           TERM4A= RATE2*HOXCO2*(1-QBED)
           T4AAVE= T4AAVE + TERM4A
           TERM4B= RATE2*HOXCO*QBED
           T4BAVE= T4BAVE + TERM4C
           TERM4C= BEDCEL(L+9*NI)*HCO2C
           T4CAVE= T4CAVE + TERM4C
           TERM4D= BEDCEL(L+10*NI)*HH2OC
           T4DAVE= T4DAVE + TERM4D
           T5AVE = T5AVE + RAY(L+NI)
```

```
      TERM6=-(1015.*O2CELL+1788.*(MINORG+BEDCEL(L+7*NI))
     1          +1788.*CARBIN + 44./12.*BEDCEL(L+9*NI)*1115
     1          + 18./12.*BEDCEL(L+10*NI)*2326)*(T(L+NI)-1100.)
      T6AVE = T6AVE + TERM6
      WVAP  = BEDCEL(L+12*NI)
      WVAPAV= WVAPAV + BEDCEL(L+12*NI)
      TOUT1 = 1115*DCDT*(1-QBED)*44/12.+1194*DCDT*QBED*28/12.
     1          + (28/12.*(2*BEDCEL(L+9*NI)+BEDCEL(L+10*NI)))*1194
     1          + 2/12*BEDCEL(L+10*NI)*1194
      TO1AV = TO1AV + TOUT1
      TOUT2 = 1788.*FOUT
      TO2AV = TO2AV + TOUT2
      TOUT3 = 1788*BEDCEL(L+4*NI)
      IF(BEDCEL(L+4*NI).LT.0)TOUT3 = 0.
      TO3AV = TO3AV + TOUT3
      CON1 = TERM1 + TERM2 + TERM3 + TERM4 + TERM4A + TERM4B +
     1          TERM4C + TERM4D + TERM6 + WVAP
      CON2 = TOUT1 + TOUT2 + TOUT3
      CON3 = 58*SFAREA
      C3AV = C3AV + CON3
      CON4 = 2.0*RBOUND(ICELL(L))/(2.0-RBOUND(ICELL(L)))
     1          *SFAREA
      C4AV = C4AV + CON4
C
C     CALCULATE THE COEFFICIENTS FOR NEWTON-RAPHSON SOLUTION FOR T
C
      FC1 = CON1 - 1100 * CON2 - CON4 * RAY(L+NI) - T(L+NI) * CON3
      FC2 = CON2 + CON3
      FC3 = STEFAN * CON4
C
13    TOLD = TBED
      IF(TOLD.LE.0) THEN
      TBED = 900
      WRITE(IO,*)'BAD BED CELL, SET EQUAL TO 900K' ,I,J,K
      GOTO 999
      ENDIF
      FUNC = FC1 + FC2*TOLD + FC3*TOLD**4.0
      FUNCP= FC2 + 4.0*FC3*TOLD**3.0
      TNEW = TOLD - FUNC/FUNCP
      EPS  = ABS((TNEW-TOLD)/(TOLD+TNEW)/2))
      TBED = TNEW
      IF(EPS.GT.0.01) GOTO 13
C
C     BRACKET THE WALL TEMPERATURE TO REMOVE ANOLOMIES.
C
999   TBED = AMIN1(TNEW,1700.)
      T(L) = AMAX1(TBED,900.)
C
      COCO2 = COCO2 + BEDCEL(L+8*NI)
      RDTION = RDTION + CON4*(STEFAN*T(L)**4.-RAY(L+NI))
      O2AVE = O2AVE + O(L+NI)
      H2OAVE = H2OAVE + B(L+NI)
      CO2AVE = CO2AVE + C(L+NI)
      FUELAV = FUELAV + F(L+NI)
      SUMMER = SUMMER + BEDCEL(L+4*NI)
      TAVRGE = TAVRGE + T(L+NI)
      TW9AVG = TW9AVG + T(L)
      TCOUNT = TCOUNT + 1
      SMELTO = SMELTO + FOUT
      VELAVE = VELAVE + VELOC
      RAVG = RAVG + BEDCEL(L+5*NI)*FOUT
```

```
20      CONTINUE
        VELAVE = VELAVE/TCOUNT
        TAVRGE = TAVRGE/TCOUNT
        TW9AVG = TW9AVG/TCOUNT
        RAVG = RAVG/SMELTO
        COCO2 = COCO2/TCOUNT
        RDTION = RDTION/TCOUNT
        O2AVE = O2AVE/TCOUNT
        H2OAVE = H2OAVE/TCOUNT
        CO2AVE = CO2AVE/TCOUNT
        FUELAV = FUELAV/TCOUNT
        ENCODE(4,101,CHR1) NITER
101     FORMAT(I4)
        CHR2 = 'BED_'//CHR1
        OPEN(UNIT=17,STATUS='UNKNOWN' ,FILE=CHR2)
        WRITE(17,*)'NITER = ',NITER
        WRITE(17,*)'BED GROWTH ',SUMMER,' R ',RAVG
        WRITE(17,*)'TBED ',TAVRGE,' TSURF ',TW9AVG
        WRITE(17,*)'TOTAL INORGANIC ',TMINRG,'SMELT LEAVING ' SMELTO
        WRITE(17,*)'TOTAL CARBON IN ',TCARBN, 'CARBON CONSUMED ',CRATET
        WRITE(17,*)'C/SO4 CARBON ', CRATE1,'C/O2 CARBON ',CRATE2
        WRITE(17,*)'C/CO2 CARBON ', CRATE3,'C/H2O CARBON ',CRATE4
        WRITE(17,*)TMTCNT,' CELLS OUT OF ',TCOUNT,' ARE M-T CONTROLLED.'
        WRITE(17,*)'AIR O2 ',O2TOT,'O2 AS SO4 ',SO4TOT,' TAREA ',TAREA
        WRITE(17,*)'RADIANT FLUX = ',RDTION,' F = ',COCO2
        WRITE(17,*)'AVERAGE O2 CONC. = ',O2AVE
        WRITE(17,*)'AVERAGE CO2 CONC. = ',H2OAVE
        WRITE(17,*)'AVERAGE FUEL CONC. = ',FUELAV
        WRITE(17,*)'TERM1 = ',T1AVE/TCOUNT,'TERM2 = ',T2AVE/TCOUNT
        WRITE(17,*)'TERM3 = ',T3AVE/TCOUNT,'TERM4 = ',T4AVE/TCOUNT
        WRITE(17,*)'TERM4 = ',T4AAVE/TCOUNT,'TERM4B = ',T4BAVE/TCOUNT
        WRITE(17,*)'TERM5 = ',T5AVE/TCOUNT
        WRITE(17,*)'TERM6 = ',T6AVE/TCOUNT,'WVAP = ',WVAPAV/TCOUNT
        WRITE(17,*)'TOUT1 = ',TO1AV/TCOUNT,'TOUT2 = ',TO2AV/TCOUNT
        WRITE(17,*)'TOUT3 = ',TO3AV/TCOUNT
        WRITE(17,*)'CON3 = ',C3AV/COUNT,'CON4 = ',C4AV/TCOUNT
        WRITE(17,*)'AVERAGE VELOCITY ',VELAVE
        CLOSE(UNIT=17,STATUS='KEEP')
        RETURN
        END
```

APPENDIX VIII. SOURCE CODE FOR IMPROVED THEORY OF CHAR BURNING.

```
      REAL KR, KM, MINIT, KTOT, MRELI
       CHARACTER*1 TAB
       PARAMETER(TAB=9)
       WRITE(9,*)'ENTER  T, TIMMAX'
      READ(9,*) T, TIMMAX
C
C   INITIALIZE VARIABLES
C
      FCS=0.
      FCOX=0.
      YO2=.21
      VEL=270
      CI=3.5
     FUME = 0.
      S = 0.12
       TSTART = 1158
      TMAX = T
        SLOPE = (TMAX-TSTART)/TIMMAX
     NSKIP = 1000
      R = 0.5
      C =CI
      REL1=0.9999
      D = 0.9999
     TIME=0
      DELT=0.001
       NSTEPS = 29000
      D0 = 0.9999
       VINIT = 3.1416*D0**3/6.
     RHOCHR = 0.2
     RHOING = 2.0
        MRELI = 106+36*S-64*S*R+12*C
     XINRG = (MRELI - 12*CI)/MRELI
     TOTCO2 = 0.
     TOTCO = 0.
     CCO2 = 0.
     CCO = 0.
     ACO2 = 0.
     ACO = 0.
     TG = 1158.
      VISC = 0.00227*TG - 1.13
       DEL = 5*SQRT(VISC*D/VEL)
        VOLBL = 3.14159/6. * ((D+2*DEL)**3. - D**3.)
C
      OPEN(UNIT=2,FILE='SSCYC')
      WRITE(2,100)TIME,TAB,R,TAB,C,TAB,REL1,TAB,CCO2,TAB,CCO,TAB,FUME
100   FORMAT(F7.2,A1,F6.4,A1,F6.4,A1,F6.4,A1,E10.4,A1,E10.4,A1,F6.4)
      WRITE(9,100)TIME,TAB,R,TAB,C,TAB,REL1,TAB,CCO2,TAB,CCO,TAB,FUME
     DO 10 I = 1,NSTEPS
C
C     THE OXYGEN CONCENTRATION IS CALCULATED AT THE GAS TEMPER ATURE
C     OF 885 C(1158 K).  THE VISCOSITY AND DIFFUSIVITY ARE CALCULATED
C     AT THE "FILM" TEMPERATURE WHICH IS JUST THE AVERAGE OF GAS AND
```

```
C    PARTICLE TEMPERATURES.
C
     T = SLOPE*TIME+TSTART
     IF(TIME.GE.TIMMAX)T=TMAX
     TFILM = (TG+T)/2.
     COXBLK = YO2/82.06/TG
     VISC = 0.00227*TFILM - 1.13
     DIF = 0.00333*TFILM - 1.59
     COEFF1=1310*EXP(-14696/T)
     KR = 236 * TG * EXP(-11022/T)
C
C    DO THE NEW SS CYCLE
C
     A = (C/CI)**0.6667
     P = A/(A+0.4)
     D = D0 * ((1.-XINRG*RHOCHR/RHOING)*C/CI+
    1         XINRG*RHOCHR/RHOING)**0.3333
     RE = D * VEL/VISC
     KM = (2.0 + 0.525*RE**0.5)*DIF/D
     KTOT = 1/(1/KM + 1/KR)
      RO2 = (1-P)*KM*3.1416*D**2/VINIT*MRELI/RHOCHR*COXBLK
      RCS= COEFF1*(1.-R)*S/(0.0011+(1.-R)*S)*C
     RCOX = KTOT * P * 3.1416*D**2/
    1           VINIT*MRELI/RHOCHR*COXBLK
     IF(R.LE.0.999) THEN
               DRDT  =  (RCS-RO2/2.)/S
      R = R + DRDT * DELT
               C = C - (RCS*4/(2-FCS) + RCOX * 2/(2-FCOX))*DELT
    ELSE
     RCS = RO2
               FR = RCS/COEFF1/C
       R = 1.-(FR*0.0011)/((1.-FR)*S)
        C = C - (RCS*4/(2-FCS) + RCOX * 2/(2-FCOX))*DELT
    ENDIF
C
C    CO2/C REACTION
C
C
C
       RCO2P = P*(8E12*CCO2*C*EXP(-22492/T)*RHOCHR*VINIT/MRELI)/
    1     (1.+.91E6*CCO2+.53E6*CCO)
      RCOXP = KTOT * P * 3.1416*D**2*COXBLK*2./(2.-FCOX)
      RCSP = RCS*RHOCHR*VINIT/MRELI*4/(2.-FCS)
     CMAX = 1/82.06/TFILM
      DEL = 5*SQRT(VISC*D/VEL)
      VOLBLT = 3.14159/6. * ((D+2*DEL)**3. - D**3.)
      FCO2 = CCO2*VEL/2.* 3.14159/4. * ((D+DEL)**2. - D**2.)
      FCO = CCO*VEL/2.* 3.14159/4. * ((D+DEL)**2. - D**2.)
     ACO2 = RCOXP + RCSP - FCO2 - RCO2P
     IF(ACO2.LT.0.AND.TOTCO2.EQ.0) THEN
     ACO2 = 0.
               X1 = RCOXP + RCSP
               X2 = VEL/2. * 3.14159/4. * ((D+DEL)**2. - D**2.)
               X3  =  P*8E12*C*EXP(-22492/T)*RHOCHR*VINIT/MRELI
               X4 = .91E6
               X5 = .53E6*CCO
```

```
            ACOEF = -(X1+X1*X5)
            BCOEF = X2-X1*X4+X2*X5+X3
            CCOEF = X2*X4
            CCO2 = (-BCOEF**2+SQRT(BCOEF**2-4*ACOEF*CCOEF))/(2*ACOEF)
            RCO2P = P*(8E12*CCO2*C*EXP(-22492/T)*RHOCHR*VINIT/MRELI)/
     1     (1.+.91E6*CCO2+.53E6*CCO)
     ENDIF
       RCO2 = P*8E12*CCO2*C*EXP(-22492/T)/(1.+.91E6*CCO2+.53E6*CCO)
     C = C - RCO2*DELT
     ACO = 2*RCO2P - FCO
      TOTCO2 = TOTCO2 + ACO2*DELT
      TOTCO = TOTCO + ACO*DELT
      IF(TOTCO2.LT.0) TOTCO2 = 0.
      IF(TOTCO.LT.0) TOTCO = 0.
       DVOLBL = (VOLBLT-VOLBL)/DELT
     VOLBL = VOLBLT
       DCCO2 = ACO2/VOLBLT - TOTCO2/VOLBLT**2.*DVOLBL
       DCCO = ACO/VOLBLT - TOTCO/VOLBLT**2.*DVOLBL
     CCO2 = CCO2 + DCCO2*DELT
     CCO = CCO + DCCO*DELT
     IF(CCO2.GT.CMAX)THEN
      CCO2=CMAX
            WRITE(9,*)'CCO2 GT CMAX'
     ENDIF
      IF(CCO2.LT.0)CCO2=0
     IF(CCO.GT.CMAX)CCO=CMAX
     IF(CCO.LT.0)CCO=0
     IF(R.LT.0) R=0
     IF(C.LT.0) C=0
       REL1=(106+36*S-64*S*R+12*C)/MRELI
C    FUME=0.07/15*TIME
C    IF(TIME.GT.15) FUME=0.07
     DFDT=0.011*(1-P)
     IF(R.LT.0.01)DFDT=0.
     FUME=FUME+DFDT*DELT
     IF(FUME.GT.0.07)FUME=0.07
C
     TIME = TIME + DELT
       IF(I/NSKIP*NSKIP.EQ.I)WRITE(9,100)TIME,TAB,R,TAB,C,TAB,REL1,
     1 TAB,CCO2,TAB,CCO,TAB,FUME
C        IF(I/(NSKIP+5)*(NSKIP+5).EQ.I)WRITE(9,*)TIME,TAB,C,
C     1 TAB,CCO2,TAB,CCO,TAB,ACO,TAB,TOTCO,TAB,FCO
      IF(I/NSKIP*NSKIP.EQ.I)WRITE(2,100)TIME,TAB,R,TAB,C,TAB,REL1,
     1 TAB,CCO2,TAB,CCO,TAB,FUME
10   CONTINUE
     CLOSE(UNIT=2)
     STOP
     END
```

APPENDIX IX. DIFFERENCES BETWEEN BED.FOR AND IPCBED.FOR.

1. **BED.FOR**

```
      SARNSV = SX(I) * SY(J+1) * 1.91
      SAREWV = SZ(K) * SY(J+1) * 1.91
      SAREAH = SX(I) * SZ(K) * 1.91
```

IPCBED.FOR

```
      SARNSV = SX(I) * SY(J+1)
      SAREWV = SZ(K) * SY(J+1)
      SAREAH = SX(I) * SZ(K)
```

2. **BED.FOR**

```
      SCCO2 = VISC/DIFCO2
      SCH2O = VISC/DIFH2O
      SCO2  = VISC/DIFO2
```

IPCBED.FOR

```
PROPERTIES AT 800 C (1073 K)
      DCO28 = -0.20141+9.0103E-4*1073+6.7304E-7*1073**2.
      DH2O8 = -0.34941+1.4816E-3*1073+1.2056E-6*1073**2.
      DO28  = -0.19389+1.0385E-3*1073+9.4380E-7*1073**2.
      VISC8 = -0.13327+7.2699E-4*1073+5.9149E-7*1073**2.
```

3. **BED.FOR**

```
      REYN = 1.0 * VELOC * 100/VISC
C     SHERWOOD NUMBER
      SHCO2 = 2.0 + 0.6 * REYN**0.5 * SCCO2**0.333
      SHH2O = 2.0 + 0.6 * REYN**0.5 * SCH2O**0.333
      SHO2  = 2.0 + 0.6 * REYN**0.5 * SCO2 **0.333
C     MASS TRANSFER COEFFICIENTS
      KMCO2 = DIFCO2 * SHCO2/1.0/100
      KMH2O = DIFH2O * SHH2O/1.0/100
      KMO2  = DIFO2  * SHO2 /1.0/100
C
```

IPCBED.FOR

```
C     MASS TRANSFER COEFFICIENTS
      KMCO2 = (3.05+8.62*VELOC)*(DIFCO2/DCO28)**0.57
     1          *(DCO28/DO28)**0.57 * (VISC/VISC8)**-0.37/100
      KMCO2 = (3.05+8.62*VELOC)*(DIFH2O/DH2O8)**0.57
     1          *(DH2O8/DO28)**0.57 * (VISC/VISC8)**-0.37/100
      KMCO2 = (3.05+8.62*VELOC)*(DIFO2/DO28)**0.57
     1          *(DCO28/DO28)**0.57 * (VISC/VISC8)**-0.37/100
```

4. BED.FOR

```
13      TOLD = TBED
        IF(TOLD.LE.0)THEN
```

IPCBED.FOR

```
        TOLD = TBED
13      IF(TOLD.LE.0)THEN
```

5. BED.FOR

```
        TBED = TNEW
        IF(EPS.GT.0.01) GOTO 13
C
C       BRACKET THE WALL TEMPERATURE TO REMOVE ANOLOMIES.
C
999     TBED = AMIN1(TNEW,1700.)
        T(L) = AMAX1(TBED,900.)
C
```

IPCBED.FOR

```
        TOLD = TNEW
        IF(EPS.GT.0.01) GOTO 13
C
999     T(L) = 0.9*TBED + 0.1*TNEW
C
```